DIPLOMARBEIT

Investigation of novel immobilization matrices with scanning probe microscopy for the integration of electrochemical biosensors into bifunctional AFM tips

ausgeführt am

Institut für Chemische Technologien und Analytik

der Technischen Universität Wien

unter der Anleitung von a.o. Univ. Prof. Dr. Boris Mizaikoff und Dr. Christine Kranz

durch

Justyna Wiedemair
Florianigasse 52/11, A-1080 Wien

Atlanta, im Juli 2004

Acknowledgement

First, I would like to thank Prof. Boris Mizaikoff and Dr. Christine Kranz for the interesting topic and for the unique opportunity of performing my diploma thesis in the United States.

Many thanks to Dr. Angelika Kueng for help in the process of familiarizing myself with the instrumentation and the topic along with all the helpful discussions and assistance.

Also I would like to say thank you to all members of the Applied Sensors Laboratory for the nice working atmosphere and for spending a lot of good times together, not only at the university. In particular I would like to thank Nicola Menegazzo for all his help and support and for being a very special friend.

Furthermore I appreciate the hydrogel sample preparation by Michael Serpe and all the discussions and scientific input of Prof. Andrew Lyon.

Financial support by the “Fonds zur Foerderung der wissenschaftlichen Forschung” (FWF, grant #P14122-CHE), the “Ausseninstitut der Technischen Universitaet Wien” and the “U.S. National Institute of Health” (NIH, grant #EB000508) is gratefully acknowledged.

And finally a big thank you to my family, for always supporting and standing behind me, and all my friends back home in Europe. Without them I would not be what I am.

Abstract

The presented thesis is focused on strategies for the development of microelectrode based amperometric biosensors with the emphasis on characterization of novel immobilization materials. Experimental conditions for future miniaturization and development of atomic force microscopy (AFM) tip integrated glucose biosensors have been investigated and optimized. Furthermore, the phase transition behavior of thermally responsive hydrogel particles potentially serving as enzyme immobilization matrix has been studied by atomic force microscopy.

Amperometric glucose biosensors were prepared by (i) pH shift induced pulsed deposition of enzyme containing polymer layers, and (ii) covalent attachment of self-assembled monolayers to electrode surfaces with subsequent crosslinking of glucose oxidase via glutaraldehyde. For the first approach, the optimal sensor stability was achieved by application of one deposition cycle with maximum current response of the sensor after a storage time of 12 - 24 h. The second approach based on covalent attachment revealed improved stability of the recognition layer, however, at decreased sensitivity in comparison to the polymer entrapment based biosensor due to lower amounts of immobilized enzyme.

Manual calibration of the biosensors was compared to an automated standard addition procedure for the substrate glucose, established on the basis of flow injection analysis (FIA). While the latter approach yielded reproducible linear calibrations, high background noise limited the achievable limit of detection at the current stage of development.

Immobilized thermoresponsive hydrogel microparticles were investigated with atomic force microscopy. Responsive hydrogels are innovative materials that show a change in the physical nature of the polymer network upon exposure to certain stimuli such as modulation of the temperature or pH. These properties render them useful matrices for a variety of applications ranging from drug delivery to biosensor design. However, prior to these challenging applications fundamental knowledge on the temperature responsive behavior of individual hydrogel particles is an essential prerequisite. In-situ experiments of the volume phase transition behavior of thermo- and pH-responsive poly(N-isopropylacrylamide-co-acrylic acid) hydrogel particles after electrostatic and covalent immobilization were performed. The fundamentals for AFM investigation of volume phase transitions on individual hydrogel particles have successfully been established. Among the main findings of this study was the effect of tip-sample interaction during AFM imaging on the volume phase transition behavior of individual hydrogel particles.

TABLE OF CONTENTS

1 Introduction

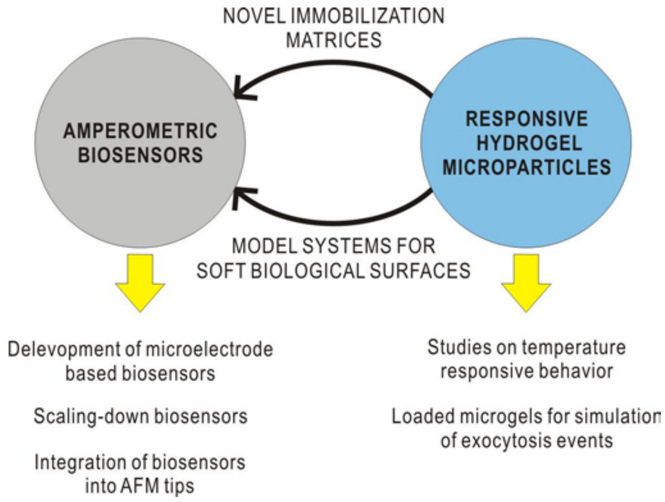

Figure 1.1: Schematic summary of the objectives of the presented thesis including future perspectives of this work.

Rapid and molecule specific determination of analytes in complex matrices is a seminal field in modern analytical chemistry. Electrochemical biosensors provide an attractive platform for this challenge. The key element in effective biosensor design is the immobilization of analyte specific biorecognition elements at the transducer surface. Enzymes are among the most commonly applied recognition elements in biosensor technology, in particular due to their high selectivity. Retaining sufficient enzyme activity along with a minimum of conformational changes of the protein structure is of particular importance during the immobilization process influencing the performance and long term stability of the sensing interface.

Miniaturization of (bio)sensor technology has gained increasing interest in the last decade. In particular, laterally resolved measurements of bioactivity at a sample surfaces requires the integration of electrochemical biosensor functionality into imaging device technology. Bifunctional atomic force microscopy (AFM) tips based on tip-integrated micro- and nanoelectrodes provide a unique platform for simultaneously obtaining laterally resolved information on multiple parameters correlated in space and time.

Thermoresponsive hydrogels are potentially attractive immobilization matrices for advanced biosensor design. Due to their high water content they provide a favorable environment for biorecognition elements, and in particular for enzymes. However, this challenging application of hydrogels requires fundamental knowledge on these novel materials, especially on their temperature responsive behavior. Scanning probe microscopy is a promising surface analytical technique for laterally resolved in-situ temperature studies of immobilized, individual hydrogel microparticles.

The main focus of the presented thesis is the in-situ characterization of hydrogel microparticles and their temperature responsive behavior with atomic force microscopy for future application as immobilization matrix for biological components (e.g. enzyme entrapment) and/or model systems for soft biological surfaces. In addition, the experimental conditions and automated calibration procedures for the development of miniaturized amperometric glucose biosensors have been optimized. It is anticipated that the combination of the investigated technologies will lead to advanced AFM tip-integrated amperometric glucose biosensors for laterally resolved investigations at cell surfaces.

.

2 Theoretical background

2.1 Biosensors

2.1.1 Basic principles and applications

The rapid and/or on-line determination of analytes in complex matrices remains a challenge in modern analytical chemistry. Biosensors are gaining increasing interest in this field, in particular due to their molecular selectivity. Based on the IUPAC definition [1] a biosensor is "a self-contained integrated device which is capable of providing specific quantitative or semi-quantitative analytical information using a biological recognition element, which is in direct spatial contact with a transducer element". The biological recognition element specifically interacts with analyte molecules creating a change of physical or chemical parameters (e.g. pH, redox state, temperature, charge, refractive index, etc.), which can be converted by the transducer into a quantifiable read out signal (Figure 2.1). Usually, a signal obtained in the biochemical domain is transduced to the electrical domain. The obtained signal can be directly correlated to the concentration of the target analyte.

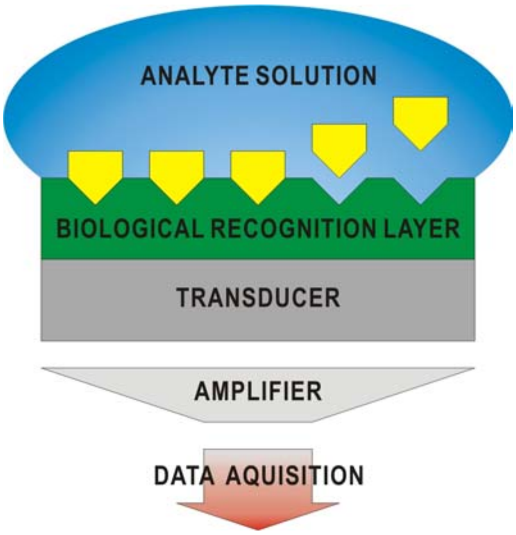

Figure 2.1: Schematic representation of a biosensor. The analyte specifically interacts with the biological recognition layer, which is in direct contact with a transducer. Data are amplified and converted into quantifiable readout signals.

As the selectivity of the biosensor mainly depends on the nature of the biological recognition element and the immobilization process ensuring intimate interaction with the transducer surface, appropriate selection of the sensor architecture and sophisticated immobilization strategies are a prerequisite. The majority of biosensors are based on enzymes serving as biological recognition elements. However, biosensors based on antibodies, cell components, whole cells, or even microorganisms can be found in literature [2, 3]. Besides high chemical specificity, enzymes provide inherent biocatalytic signal amplification. The long term stability of enzyme based biosensors relies on the ability of enzymes to regenerate and on appropriate strategies for retaining the enzyme activity after immobilization at the transducer interface. The most frequently applied transducer principles are electrochemical (amperometric, potentiometric, impedimetric, or conductometric) and optical (fluorescence, surface plasmon resonance, etc.) sensing platforms. However, mass sensitive or thermosensitive transduction principles can also be found in literature [4].

In principle, biosensors have a wide range of applications ranging from clinical analysis to environmental monitoring and can be considered a valuable asset to modern analytical chemistry. Among the main advantages is the high selectivity of the biological recognition element, which enables the analysis of complex samples mixtures frequently without any preceding separation procedures. Recent progress in miniaturization of biosensors results in faster response times and reduced costs due to the minimized consumption of biological components and reduced sample volumes. Biomedical and clinical analysis are certainly amongst the most promising applications for miniaturized biosensing devices [5, 6].

Among the described transduction principles, the presented work is focusing on novel strategies for miniaturized amperometric biosensors.

2.1.2 Design and fundamental principles of amperometric biosensors

Amperometric biosensors are based on the measurement of a current resulting from the electrochemical oxidation or reduction of an electroactive species, which is produced or consumed within the biocatalytic layer adjacent to the electrode surface. The obtained current is proportional to the bulk concentration of the analyte, if the biocatalytic reaction rates show a first order dependence.

One of the main challenges in biosensor design is the immobilization of the enzyme at the transducer interface. In particular, specific and fast electron transfer between the recognition element and the electrode surface have to be maintained, while avoiding loss of catalytic enzymatic activity induced by e.g. conformational distortion during immobilization. Direct electron transfer from the active site of the enzyme to the electrode surface via electron tunneling represents the ideal case. However, direct electron transfer is difficult to achieve since the redox centers of most oxidoreductases are deeply buried within the three dimensional protein structure [3]. Hence, the comparatively long distances to the electrode surface prevent regeneration of the active site via electron tunneling. Therefore, alternative approaches for enzyme immobilization have been developed and are discussed in the following section.

In recent decades, amperometric biosensor design has evolved through several phases of development [3]: Early biosensor architectures ("first generation") were predominantly based on direct adsorption of enzymes such as glucose oxidase at electrode surfaces [7]. Natural co-substrates (e.g. molecular oxygen or NAD^+) were used for recycling of the prosthetic group. These co-substrates act as electron-transfer shuttles between the enzyme and the electrode. However, unpredictable concentrations of natural co-substrate and desorption of the weakly immobilized enzyme generally led to unreliable analytical results and insufficient stability inspiring further evolvement of immobilization strategies. Artificially added redox mediators were used in the so called "second generation" of biosensors [8]. However, this biosensor design relies on a mediator, which is not immobilized in proximity of the electrode surface leading to "bleeding" of the mediator. Hence, applicability in sensitive environments such as biomedical in-vivo glucose analysis is limited. The "third generation" of biosensors (reagentless biosensors) is based on immobilization of the enzymatic component and covalent attachment of the artificial mediator. This approach leads to enhanced electron transfer via "electron hopping mechanisms" [9] and avoids the problem of decreasing sensor response due to leaching of the mediator.

In general, a variety of enzyme immobilization techniques can be applied at electrode surfaces, including drop or dip coating of solutions containing appropriate cross linkers in presence of the biological recognition element [10], or use of sol-gel matrices [11, 12]. Screen printing techniques [13] or spin coating techniques [14] are of increasing importance, since better control of the immobilization process can be achieved, which is of particular importance for developing miniaturized sensor systems [13, 14].

Self-assembled monolayers (SAMs) provide a well controlled chemical toolbox for immobilizing biological recognition elements. These highly ordered thin films provide the opportunity to attach enzymes at a defined distance from the transducer interface with high reproducibility. As an example, gold electrodes can be modified with functionalized thiolate SAMs (e.g. cystaminiumdihydrochloride). Subsequently, the enzyme can either be covalently coupled to the monolayer or cross linked via glutaraldehyde [15].

Entrapment of biological recognition elements within electrochemically formed polymer films is an attractive immobilization strategy for amperometric biosensors, as the immobilization can be localized at and confined to the electroactive area of the sensor. Hence, conducting polymers such as polypyrrole, polyaniline, polythiophene and their functionalized derivatives are frequently applied as immobilization matrix. Enzyme entrapment is achieved by electropolymerization in presence of the biological component. Several extensive reviews on biosensors based on conducting polymers have been published in literature [16-19]. Among the disadvantages of this entrapment technology is the stiffness of the polymer backbone leading to decreased diffusion kinetics of the redox mediator and in consequence a decreased electron transfer rate [3]. Recently, an immobilization technique based on electrochemically induced, localized deposition of enzyme-containing polymer suspensions has been reported [20]. Oxidation of water at the electrode surface leads to a locally induced pH shift and to a significant change in polymer solubility. Therefore, the polymer locally precipitates at the electrode surface entrapping simultaneously present enzyme molecules.

Redox hydrogels are another promising group of polymers, which can be applied as entrapment matrix. These materials are particularly suitable for the construction of reagentless biosensors [3]. The attractive advantages of redox hydrogel based immobilization matrices result from following properties: (i) the redox mediator is covalently bound to the backbone of the polymer matrix. Hence, this approach ensures a high local concentration of redox relays enabling fast electron transfer; (ii) the high water content of the hydrogel provides a favorable environment for enzymes maintaining high activity; (iii) the flexibility of the backbone leads to advantageous diffusion kinetics for the enzymatic substrate and its reaction products; and (iv) redox hydrogels show excellent biocompatibility along with reduced biofouling of the transducer surface. However, especially for miniaturized biosensors the electrode modification procedure for immobilizing the biological recognition element has to be improved. In principle, the combination of conducting polymers with hydrogels may provide an optimal strategy for the formation of conducting redox hydrogels merging the advantages of both approaches [3].

2.1.3 (Thermo)responsive hydrogels

Hydrogels are promising materials serving as immobilization matrices in advanced biosensor design [3]. Especially so called responsive or “smart” hydrogels are material systems attracting substantial interest e.g. in the field of drug delivery. Individual environmentally responsive hydrogel particles or clusters of particles may also prove valuable as tunable model compartments mimicking e.g. soft biological surfaces or exocytosis by triggering molecular release events.

Responsive hydrogels are defined as highly solvent swollen, mostly hydrophilic and crosslinked polymers, which show an abrupt change of the physical nature of their polymer network upon exposure to certain stimuli (e.g. temperature, pH, etc.). In their swollen state, polymer-solvent interactions are thermodynamically favorable. However, upon subsequent variation of the stimulus the solvation behavior of the polymer chains is changed and polymer-polymer interactions are thermodynamically preferable. The state where the stimulus induced change occurs is called the volume phase transition (VPT) of the hydrogel.

Poly(N-isopropylacrylamide) (polyNIPAM) based hydrogels are among the most popular representatives of temperature responsive hydrogels [21-23]. Depending on their composition, the volume phase transition temperature (VPTT) can be deliberately tuned. Co-polymerization of acidic monomers such as acrylic acid (AAc) additionally leads to pH responsive behavior. Hence, the physical nature of the hydrogel depends on both the temperature and the pH of the solution [24].

Synthesis of small hydrogel particles (nanospheres; microgels) is usually achieved by free radical precipitation polymerization [21]. An initiator (e.g. persulfate) is added to the monomer solution, which contains cross-linking co-monomers (e.g. N, N'-methylene(bisacrylamide), BIS). At temperatures of about 60-70 °C the persulfate forms free radicals initiating the polymerization process. The polymerization process is followed by several cleaning steps removing both the sol (i.e. linear or only slightly branched polymer constituents) and the polydisperse fraction of the hydrogel. Besides uniform microgels also multiresponsive core-shell hydrogel nanoparticles can be designed following appropriate multistep synthesis protocols [25].

Dynamic light scattering (DLS) techniques or photon correlation spectroscopy (PCS) are frequently applied to determine particle size and size distribution in microgels, especially, for solvated polymer particles [21, 26]. Optical microscopy is applied for studying immobilized hydrogel microspheres [27]. Here, it should be mentioned that single hydrogel particles can be depicted, however, only for large particles (diam. > 1 µm) the volume phase transition can be observed. Hydrogel films can be investigated with surface plasmon resonance (SPR) techniques [28, 29]. The combination of this surface sensitive technique measuring minute refractive index changes with confocal fluorescence microscopy, ellipsometry or quartz crystal microbalance (QCM) devices, leads to a deeper insight into hydrogel formation processes and yields optical and mechanical properties of hydrogel films. Atomic force microscopy (AFM) is a promising technique to study the structure and mechanical properties of hydrogels in-situ [30-32]. However, to date this technique was mostly applied to investigate hydrogel films. In-situ AFM studies at single hydrogel particles along with the investigation of their temperature responsive behavior have not yet been reported in literature.

Upon passing the VPT, the volume and shape of hydrogel particles rapidly change. Following this behavior, two different types of hydrogels can be differentiated [23]: (i) rapid collapse of the polymer network leading to expulsion of up to 90 % of the contained solvent [33]. This behavior is usually defined as negative temperature behavior. (ii) In contrast, hydrogels, which swell upon passing the VPT due to uptake of solvent show positive temperature behavior.

Within this thesis only the first type of particles was investigated. Under certain conditions, hydrogels can be loaded with e.g. drugs inside the hydrogel particle. The abrupt deswelling process allows delivering of the incorporated species to a specific site. Hence, drug release can be triggered by e.g. temperature induced deswelling. Likewise, entrapment of enzymes instead of drugs can be used to design novel biosensors based on the unique features provided by responsive hydrogels. Furthermore, the simulation of abrupt release events while passing the VPT of the hydrogel could render responsive hydrogels an interesting model system for miniaturized biosensor optimization prior to work at live cells. While temperature induced release of entrapped molecules can be performed and measured in bulk solution, laterally resolved investigation of local release events at single particles remains a challenge that has not been reported yet. Imaging techniques based on scanning multifunctional probes in close proximity across the surface of individual hydrogel particles is a promising approach in this field.

Besides the deswelling behavior, the volume phase transition is usually associated with a change in particle stiffness. If the particles contain acidic side chains (i.e. also show pH responsive behavior), pH changes usually also result in changes of the water content and, consequently, the particle stiffness.

In order to study the functionality of responsive hydrogel particles and their potential application as immobilization matrix for biosensors, laterally resolved information on single particle behavior during their transition state is a fundamental prerequisite. The temperature dependent behavior and morphology changes during the transition state are interesting aspects, which can be studied with scanning probe techniques such as atomic force microscopy (AFM). Throughout this thesis, the main emphasize was focused on fundamental studies for investigating temperature dependent deswelling of individual hydrogel particles with AFM. Based on the obtained results, the remaining challenges and future applications will be discussed.

As already indicated, hydrogels are interesting candidates for immobilizing enzymes at a transducer surface due to their hydrophilic nature. Compared to conventional polymer matrices, immobilization in hydrogel matrices provides improved diffusion kinetics and biocompatibility, along with reduced biofouling. Additionally, the mass transfer rate between the enzyme containing hydrogel layer and the bulk solution is increased upon passing the VPT resulting in strongly reduced response times of a biosensor [34]. First results indicate another unique feature of temperature responsive hydrogels: enzymes being entrapped in the network of responsive cross-linked hydrogels retain high enzyme activity even if the denaturation temperature of the protein is passed. Apparently, the collapse of the polymeric network and consequently tighter entrapment of the protein molecules protects the enzyme and prevents denaturation beyond the usual solution denaturation temperature. Hence, hydrogel matrices are potential alternatives for enzyme based measurements at harsh environmental conditions. Finally, the attachment of hydrogel layers via covalent binding at Au surfaces is a well known procedure. Consequently, the modification of electrode surfaces with responsive hydrogel particles and films can be envisaged.

2.1.4 Miniaturization of biosensors

Miniaturization and integration of biosensors are intensively studied aspects in recent biosensor research [35]. Faster response times and reduced costs of fabrication due to minimized consumption of potentially expensive analytes and samples are among the key interests in this respect.

Miniaturized and highly integrated biosensors utilizing “on chip technology” have successfully been demonstrated [36]. However, application of these devices is usually restricted to bulk measurements. Obtaining laterally resolved information (“imaging biosensors”) is of high importance, especially in biomedical sciences. Complex biological samples require the simultaneous measurement of multiple parameters correlated in space and time [37]. Accurate positioning and scanning (imaging mode) of miniaturized biosensors in close proximity to the sample surface enables laterally resolved sensing of individual (re)active sites (see also 2.2.1.2 and 2.2.1.3).

In order to develop and optimize miniaturized systems, usually a “macroscopic” version of the device is developed and characterized. For example, the development of integrated scanning amperometric biosensors requires preliminary tests performed at microelectrode based enzymatic biosensors. The process of transferring the geometric factors and the obtained performance of the “macroscopic” version to the miniaturized device is typically called “scaling down". In this thesis, first steps towards miniaturization of a previously optimized microelectrode based glucose biosensor into AFM tip integrated electrodes were performed.

2.2 Methods

2.2.1 Scanning probe microscopy

The term scanning probe microscopy (SPM) covers a variety of techniques providing measurements of surface topography and laterally resolved physical-chemical surface properties with high lateral resolution. The basic principle of SPM techniques relies on the specific tip-sample interaction as the probe is scanned in close proximity across the sample surface. The main difference between individual SPM techniques derives from the fundamental physical principle of the selected tip-sample interaction determining the probe distance regulation. Depending on the tip-sample interaction, SPM can be classified into various techniques such as scanning tunneling microscopy (STM), atomic force microscopy (AFM), scanning electrochemical microscopy (SECM), and near-field scanning optical microscopy (NSOM) listing the most important representatives. With the development of STM Binnig and Rohrer laid out the fundamentals for a whole family of scanning probe techniques, which was honored with the Nobel prize in physics in 1986 [38, 39]. In the same year, G. Binnig et al [40] introduced the AFM. Due to their relevance in the present thesis, AFM and SECM will be discussed in detail in the following chapters.

2.2.1.1 Atomic force microscopy (AFM)

AFM has rapidly developed into a routine tool for surface scientists in vacuum and ambient environments. In contrast to STM, no limitations due to the electrical properties of the sample restrict the application of AFM.

In AFM a sharp tip, which is mounted on a soft cantilever is scanned in close proximity across a sample surface detecting variations in physical and chemical attractive and repulsive forces at the molecular and atomic level. Due to force interactions between the sample and the tip the cantilever is actuated. The resulting cantilever displacement provides the required information for imaging the topography of the sample surface. Repulsive short range forces, electrostatic forces, van der Waals forces, magnetic forces or capillary forces may cause bending of the cantilever. Depending on the measurement mode, different forces are dominating during the tip-sample interaction. For example, in AFM non-contact mode long range forces (e.g. electrostatic forces, van der Waals forces, magnetic forces or capillary forces) are dominating, whereas in AFM contact mode repulsive short range forces are mainly responsible for the tip-sample interaction. The proportional relationship between force and displacement of the engaged cantilever is described by Hook's law.

Piezoelectric (x, y, z) positioning elements and a feedback control system are applied to keep the probe in constant distance to the sample surface. In most commercial systems the deflection of the cantilever is detected with an optical measurement, though other measurement principles can be used. During optical detection, a radiation from a laser diode is focused on the tip end of the cantilever and reflected onto a split photodiode. In most cases, photodiodes with four commensurate segments (upper and lower; left and right) are used. The read-out between the upper and the lower part provides information on the cantilever deflection (topography), whereas the signal difference between the left and right photodiode segment reflects frictional information (friction force microscopy, FFM) due to e.g. torsion of the cantilever.

Two basic operational principles can be applied during AFM studies: in the constant height mode the z-coordinate is not adjusted during scanning and the deflection of the cantilever is directly measured. Consequently, measuring in constant height mode is suitable for flat samples, small scan areas and high scan rates. If thermal drifts are efficiently eliminated high resolution imaging down to the atomic level is enabled. However, this mode is limited to flat samples due to potential tip crashes at substrates with high surface roughness. In this case, the vertical position of the tip has to be re-adjusted. The height information measured using the deflection of the cantilever is compared with a default value based on a feedback loop. The feedback system controls the piezoelectric positioning system to maintain the default deflection value constant during the AFM measurement. This principle leads to so called constant force measurements (constant force mode). The constant force mode is typically used for imaging rough samples and when scanning large areas.

In *non contact mode AFM* the cantilever is scanned at a distance > 10 Å across the sample surface. As a consequence, at these distances only long range forces (e.g. electrostatic forces) are causing deflection of the cantilever. In general, the achievable resolution does not favorably compare to contact mode imaging, although, atomic resolution in non contact mode AFM was reported in literature for imaging semiconductors and insulating surfaces in ultra high vacuum (UHV) conditions [41, 42]. Applications of non contact mode AFM are focused on the investigation of long range forces and for imaging delicate samples such as liquid/air interfaces [43].

In contact mode AFM the tip is in physical contact with the sample surface during imaging. Considering an ideal tip, only a couple of atoms of the tip material are interacting with the sample surface. The orbitals of the atoms in this small area (apex of the tip) are overlapping with the molecular or atomic orbitals of the sample. Due to this overlap, inter-atomic repulsive short range forces arise, which are among other interactions responsible for deflection of the cantilever. Atomic resolution can be achieved by successful elimination of other forces (e.g. capillary forces due to thin films of humidity covering every surface at ambient conditions) and thermal drifts.

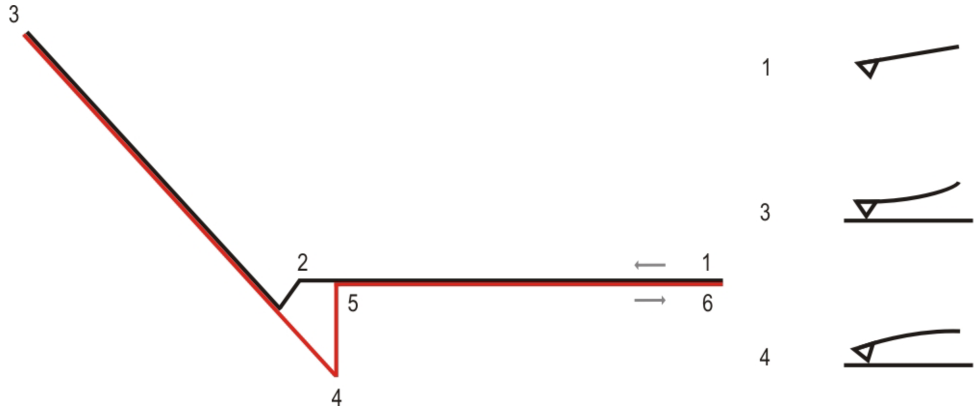

Figure 2.2: Idealized force distance curve and schematic depiction of AFM cantilever deflection (black line: approaching, red line: withdrawing the tip). (1) At a large tip-sample distance the tip does not interact attractively with the sample and the cantilever deflection is not altered. (2) The AFM tip is engaged at the surface. Upon further decreasing the distance of the cantilever, the interaction between the probe and the surface follows Hook's law. (3) The deflection of the cantilever reaches its maximum value, and the distance is increased again. (4) The point were the tip should withdraw from the surface is delayed due to (attractive) adhesive interactions in respect to the approaching curve. To minimize forces, measurements should be performed as close to point (4) as possible. (5) The tip withdraws from the surface and returns to the initial state (6).

Besides recording topographical images, AFM is frequently used for force spectroscopy by recording so called force distance curves. The tip-sample interaction at small distances to the sample surface is measured and can be a valuable parameter for the characterization of the sample elasticity. Figure 2.2 shows an idealized force distance curve. At large distances the tip does not interact with the sample. When the tip is approaching the sample surface probe/sample interaction resumes, however, with forces much lower than the restoring force of the cantilever. The cantilever abruptly engages with the sample surface due to attractive van der Waals interactions, which then exceed the restoring force of the cantilever. The engagement is also described as the tip "jumping" to the surface. Upon further decreasing the distance, the cantilever deflection is increased. This part of the force distance curve can be characterized by Hook's law, showing a linear dependence between force and distance. If the tip sample distance is increased again, the tip is withdrawn from the surface. Adhesive forces between the probe and the sample delay the probe/sample disruption in respect to the approaching curve. Ideally, measurements should be performed at minimized forces to avoid excessive forces at the sample surface, which may mechanically affect or destroy the sample. In general, contact mode AFM is mainly applied to imaging of comparatively hard sample surfaces.

The introduction of intermittent contact mode AFM (dynamic mode, acoustic mode or tapping mode AFM; the latter is a trademark of Digital Instruments) was a significant step facilitating the investigation of soft sample surfaces such as biological species and polymers. Dynamic mode measurements can be performed in air and liquid phase [44, 45]. In dynamic mode the cantilever is oscillated at its resonance frequency using either acoustic or magnetic excitation. In contrast to permanent contact with the sample, intermittent contact with the surface results in reduced tip-sample contact time and hence, minimized frictional forces [46, 47].

Valuable information on sample properties such as elasticity or frictional forces can be obtained by recording phase images (in dynamic mode AFM) or frictional force measurements (in contact mode AFM), respectively. Besides the elasticity information, phase imaging is a promising technique to discriminate chemically different areas at the sample surface. However, element specific or direct chemical information cannot be obtained with this technique, in particular if unknown samples are investigated. Chemical modification of AFM tips extends the information content obtained by conventional force spectroscopy utilizing molecular interaction forces between the modified tip and the sample surface.

Single bond rupture events and the determination of binding constants were first reported in 1994 by Gaub and co-workers [48] and Colton and co-workers [49]. Extensive reviews on single-molecule force spectroscopy have recently been published [50-53]. Especially in the field of biosciences the simultaneous detection of surface topography and chemical functionality enables investigation of structure-function relationships. This promising approach yields enhanced insight into biological and biochemical mechanisms. Molecular recognition force microscopy (MRFM) is an excellent technique for the characterization of single ligand-receptor binding and dissociation combining dynamic force microscopy with simultaneous molecular recognition. Affinity constants, rate constants and energy barriers have been estimated and bond widths of binding pockets have been determined [54-57]. Recently, the determination of receptor sites with an accuracy at the nanometer scale has been reported [58]. An antibody for lysozyme was tethered to a magnetically oscillated AFM tip and used for imaging immobilized lysozyme molecules with high resolution. However, this principle can be theoretically extended to any ligand-receptor pair opening the field for a variety of applications. Another example is studying the Na+/D-Glucose co-transporters in brush border membrane vesicles with a PAN3-antibody modified AFM tip [59]. Single antibody-antigen recognition events can be observed by recording of force distance cycles during dynamic force imaging.

The lack of direct chemical information is among the major drawbacks of conventional AFM with non-modified probes. Nonetheless, AFM is an attractive surface analytical technique for imaging with high lateral resolution and for obtaining topographical information on surface processes on a wide variety of different sample surfaces in UHV and at ambient conditions. Additionally, direct surface structural information goes along with a high dynamic scan range covering approx. 5 orders of magnitude.

2.2.1.2 Scanning electrochemical microscopy (SECM)

Since the introduction of ultramicroelectrodes (UMEs), unprecedented advances in electroanalytical chemistry have been achieved. UMEs are commonly defined as electrodes with at least one dimension (“critical dimension”) of the electroactive surface in the range of 25 µm to a few nanometers [60]. There are different types of microelectrodes including disk, ring, ring-disk, spherical or conical electrodes. Disk electrodes are among the most widely used and studied UME types. The dimensional aspect has a major impact on the mass transport phenomena at the electrode surface. Mass transport towards a macroscopic electrode is described by planar diffusion. In contrast, due to the minimized electroactive area and edge effects, microelectrodes are characterized by hemispherical diffusion behavior, which is shown in Figure 2.3. Resulting, microelectrodes provide attractive features in terms of their electrochemical behavior making them particularly suitable for imaging applications. Hemispherical diffusion results in an enhanced mass transport causing the thickness of the diffusion layer to rapidly reach a steady state value. At macroelectrodes, the thickness of the diffusion layer is strongly time dependent, as described by the Cotrell equation. For this consideration the current is represented by the diffusional flux of the electroactive species (convection and migration are neglected). By solving Fick’s second law of diffusion, the planar diffusion towards the electractive area results in a concentration gradient resulting in a time-dependent Faraday current. The relationship of time dependent current and the diffusion behavior is given by the the Cotrell equation:

$$i(t) = \frac{n * F * A * D^{1/2} * c}{\pi^{1/2} * t^{1/2}} \tag{1}$$

where *n* is the number of electrons transferred at the electrode, *F* is the Faraday constant, *A* is the area of the elctroactive surface, *D* is the diffusion coefficient of the redox species in solution, *c* is the concentration of the redox mediator and t is the time.

In the case of microelectrodes the Cotrell equation has to be modified by an additional, non time dependent, term due to hemispherical diffusion. Due to the smaller electrode area the diffusion layer exceeds the dimension of the electroactive area. The obtained Faraday current depends on the time scale of the experiment. In case of short experiments the planar diffusion prevails and the current response is determined by the time dependent term of the Cotrell equation. At longer time scales additional radial diffusion dominates and the enhanced mass transfer towards the electrode results in a steady state current response, which is described by the second term of the modified Cotrell equation:.

$$i(t) = \frac{n * F * A * D^{1/2} * c}{\pi^{1/2} * t^{1/2}} + \frac{n * F * A * D * c}{r} \tag{2}$$

where *n* is the number of electrons transferred at the electrode, *F* is the Faraday constant, *A* is the area of the elctroactive surface, *D* is the diffusion coefficient of the redox species in solution, *c* is the concentration of the redox mediator, *t* is the time and *r* is the electrode radius.

For UMEs, double layer charging effects are minimized and the ohmic drop is strongly reduced. Their small dimensions and advantageous electrochemical behavior renders microelectrodes a versatile component of electrochemical imaging systems, usually referred to as scanning electrochemical microscopy (SECM) [61, 62].

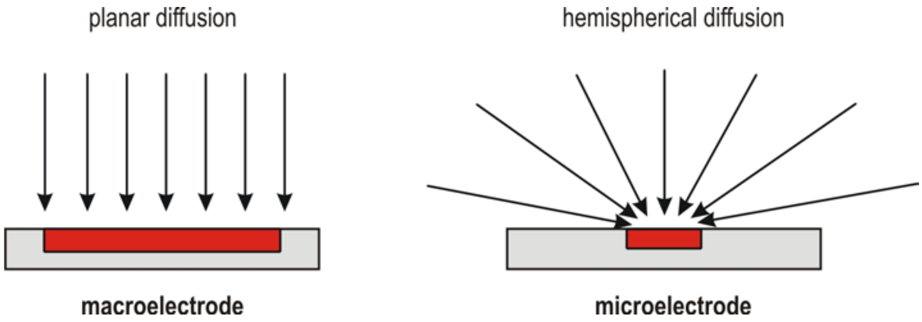

Figure 2.3: Comparison of the diffusion behavior at a macro- and microelectrode.

With the investigation of local concentration profiles using an UME and the description of the faradaic current at an UME in the late 1980's Engstrom and co-workers [63] and Bard and co-workers [64-66], respectively, laid the fundamentals for scanning electrochemical microscopy (SECM). This in-situ scanning probe technique is a powerful method for the investigation of (electro)chemical surface and interface processes with increasing importance in the biological and biomedical disciplines.

In SECM, a biased UME is scanned in close proximity across a sample surface and the faradaic current measured at the UME is recorded. Signal generation in SECM is based on surface induced changes of the faradaic current due to hemispherical diffusion of redoxactive species in solution to the biased UME. Besides the (electro)chemical properties of the sample surface, the measured current is strongly dependent on the distance between the UME and the sample surface topology. Hence, accurate positioning of the microelectrode is of major importance and will be discussed below. While different electrode geometries such as ring, disk or conical microelectrodes can be used for SECM experiments [67-70], predominantly disk UMEs are reported as scanning probes.

There are several modes of operation in SECM, with the feedback mode [66] and the generation/collection mode (*GC mode*) [71] as the most prominently applied techniques. Direct mode SECM is mainly used for surface modifications and should therefore only be mentioned here for completion [72].

The diffusion controlled steady state current $i_{T\infty}$ arising at a biased disk microelectrode in bulk solution (i.e. at least several tip diameters away from the surface, implied by the subscript ∞) is described by following equation [73]:

$$i_{T\infty} = 4nFDcr \tag{3}$$

where *n* is the number of electrons transferred at the electrode, *F* is the Faraday constant, *D* is the diffusion coefficient of the redox species in solution, *c* is the concentration of the redox mediator and *r* the disk radius.

For measurements in feedback mode the solution contains one redox form of a quasi reversible redox couple, which is usually artificially added to a supporting electrolyte solution. By applying the respective potential at the microelectrode, the redox species is either oxidized or reduced resulting in a diffusion-limited faradaic current measured at the UME. Depending on the (electro)chemical properties of the investigated sample surface, the concentration of the redox mediator and, hence, the faradaic current is influenced by the surface properties when the tip is in close proximity to the sample surface. If the tip is approaching an insulating surface, at distances smaller than few electrode radii hemispherical diffusion of the redox active species towards the UME is blocked and the current measured at the electrode decreases compared to $i_{T\infty}$ (negative feedback). In contrast, if the tip is approaching a conducting or electrochemically active surface, the species oxidized or reduced at the UME can be regenerated by the sample surface leading to a recycling effect in the vicinity of the microelectrode. Hence, the faradaic current measured at the UME is increased compared to $i_{T\infty}$, which is called positive feedback. Current-distance curves (or so called "approach curves") are recorded to determine the UME tip-to-sample distance. A schematic representation of typical approach curves is given in Figure 2.4.

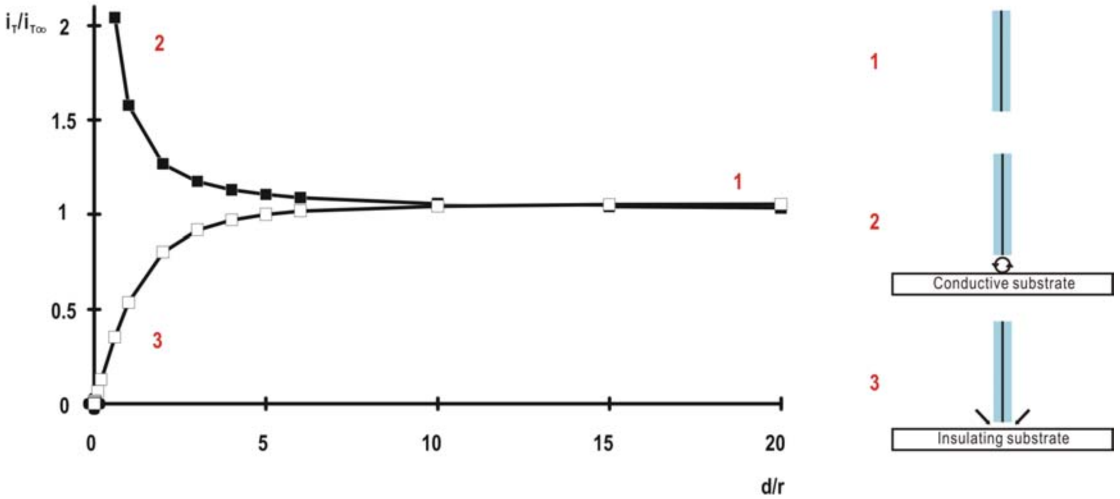

Figure 2.4: Idealized SECM approach curves in feedback mode approaching a conductive sample surface (2) and an insulating sample surface (3). (1) The microelectrode is several radii away from the surface, the diffusion controlled steady state current $i_{T\infty}$ is recorded. (2) Positive feedback. Upon approaching the microelectrode towards the conducting surface the current signal increases due to the regeneration of the redox species at the substrate. (3) Negative feedback observed when approaching an insulating surface. The diffusion of the redox species towards the UME is blocked and the current signal decreases.

It should be noted that for optimized diffusion conditions during feedback mode SECM experiments the insulating shield of the electrode needs to have a certain thickness correlated to the dimensions of the electroactive area (RG value, $RG = \frac{r_{shield}}{r_{electrode}}$) [66]. During negative feedback the diffusion rate and diffusion efficiency into the narrow gap between electrode and sample surface is strongly dependent on the dimension of the microelectrode and the insulating glass shielding. Derived from numerical simulations for approaching insulating and conductive sample surfaces, this effect is less prominent for positive feedback, as the resulting current mainly depends on the regeneration of the electroactive species and less on diffusional transport in the tip-sample gap. It has been found that for RG values of 5 – 10, theoretical approach curves correspond well with the experimentally obtained data [66].

In the generation/collection mode locally produced electroactive species are mapped when the UME is in close proximity to the sample surface. Two different approaches are described in literature: (i) the substrate generation/tip collection (SG/TC) and (ii) the tip generation/substrate collection (TG/SC) mode. In SG/TC mode, the substrate is used to generate a reactant, which is then detected (collected) by the microelectrode. The first paper relevant for the development of SECM, which was published in 1986 by Engstrom et al using an UME to study concentration profiles near electrode surfaces is an excellent example of this operation mode [63]. In TG/SC mode, the tip generates a species, which is then collected by the substrate acting as detecting electrode. Although the lateral resolution obtained in feedback mode can not be achieved in generation collection experiments, this mode is frequently used for investigations at biological samples due to the higher sensitivity.

In SECM imaging the microelectrode is typically scanned in a (x, y) plane across the surface (constant height mode) after recording of approach curves to determine the UME to sample distance. The experimental results are plotted as faradaic current versus distance curves and compared with theoretical approach curves, which are usually based on well established numerical simulations for different electrode geometries [66, 74]. However, this approach is limited to amperometric electrodes. Positioning of non-amperometric UMEs (such as biosensors or potentiometric electrodes) requires alternative position strategies. Additionally, several problems arise when imaging is performed in constant height mode. The lateral resolution of SECM in conventional constant height is not comparable to other SPM techniques such as AFM and STM. High lateral resolution could be achieved using nanometer-sized electrodes, which in turn require a significantly reduced working distance in contrast to micrometer-sized electrodes. If sub- microelectrodes or nanoelectrodes are used for imaging, the tip to sample distance, which again needs to be within several radii of the electroactive tip area, may easily lead to tip crashes when scanning over rough or tilted sample surfaces in constant height. Hence, tip and sample may be destroyed. Furthermore, images recorded at a fixed (constant) height may represent a convolution of electrochemical surface properties and topography, which is especially critical for unknown sample topographies [75]. Consequently, separation of electrochemical and topographical information along with reduction of the electrode size is required for high resolution electrochemical imaging. In addition, quantification of the obtained electrochemical data requires precise knowledge of the electrode-sample distance. These aspects clearly document that current independent positioning is the key problem of conventional SECM.

Early attempts have been made towards solving the "fixed height" problem [76-78]. which were still mainly dependent on the electrochemical signal [75]. In 1995 Ludwig et al. [79] introduced the first promising approach, which enabled scanning the UME at a constant distance across the sample surface. Adapted from the distance control in NSOM [80], a fiber-shaped microelectrode is laterally vibrated at its resonance frequency while approaching the sample surface. Due to hydrodynamic interactions with the sample surface the vibration amplitude is damped in close proximity. The damping of the vibration is detected with an optical system using radiation of a laser diode focused onto the fiber electrode tip. A feedback loop then regulates the position of the UME independent of the measured faradaic current by keeping the vibration damping at a constant value. Recently, alternative non-optical shear force based constant distance control techniques have been introduced [81]. Alternative piezoelectric shear force detection based on tuning fork or a system containing two piezoelectric plates have been integrated into SECM for distance control. Applying the constant distance mode based on shear force detection also allows positioning of nanoelectrodes and non-amperometric UMEs.

2.2.1.3 Combined AFM-SECM

Recently, smart combination of scanning probe microscopy techniques has been described in literature overcoming some of the limitations discussed in the previous chapters of this thesis. For example, AFM provides only limited chemical information, whereas SECM still can not compete with the lateral resolution obtained by STM and AFM. Merging complementary techniques is a promising approach of overcoming these limitations. Combinations of SECM and STM [82, 83], SECM and NSOM [84, 85], and SICM and NSOM [86] have been reported in literature. Due to relevance for the presented work, this chapter will exclusively focus on the combination of AFM with SECM, and the development of scanning electrochemical micro- and nanobiosensors. By merging the principle of SECM with the technology of AFM, simultaneous imaging of topography and electrochemical reactivity at surfaces and interfaces can be achieved.

Recently, two approaches combining AFM and SECM have been realized. Macpherson et al [87-89] fabricated bent Pt wire nanoelectrodes, which are shaped like AFM cantilevers and insulated except for the very tip of the wire. Although high lateral resolution in SECM can be achieved with these small tips, usually the simultaneous measurement of topography and electrochemistry is restricted to contact mode imaging of robust, non-conductive samples. Non-contact mode imaging can be used for conductive samples operating in the lift mode of AFM. In lift mode, the topography is imaged within a first scan and the recorded data is subsequently used to maintain a constant distance between the tip and the surface. After the tip is “lifted” from the surface the electrochemical data are recorded in a second scan. To date, imaging in AFM dynamic mode has not been reported with these combined probes due to the variation of spring constants of these hand made tips [37].

The second approach is based on the integration of submicro- and nanoelectrodes into scanning probe cantilevers by microfabrication and 3-dimensional focused ion beam milling, and was first introduced by Kranz et al. [90] in 2001. Commercially available silicon nitride AFM probes are sputtered with a layer of conductive material (mainly Au or Pt) and subsequently insulated with silicon nitride by plasma enhanced chemical vapor deposition (PECVD). Alternatively, Parylene C is used for insulation deposited by chemical vapor polymerization (CVP). Focused ion beam technology (FIB), frequently used as maskless micro- and nanofabrication tool in semiconductor industries [91], is applied to reproducible expose an electroactive area recessed from the apex of the insulating AFM tip [92]. The length of the AFM tip is correlated to the dimensions of the integrated electrode to ensure an optimum working distance between electrode and sample surface. High resolution AFM imaging is achieved by re-shaping the AFM tip via FIB milling. Frame-, ring- or disk-shaped electrodes can be integrated into AFM tips based on this technology with sizes down to 100 nm so far achieved for tip-integrated disk electrodes [93]. Figure 2.5 shows images of an integrated AFM tip prior and after FIB milling.

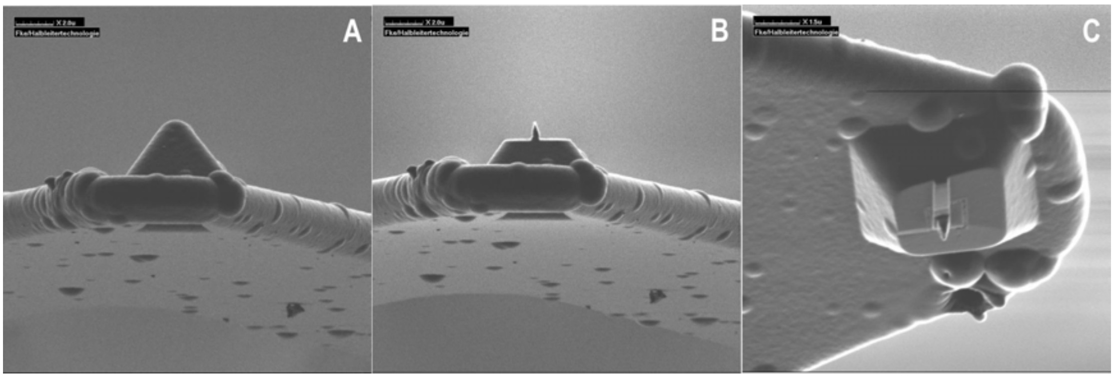

Figure 2.5 Modified AFM cantilever prior (A) and after (B, C) the FIB microstructuring process. The integrated electrode as well as the reshaped AFM tip can be clearly seen (height of the reshaped AFM tip 450 nm, edge length of the frame electrode 960 nm).

As the reshaped AFM tip acts as a spacer between the sample and the electrode, a fixed tip to sample distance can be maintained throughout the entire measurement. Hence, non-amperometric probes such as integrated biosensors or potentiometric microelectrodes can be positioned at an exactly defined distance from the sample surface. Simultaneously recorded AFM and SECM images of both conductive and insulating samples can be obtained in contact and dynamic mode operation of AFM [94]. The resonance frequency of the modified cantilever remains virtually unaltered and the resulting amplitude of the tip does not significantly disturb the electrochemical current response of the sub-micrometer-sized electrode [94]. Hence, these combined microfabricated AFM-SECM probes can be applied to a variety of interfacial problems ranging from biological/biomedical applications to material characterization and surface modification. Especially in the biological and biomedical field, combined AFM-SECM promises to become a powerful and versatile tool, as many biological processes induce structural changes in combination with electrochemical signals [93]. As an example, simultaneously obtained topographical and electrochemical information on enzyme activity in contact mode AFM and GC mode SECM [95] and in dynamic mode and GC mode SECM have recently been reported [93].

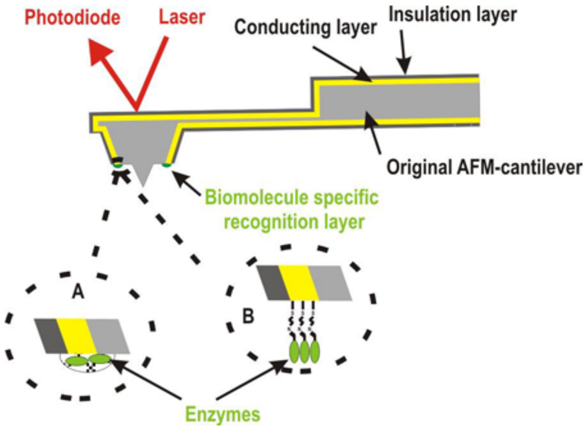

Figure 2.6: Scheme of an AFM tip integrated biosensor. Immobilization of the enzyme over entrapment in a polymer matrix (A) and crosslinking with glutaraldehyde to a SAM system (B).

Furthermore, this concept can be extended to electrochemical micro- and nanobiosensors integrated into bifunctional scanning probes, which enables precise positioning of miniaturized biosensors in close proximity of the sample surface. Well established surface modification processes for biosensors can be adapted to immobilize biological recognition elements at the surface of the integrated electrode. Techniques adressing the electroactive area are especially favorable for site specific modification. pH shift induced deposition of polymer films and SAM modification of electrodes are therefore of particular interest (see Figure 2.6). Deposition of the enzyme at the electrode surface enables highly specific detection of analyte molecules generated at the sample surface. Hence, surface topography and localized generation of biologically relevant analytes can be mapped simultaneously, enabling for the first time sufficient spatial and temporal resolution for the investigation of cellular processes. Besides monitoring of localized events at individual reaction sites, measurements with AFM tip integrated biosensors combined with appropriate theoretical considerations are promising concepts for the quantification of bioprocess kinetics.

Here it should be noted that the integration of microsensors into AFM-SECM tips is not limited to the amperometric biosensors discussed in this thesis, but also the integration of potentiometric sensors, such as pH electrodes, is feasible with this technology [37].

2.2.2 Electrochemical techniques for fabrication and characterization of biosensors

2.2.2.1 Pulsed electrochemical deposition

Electrochemical polymerization is an attractive immobilization technique for the entrapment of enzymes into polymer films addressing the electroactive area with site specificity. Traditional electrochemical techniques for the formation of polymer films including galvanostatic, potentiostatic or multi sweep deposition procedures have limitations mostly attributed to the diffusion of monomers/oligomers often leading to poor polymer film formation. By developing a pulsed technique for the electrochemical deposition of polymer films at electrode surfaces Schuhmann et al [96] reported an attractive alternative overcoming problems occurring for conventional deposition methods. In principle, this method can be applied to any electrochemically induced polymerization such as the formation of conducting polymers and pH shift induced polymer deposition.

The formation of polymer films at electrode surfaces can be envisaged as the result of several consecutive steps including the diffusion based mass transport of the monomer to the electrode surface, the oxidation/reduction of monomers (for conductive polymers) or water oxidation (for pH shift induced polymer films) at the suitable potential, formation of oligomers, reduction/oxidation of the formed oligomers, chain propagation and - upon passing a polymer specific solubility limit - precipitation at the electrode surface. However, these steps are strongly correlated to and influenced by the experimental conditions (e.g. concentration of monomer/oligomer, potential, pH changes, solvent, etc.), thus rendering electrochemical polymerization a highly complex and difficult to control process.

The main problem occurring with classical electrochemical methods is the diffusion behavior of monomers and oligomers influencing the concentration profiles and, therefore, the probability for chain propagation and polymer formation. During pulse deposition, diffusional mass transport to/from the electrode surface is optimized. Either the potential or the current (potentiostatic or galvanostatic pulse method) is instantaneously changed. If the conductivity of the formed polymer is low, the resistance of the film increases with the thickness of the deposited matrix leading to an additional potential drop when a constant potential is applied. However, in this case the galvanostatic approach allows compensation of the potential drop as the potential will be automatically increased to allow the predefined current to flow.

In the case of pH shift induced polymerization of biomolecule containing films, a potentiostatic triple pulse deposition protocol was established [20]. For a predefined, short period of time a potential is applied to oxidize water, followed by a period with an intermediate potential and a period at a potential, where no reaction occurs. The time period for the latter step has to be selected long enough to allow reestablishing the bulk concentrations of the monomers and the biological recognition element in vicinity of the electrode prior to a possible next deposition cycle. Depending on the desired film thickness repeated cycles can be applied.

2.2.2.2 Cyclic voltammetry

Cyclic voltammetry is a routine method in the field of dynamic current measurement techniques. Various redox processes can be studied with respect to their thermodynamics and information about kinetics of electron transfer reactions can be gained.

In a cyclovoltammetric experiment the potential applied to the working electrode is linearly varied with time defined as the sweep rate ($\Delta E/\Delta t$). The potential is scanned from a start value to a maximum potential and reversed again. If the applied potential range includes the standard reaction potential of a redox active species in bulk solution, the recorded current profile is determined by the oxidation and reduction peak correlated to the applied potential. The resulting current potential curve is called cyclic voltammogram (CV). Figure 2.7 (1) shows the linear change of potential and (2) represents a cyclic voltammogram recorded at a microelectrode. Due to the unique features of microelectrodes, the shape of the voltammogram follows a characteristic sigmoidal curve, in contrast to the peak shaped CVs obtained at macroelectrodes.

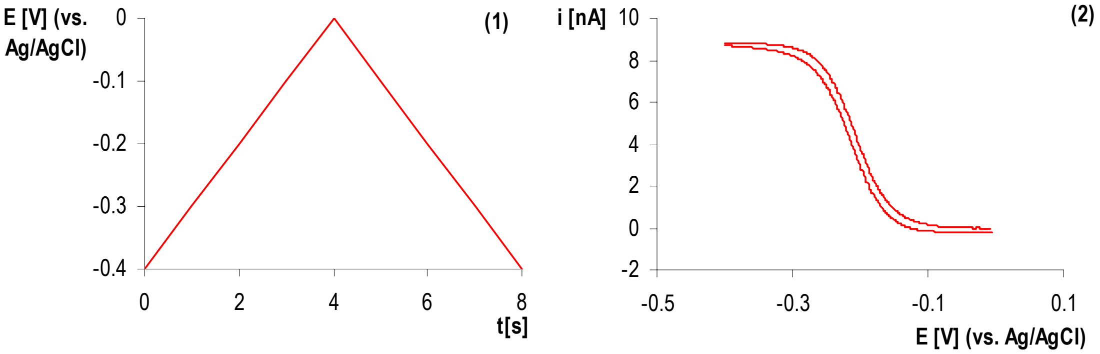

Figure 2.7: (1) Linear potential sweep applied during a cyclovoltammetric experiment (1 cycle). (2) Resulting characteristic sigmoidal cyclic voltammogram recorded at a 10 µm Au microelectrode. Reduction of 10 mM $Cl_3Ru(NH_3)_6$ (RuHex) in 0.5 M aqueous KCL, sweep rate 0.1 V s^{-1} vs. Ag/AgCl reference electrode.

From this data, the radius of the microelectrode can be calculated following equation (1). It should be emphasized that the scan rate is of particular importance in cyclic voltammetry. The heterogeneous charge transfer across the electrode interface can be described by the Butler-Volmer equation

$$i = i_0 * \left[\exp\left(\frac{\alpha * z * F * \eta}{R * T} \right) - \exp\left(- \frac{(1-\alpha) * z * F * \eta}{R * T} \right) \right] \qquad \textbf{(4)}$$

where i_0 is the exchange current, α is the symmetry factor, z is the number of electrons transferred at the electrode, F is the Faraday constant, η is the overpotential, R is the molar gas constant and T the absolute temperature.

The overpotential η represents the deviation of the potential E from the equilibrium potential E^0 and the exchange current i_0 is defined as rate constant of electron transfer at no overpotential [97]. The rate constant (i.e. the exchange current) depends on the concentration of the species at the electrode surface, which is determined by the diffusion coefficient. Besides the heterogeneous charge transfer the mass transport has to be considered with two exceptions [98]. (i) If the standard rate constant of the charge transfer process is very high (> 10^{-1} cm s^{-1}, reversible case) the reaction and the resulting current are limited by diffusion. In this case the concentration of the species at the electrode surface only depends on the applied potential. Hence, a dynamic equilibrium is established and the Butler-Volmer equation is simplified to the Nernst equation. (ii) In contrast, a very low charge transfer rate constant (< 10^{-5} cm s^{-1}, irreversible case) is given, if the charge transfer is the reaction limiting step.

In this thesis cyclic voltammetry was applied for characterization and cleaning of microelectrodes as well as for studies on the polymer permeability.

3 Experimental

3.1 Materials

Chemicals used throughout this thesis are summarized in Table 1:

Acetic acid	100 %	Fisher Scientific (Pittsburgh, PA, USA)
Cystaminiumdihydrochloride	> 98 %	Fluka (Buchs, Switzerland)
Dinatriumhydrogenphosphate	98.5 %	Fisher Scientific (Pittsburgh, PA, USA)
D(+)-Glucosemonohydrate	≥ 99 %	Fluka (Buchs, Switzerland)
Glucose oxidase (from Aspergillus niger)	(150,000 U g^{-1}, solid)	Fluka (Buchs, Switzerland)
Glutaraldehyde	(~ 50 % in water)	Fluka (Buchs, Switzerland)
Hexachloroplatinate	min. 37.5 % Pt	Mallinckrodt (Phillipsburgh, NJ, USA)
Hexaminorutheniumchloride	98 %	Aldrich (Milwaukee, WI, USA)
Horseradish peroxidase	(987,000 U g^{-1}, solid)	Sigma-Aldrich (St Louis, WI, USA)
HPLC grade water	HPLC grade	J. T. Baker (Phillipsburgh, NJ, USA)
Hydrochloric acid	37.5 %	Fisher Scientific (Pittsburgh, PA, USA)
Hydrogenperoxide	30 % in water	J. T. Baker (Phillipsburgh, NJ, USA)
Hydroxymethylferrocene	97 %	Aldrich (Milwaukee, WI, USA)
Natriumdihydrogenphosphate monohydrate	≥ 99 %	Fluka (Buchs, Switzerland)
Potassiumchloride	puriss. p.a. > 99.5 %	Fluka (Buchs, Switzerland)
Potassiumferrocyanide	99 %	Aldrich (Milwaukee, WI, USA)
Sodium acetate	99 %	Aldrich (Milwaukee, WI, USA)
Sulfuric acid	95.8 %	J. T. Baker (Phillipsburgh, NJ, USA)

Table 1: Summary of the chemicals used in this thesis.

Unless otherwise stated, all aqueous solutions were prepared with deionized water (Millipore).

Soda lime capillaries used for the preparation of microelectrodes were purchased from Hilgenberg GmbH (Malsfeld, Germany; outer diameter 1 mm, wall thickness 0.5 mm, capillary length 10 mm) and gold microwire was obtained from Goodfellow (Huntingdon, England; diameter 25 µm and 10 µm, purity 99.99+ %, hard temper). Conductive silver epoxy (Epo-Tek H20E) was obtained from Polytec (Waldbronn, Germany) and insulating varnish (MR 8008) from Elektrolube (Wargrave, England).

Anodic electrophoretic deposition paint (EDP, Elektrodepositionslack Glassophor ZQ 8-43225, Canguard) from BASF Farben und Lacke GmbH (Muenster, Germany) was used as an immobilization matrix for enzyme entrapment.

Immobilization of the thermoresponsive microgels was performed on modified glass substrates (micro cover glasses from VWR, West Chester, PA, USA).

For measurements with bifunctional AFM probes a periodic micropattern (silicon nitride on gold, Quantifoil Micro Tools, Jena, Germany) was used as a substrate. Membranes for glucose transport measurements were bought from Osmonics Inc. (Poretics, polycarbonate membranes, pore size 200 nm, General Electric Comp., Fairfield, CT, USA).

Depending on the performed AFM measurements different AFM probes have been used. AFM contact (at ambient conditions and in liquids) and dynamic mode measurements (in liquids) were performed with Veeco NanoProbe tips (silicon nitride, gold coated, force constant: 0.06 N m^{-1}). For dynamic mode measurements in air uncoated silicon cantilevers (Nanosensors, force constant: 39-52 N m^{-1}) and for the heating experiments aluminium coated silicon cantilevers (µ-Masch, CSC38/AlBS, force constant: 0.01-0.08 N m^{-1}) were used.

3.2 Instrumentation

For electroanalytical measurements (cyclic voltammetry and constant potential amperometry) two different potentiostats were used (electrochemical workstation CHI 660A, CH Instruments, Austin, TX, USA, and Jaissle Bi-Potentiostat PG 100, Waldbronn, Germany). Measurements that required recording of currents in the sub-nanoampere range were shielded with a faraday cage (CH Instruments, Austin, TX, USA, and Warner Instruments, Hamden, CT, USA). The FIA system for the automated glucose calibrations was purchased from FIAlab (FIAlab-3500, Bellevue, WA, USA).

Atomic force microscopy was performed with a PicoPlus SPM system (Molecular Imaging, Tempe, AZ, USA) using the large multipurpose scanner (maximum scan range: 100*100 µm). A major advantage for many applications such as experiments with a heated sample stage or electrochemical experiments is a “top down configuration” of the AFM scanner (see Figure 3.1). The AFM cantilever is mounted onto the piezoelectric scanner and moved across the sample surface.

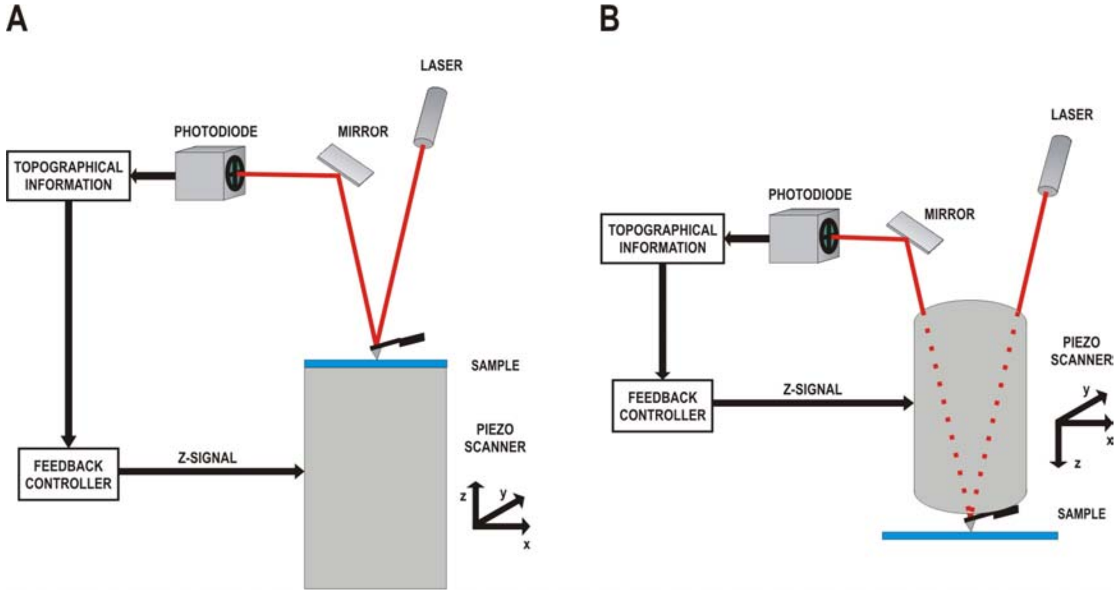

Figure 3.1: Comparison between the two most common piezo scanner configurations. (A) The sample is scanned in respect to the tip. (B) The tip is scanned at the sample (top down configuration). The system applied in studies of this thesis (MI PicoPlus SPM system) is based on design B.

During heating experiments investigating temperature responsive hydrogels the AFM was combined with a temperature stage (hot MAC sample stage, Molecular Imaging, Tempe, AZ, USA) and the temperature was adjusted by a temperature controller (Lake Shore, 321 Autotuning Temperature Controller, Westerville, OH, USA). AFM image processing was performed with the Molecular Imaging (MI) PicoScan 5.3. software. Additionally, further optimization of the obtained hydrogel images in respect to tip artifacts in deswollen condition (SPIP software, version 2.3206., from Image Metrology, Lyngby, Denmark) was attempted. However, according to personal communication with the developers at SPIP unfortunately, this software is not suitable for tip deconvolution on images of very soft samples. Hence, as clearly seen in the obtained images, due to the sudden change in height and stiffness, most images show tip-related artifacts.

Optical characterization of samples at various stages during this work was done with an optical microscope (BX 41, Olympus, Melville, NY, USA).

3.3 Fabrication of glucose microbiosensors

3.3.1 Ultramicroelectrode (UME) preparation

The preparation of UMEs will be discussed in a brief section as excellent reviews on the preparation of UMEs can be found in literature [61, 62, 99]. Disk electrodes are among the most intensively studied electrode types with respect to their theoretical and experimental behavior and are comparatively easy to prepare. Au disk microelectrodes were prepared by encapsulating gold wires (25 µm and 10 µm diameter) into soda lime glass capillaries. Following preparation protocol was followed:

Soda lime glass capillaries were cut into pieces with a length of approx. 4 cm and sealed on one end with a Bunsen burner. Then a section of Au wire (25 µm or 10 µm in diameter) with a length of approx. 1 cm was inserted into the capillary. The capillary was placed into a home made sealing setup schematically shown in Figure 3.2.

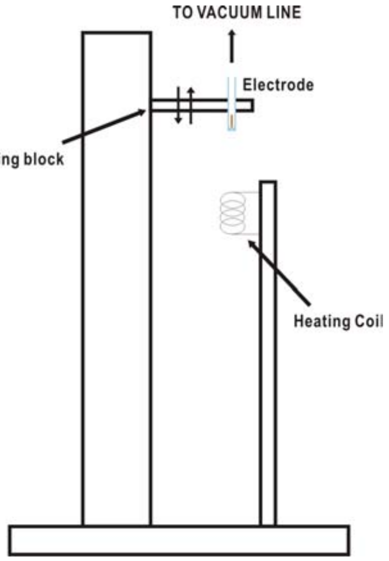

Figure 3.2: Scheme of home built electrode sealing setup (not to scale). After being adjusted to the correct (x, y) position (centered above the coil), the positioning block can be moved vertically by a micromanipulator to position the electrode within the heating coil, while vacuum is applied to the open end of the capillary.

The positioning block can be moved in the z direction by a micromanipulator. In a first step, the capillary containing the Au microwire was lowered until the encapsulated end of the capillary reached the upper part of the heating coil in order to soften the soda lime glass. At this point the open end of the capillary can be connected to a vacuum line without pulling out the microwire. The capillary was lowered further and approximately half of the wire was sealed in. After half of the wire was sealed into the glass, the positioning block was moved up again and the current supply was switched off allowing the setup to cool down. The sealed capillaries were inspected under an optical microscope to ensure there were no air bubbles.

To expose a disk-shaped electroactive area, the capillary was grinded with successive grades of silicon carbide grinding paper (1200 and 2400 grit) and then successively polished with diamond paste (6 µm, 3 µm, 1 µm and 0.05 µm particle size) until a scratch free mirror-like surface was obtained. Electrodes for SECM experiments were subsequently grinded to a conical shape of the insulation glass ensuring a RG value of approximately 10.

Electrical connection of the Au wire at the opposite end was obtained by connecting to a copper wire via silver epoxy. After curing the silver epoxy at around 70 to 80 °C, the open end of the electrodes was sealed with insulating varnish.

Prior to electrochemical characterization, the prepared electrodes were thoroughly cleaned. Remains of the polishing paste were removed by ultrasonication in deionized water for 15 min. After dipping into piranha solution (3 parts of H_2SO_4 and 1 part H_2O_2) for 10 – 30 min, the electrodes were cycled in degassed 0.5 M H_2SO_4. The applied parameters are listed in Table 2. A $Hg/HgSO_4$ reference electrode and Pt counter electrode were used:

Technique	**Initial potential [V]**	**Final potential [V]**	**Comment**
Cyclic voltammetry	-0.81	2	1 cycle @ 0.1 V s^{-1}
Cyclic voltammetry	-0.61	1	10 cycles @ 0.1 V s^{-1}
Amperometry	0.21	0.21	for Polarization

Table 2: Parameters for the electrochemical cleaning procedure of electrodes in 0.5 M H_2SO_4. Potentials are against $Hg/HgSO_4$ reference electrode.

3.3.2 UME characterization

The electrode radius and the sealing efficiency of the cleaned microelectrodes were determined by recording cyclic voltammograms.

Cyclic voltammetry was performed in 10 mM $Cl_3Ru(NH_3)_6$ (RuHex) in 0.5 M KCl supporting electrolyte solution. An Ag/AgCl reference and a Pt counter electrode completed the three-electrode setup. The standard reduction potential of $Ru(NH_3)_6^{3+}$ is 0.05 V vs. NHE. The potential sweep was performed from -0.4 to 0.1 V at a sweep rate of 0.1 V s^{-1}. Several cycles (typically 3 each) were recorded and the third run was used for data evaluation.

Besides electrochemical characterization, the quality of the microelectrodes and the uniformity of the electroactive area were investigated by optical microscopy. The diameter of the electroactive areas obtained from the electrochemical and the optical characterization were compared.

3.3.3 Immobilization of glucose oxidase (GOD)

Immobilization of the biological recognition element is among the most important aspects of micro- and nanobiosensor development.

Glucose oxidase was immobilized using two different approaches: pH shift induced deposition of GOD containing polymer films [20] and covalent binding via a ω-functionalized thiol/disulfide self-assembled monolayer (cystaminiumdihydrochloride) with subsequent formation of a GOD gel crosslinked with the covalently attached glutaraldehyde matrix [15, 100].

For the enzyme entrapment via polymerization, stock solutions of GOD were prepared by dissolving the enzyme (5 mg mL^{-1}) in HPLC grade water and adding a Canguard polymer suspension (70 µL mL^{-1}). The solutions were stored at 4 °C for 30 minutes prior to polymerization. Each microelectrode was freshly cleaned prior to the electropolymerization procedure. Polymer film formation was achieved by applying a potential-pulse profile (2.2 V for 0.2 s, 0.8 V for 1 s and 0 V for 5 s vs. Ag/AgCl) from 1 to up to 5 potential cycles. Most immobilization procedures were performed with one cycle (see chapter 4.1.2). Modified electrodes were rinsed with water and phosphate buffer (0.1 M, pH 7.4) and stored in cooled (4 °C) phosphate buffer until electrochemical analysis. Typically storing times of 12-24 h were used to obtain optimized current response. Long term studies revealed that enzymes need a certain recovery time after the high potential of the immobilization process is applied (further explanation can be found in chapter 4.1.2).

In a series of experiments the electrodes were platinized before pH shift induced polymerization. In reference to literature, a controlled rough surface is obtained, which provides improved adhesion of the chemisorbed polymer [96]. Platinization of the microelectrodes was performed via cyclic voltammetry in hexachloroplatinate (H_2PtCl_6)/0.1 M KCl electrolyte solution. 4 mg of hexachloroplatinate were dissolved in 10 mL of 0.1 M KCl and the solution was degassed for 20-30 minutes. Three cycles from -0.4 V to 0.5 V vs. Ag/AgCl with a linear sweep rate of 0.01 V s^{-1} were performed. Platinization was not performed on all electrodes, since no difference in the polymer adhesion at the selected experimental conditions was noticed.

Studies on the permeability of the polymer matrix were performed via cyclic voltammetry in 20 mM $Cl_3Ru(NH_3)_6$ (RuHex) solution in 0.5 M KCl supporting electrolyte. Sweep parameters were the same as for electrochemical electrode radius determination (see chapter 3.3.2).

The covalent attachment via self-assembled monolayer was obtained by following procedure: freshly cleaned microelectrodes were immersed into 1 % aqueous cystaminiumdihdrochloride solutions for 30 min and then rinsed with phosphate buffer (0.1 M, pH 7.4). Enzyme solutions were prepared by dissolving GOD in phosphate buffer (1 mg GOD/90 µL buffer) and subsequent adding 5 % aqueous glutaraldehyde (10 µL mg^{-1} GOD). After formation of the SAM monolayer, the electrodes were immersed into the enzyme solution and kept there for 2 h. Unlike the biosensors with the polymer entrapped GOD, the SAM modified enzyme electrodes were characterized immediately after deposition of the recognition layer in order to avoid loss of enzyme activity.

3.3.4 Manual glucose calibration

Glucose calibration was done by constant potential amperometry using an electrochemical cell equipped with a Pt counter electrode and an Ag/AgCl reference electrode containing 0.1 M phosphate buffer pH 7.4. Due to the obtained currents in the pA range these experiments were performed in a Faraday cage. The enzyme electrode was held at a potential of 0.6 V vs. Ag/AgCl in order to oxidize enzymatically produced hydrogen peroxide. A 0.2 M glucose stock solution (glucose in deionized water) was prepared and a calibration curve was recorded by standard addition of glucose. In between each addition, a delay time of 50-100 s was applied in order to obtain a stabilized current response prior to the next injection. After each addition of glucose the solution was stirred for approx. 5-10 s ensuring a homogeneous distribution of the substrate. During the actual current recording the stirring was stopped leading to an improved signal-to-noise ratio. However, using this approach information about the response time of the micro biosensor could not be achieved, because current recording was stopped for a certain period of time.

3.3.5 Flow injection analysis (FIA) for glucose calibration

FIA for glucose calibration of enzyme electrodes was performed with a home built FIA cell and a FIAlab-3500 system. The flow cell was optimized with respect to volume and shape preventing excessive turbulences of the flow and maintaining a homogenous concentration level throughout the cell. Figure 3.3 shows a schematic of the selected flow cell architecture (cell volume approx. 40 µL, pathlength approx. 8 mm).

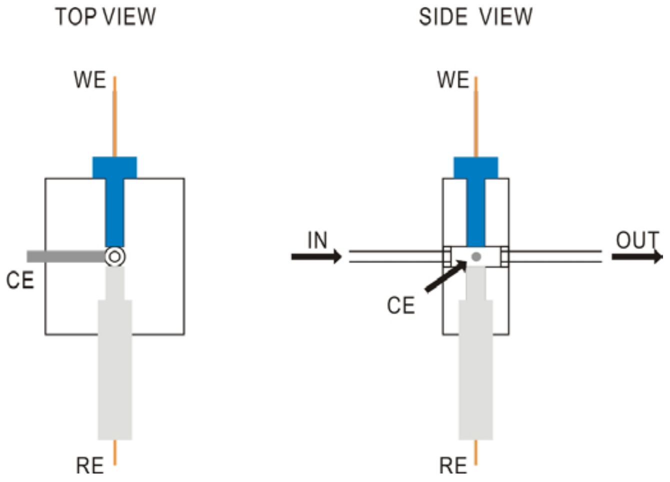

Figure 3.3: Scheme of the home built FIA flow cell (not to scale). The platinum counter electrode (CE) was glued into the plexiglas block prior to drilling the flow channel. The diameter of the flow channel was designed such that sufficient separation of the electrodes was ensured. Then the tubes were glued into the cell over small junction plugs. The Ag/AgCl reference electrode (RE) and the working electrode (WE) can be sealed into the flow cell using standard FIA fittings. Junctions between screws, electrodes and the flow cell body were sealed with a teflon tape to avoid leaking.

Prior to application of the flow cell for automated glucose calibration, preliminary studies of the cell behavior and optimization of the flow parameters for the investigated system were performed with constant potential amperometry using ferrocyanide ($Fe(CN)_6^{4+}$) solutions (10 mM, 5 mM and 2.5 mM in 0.5 M aqueous KCl as supporting electrolyte). The electrochemical flow cell housed in a faraday cage was equipped with an Ag/AgCl reference electrode, a Pt counter electrode and a polarized 10 µm Au working electrode (0.2 V vs. Ag/AgCl). 0.5 M KCl solution was used as a carrier. Different sample loop volumes were tested resulting in an optimum loop volume of 50 µL for a flow cell volume of approx. 40 µL. Due to the use of a peristaltic pump, the flow rate had an effect on the background noise. It is well known in FIA that tailing and heading effects of the respective peaks are strongly influenced by the flow rate. Concerning flow rates, an additional aspect for the glucose calibration arises: high flow rates may result in delamination of the precipitated polymer from the electrode surface. Following these considerations, the flow rate for the given setup was optimized to a value between 14 and 20 µL s^{-1} in preliminary studies.

For glucose calibrations, the working electrode (GOD microbiosensor) was biased at a potential of 0.65 V vs. Ag/AgCl to oxidize enzymatically produced hydrogen peroxide, and measurements were performed in a faraday cage. 0.1 M phosphate buffer (pH 7.4) was selected as a carrier. 10 mM glucose (glucose in buffer pH 7.4) stock solutions were used in order to prepare dilution series with different concentrations (typically 5 mM, 2 mM, 1 mM, 0.5 mM, 0.2 mM, 0.1 mM, 0.05 mM, 0.02 mM and 0.01 mM). Prior to the first sample injection a delay time was applied to stabilize the current response.

3.3.6 AFM tip integrated biosensors

To demonstrate the capability of the integrated AFM/SECM probes, simultaneous electrochemical and topographical images were recorded. Imaging height and current information in dynamic mode AFM and feedback mode of SECM was performed using a microstructured gold grating sputtered on a silicon nitride substrate (periodicity of elevated gold structures 10 µm). The bifunctional AFM tip, which was used for imaging the micropattern has an integrated electrode with a electrode edge length of 560 nm and a re-shaped tip height of 360 nm. The AFM liquid cell equipped with a three electrode setup (Ag/AgCl reference and Pt counter electrode) was used. A 30 mM ferrocyanide solution in 0.5 M KCl as supporting electrolyte was added as a quasi-reversible redox mediator for the SECM feedback experiment. Figure 3.4 shows a scheme of the experimental setup and the anticipated topography/height response. The working electrode was biased at a potential of 0.65 V vs. Ag/AgCl driving the oxidation of ferrocyanide to ferricyanide.

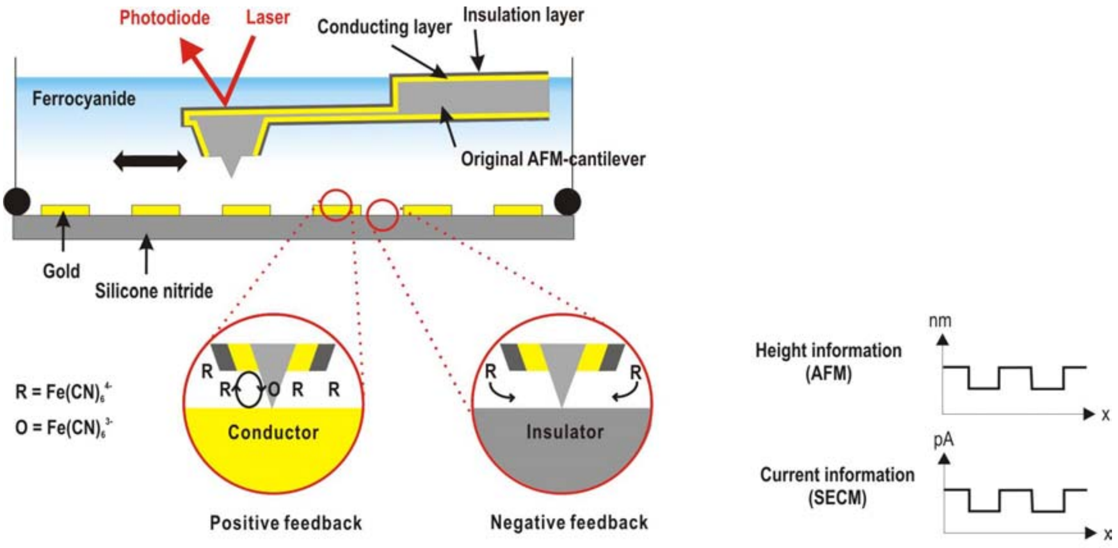

Figure 3.4: Experimental setup for simultaneous measurement of topography and electrochemical properties using a bifunctional AFM tip. When the tip is scanned in close proximity across the conductive gold grating positive feedback occurs, as shown in the proposed topography and current response scheme. In contrast negative feedback is observed over the insulating silicon nitride region.

Prior to the engagement of the integrated tip, the diffusion limited steady state faradaic current is measured at the integrated electrode. When the bifunctional probe is engaged the distance between the electrode and the sample is determined by the re-shaped AFM tip, which is usually half of the electrode edge length to ensure an optimum working distance for the electrochemical measurement. At this distance, the current recorded at the electrode is influenced by the topological features and nature of the sample surface. The conductive gold gratings enable recycling of the redox mediator (reduction of ferricyanide to ferrocyanide) leading to an increased current (positive feedback) compared to the steady state faradaic current in bulk solution, whereas the insulating silicon nitride areas are blocking the diffusion towards the integrated microelectrode inducing a decrease of the current (negative feedback).

To demonstrate the feasibility of the previously on microelectrodes studied enzyme immobilization techniques, two different types ob tip integrated biosensors were prepared.

Covalent attachment of horseradish peroxidase via cystaminiumdihydrochloride based self-assembled monolayers and glutaraldehyde as crosslinking agent was used for the development of a hydrogen peroxide sensor and previously developed polymer entrapment of glucose oxidase, which was recently applied in the host research group [101], for miniaturization of a glucose biosensor. For the covalent approach the bifunctional AFM tips were immersed into 0.1 M cystaminiumdihdrochloride (in acetate buffer, 0.1 M, pH 5.5) for 30 min. After rinsing the sample 5 times with acetate buffer the peroxidase (1 mg peroxidase in 100 µl phosphate buffer (pH 7.0), containing 2.5 % (v/v) glutaraldehyde) was immobilized onto the integrated electrode for 2 h. After thoroughly rinsing the sample with buffer solution several times the sample was stored at 4 °C until analysis.

The AFM tip integrated biosensor was studied using a periodic micropattern (silicon nitride on gold, Quantifoil Micro Tools, Jena, Germany) exhibiting a micropattern with 1 µm gold spots. Generation/collection (TG/SC) mode of SECM and contact mode AFM were used for simultaneous detection of enzyme activity and AFM topography. Images were recorded in 2 mM hydroxymethylferrocene (FMA) as electron donator, in phosphate buffer (0.1 M, pH 7/0.1 M KCl). Hydrogen peroxide (0.5 mM) was added, serving as substrate of the enzymatic conversion. The tip was held at a potential of 0.05 V vs. Ag/AgCl. Figure 3.5 (A) shows a scheme of the experimental setup, (B) shows the involved reactions, which will be further discussed in chapter 4.1.3.

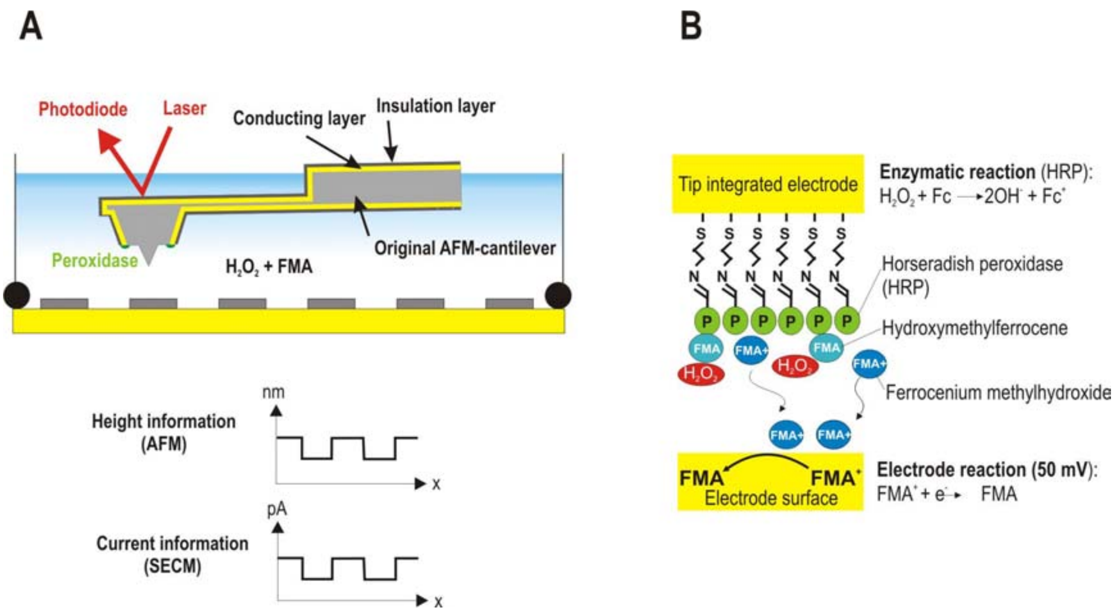

Figure 3.5: (A) Scheme of the tip generation/substrate collection experiment involving simultaneous detection of tip integrated enzyme activity and AFM topography. The current measured at the sample, which serves as a interconnected microelectrode array, reflects the enzyme activity integrated into the AFM tip. An enhanced current response can be detected in close proximity above the gold spots due to the reaction scheme presented in (B).

By using the approach via pH shift induced polymer entrapment an AFM tip integrated glucose biosensor was prepared. Polymerization was performed using the same conditions as previously described in chapter 3.3.3 for the fabrication of the glucose micro biosensors. Similar to the microelectrode modification, 1 deposition cycle was used for enzyme entrapment in the polymer suspension. The biosensor was stored in phosphate buffer (0.1 M, pH 7.4) at 4 °C for two hours prior to use.

The biosensor was used to study glucose diffusion from the pores of a track-etched membrane (polycarbonate, pore diameter 220 nm). Two different sensing approaches were realized: detection of glucose via (i) the oxidation of hydrogen peroxide and (ii) the reduction of ferrocenemethanol in combination with HRP. The involved reactions will be explained in detail in chapter 4.1.3. The lower compartment (under the membrane) contained a 50 mM solution of glucose. For the first approach phosphate buffer (0.1 M, pH 7.4) was filled in the upper compartment, and the tip was biased at a potential of 0.65 V vs. Ag/AgCl. For the latter approach 0.5 mL of peroxidase solution (4 mg horseradish peroxidase/1 mL 0.1 M phosphate buffer pH 7.0) and 0.5 mL of a solution of 2 mM hydroxymethylferrocene were mixed together and filled to the upper compartment. The tip was biased at a potential of 0.05 V vs. Ag/AgCl.

3.4 Thermoresponsive hydrogel microparticles

3.4.1 Microgel synthesis and immobilization

Microgel samples were obtained from a collaboration with the research group of Dr. Andrew Lyon (Research Group on Soft Materials Chemistry and Physics, School of Chemistry and Biochemistry, Georgia Institute of Technology). In the following, only the immobilization procedure is discussed in more detail, as the sample behavior strongly depends on the immobilization technique and procedure.

The microgels were composed of 88.6 % N-isopropylacrylamide (NIPAM), 10 % acrylic acid (AAc) and 1.4 % N,N'-methylene(bisacrylamide) (BIS), and were synthesized via surfactant free, aqueous free-radical precipitation polymerization, following a previously established protocol [25, 33].

For immobilization of the particles, functionalized gold substrates were prepared. Thin circular glass cover slips (micro cover glasses, VWR) were cleaned in Ar plasma (for a period of ≥ 20 min) and subsequently exposed to a 3-mercaptopropyltrimethoxysilane (1 %) in pure ethanol) solution for two hours. After silanization, the substrates were dried. A 50 nm thick gold film was evaporated (Au purity 99.999 %) using a thermal evaporator under low pressure. Surface functionalization was done by soaking the slides for 24 h in a 1 mM (95 % ethanol) 2-mercaptoethylamine solution. After rinsing with ethanol, the slides were stored in ethanol prior to microgel deposition, which was usually performed the next day.

Throughout this work, hydrogel particles deposited via two different approaches were investigated (electrostatic adhesion and covalent binding). A suitable particle distribution at the substrate surface was important for subsequent AFM experiments. The particle density is directly influenced by the concentration of the deposition solution and the exposure time. Several trials followed by investigations with optical microscopy and AFM led to a surface coverage optimized for the envisaged AFM experiments (see Figure 3.6).

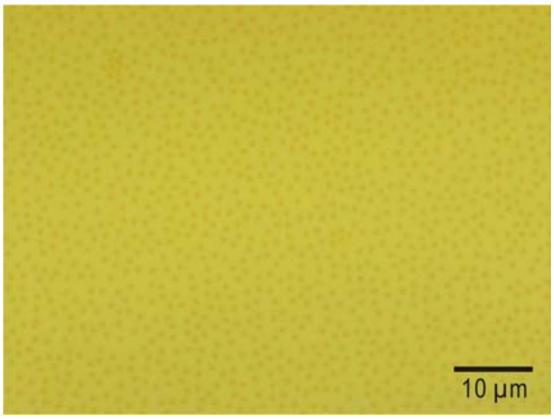

Figure 3.6 100 fold magnification of electrostatic bound hydrogel microparticles on gold in the deswollen state. Estimated surface coverage 30-50 %.

For electrostatic binding the surface was functionalized by 2-mercaptoethylamine leading to a positively charged surface, while the acrylic acid co-monomers provide the hydrogel network with negative charges. The substrates were removed from the ethanol, rinsed with deionized water and dried under nitrogen stream prior to immobilization. A droplet of 10 % microgel solution (v/v in deionized water) was deposited at the substrate surface. After 10 min the sample was rinsed with deionized water and dried in a gentle N_2 stream.

For covalent attachment of the hydrogel particles to the surface, the same modification protocol for the gold substrates was applied. The concentrated microgel solution was diluted to 10 % (in phosphate buffer, pH 4.7) and an equivalent of 35 mM 1-ethyl-3-(3-dimethylaminopropyl)carbodiimid hydrochloride (EDC) was added. Immediately afterwards, the rinsed (deionized water) and dried (N_2 stream) substrates were submersed into the solution. The surface was exposed to the hydrogel solution over night under constant shaking. Then the cover slips were removed, rinsed with water and dried under a N_2 stream.

3.4.2 AFM imaging of hydrogel microparticles

Prior to investigations of the temperature responsive behavior of isolated hydrogel microspheres, several preliminary experiments were performed.

AFM studies of the samples at ambient conditions were usually performed in AFM contact mode (silicon nitride cantilevers with gold coating). The MI liquid cell was used for first imaging experiments in buffered solutions and AFM contact and dynamic mode measurements were performed. For the temperature controlled deswelling experiments (see chapter 3.4.3), imaging was only possible in AFM dynamic mode due to the very soft particle surfaces.

In a first set of experiments, the swelling behavior was investigated using the AFM flow cell. After recording an image at ambient conditions (contact mode AFM), the tip was withdrawn from the surface (10 µm) and distilled water was added. As rapid as possible the laser was readjusted and the tip was again approached towards the surface. Typically, approx. 2-3 min after adding water the first AFM images could be recorded. Here the goal was more to depict as many pictures as possible as to get optimized image quality. Therefore, comparatively high scan rates were selected (approx. 1.5-3 Hz). Imaging was restricted to contact mode operation since dynamic mode imaging requires slower scan rates.

Another important aspect of these studies was to investigate possible correlations of the applied forces on the particle height in both ambient and liquid conditions. For this purpose, several sample areas were imaged while changing the applied force, either via the force setpoint (contact mode) or the amplitude setpoint (dynamic mode). The particle shape in liquid conditions (pH 3, HCl solution) was found to be highly dependent on the applied force (see chapter 4.2.1).

3.4.3 In-situ AFM studies on temperature responsive deswelling of hydrogel microparticles

Due to the strong dependence of the particle size and shape on the applied force, the experimental parameters have to be carefully selected and controlled. Next to the experimental settings, the force applied to the microparticles is dependent on additional aspects such as e.g. the stability of the investigated sample area, individual hydrogel to substrate binding strengths and the exact characteristics of the AFM tip (e.g. exact force constant, etc.). Given these uncertainties, the height values obtained during AFM investigations at soft surfaces are considered to be relative values, although, an average range can be determined. Hence, in order to at least semi-quantitatively compare the shapes of the particles prior to and after the VPT, it is necessary to carefully control the applied forces.

Considering these aspects following procedure was applied: after optimization of all parameters prior to approaching the tip to the sample surface, the tip was continuously held at the surface during an entire heating cycle. This experimental approach enabled obtaining the variation of the height values during an entire temperature sweep resulting in one set of data allowing to compare the retrieved height information. During the experiment the parameters were not changed, however, small changes of the effective parameters due to the natural drift of the scanner and due to the temperature change were regarded as negligible. Therefore data for one temperature sweep could be compared and evaluated. However, series obtained within different temperature experiments recorded with different AFM tips can not be compared.

All temperature controlled deswelling experiments were performed with dynamic mode AFM in pH 3 (distilled water with HCl) solution. Aluminium coated silicon AFM tips were selected for in-situ studies on the temperature responsive behavior of the hydrogels, since back-side gold coated silicon nitride cantilevers showed strong drifting behavior during temperature cycling. The temperature was varied in a range of 25 to 33 °C, with a typical temperature ramp of 0.5 °C min^{-1}. Most images were recorded while changing the temperature in increments of 1 °C, while the tip was permanently scanned across the sample surface. Images were recorded after tempering the sample at the respective temperature. In a separate set of experiments, the tip was held at the sample surface without scanning during the incremental increase of the temperature and images were discontinuously recorded at 25, 26, 27, 28 and 29 °C each, or at 25 and 30 °C (i.e. prior to and after VPT) only. Further details on the variations of these experiments are described in chapter 4.2.2 and directly related to the obtained results.

Table 3 summarizes the parameters that were applied during typical in-situ AFM experiments.

Resonant frequency [kHz]	**Free amplitude**	**Amplitude setpoint**	**Integral servo gain**	**Proportional servo gain**	**Scan speed [Hz]**
31-34	~8	7-4	0.08-0.14	0.07—0.16	0.5-0.8

Table 3: Average range for parameters applied during typical in-situ AFM experiments of temperature responsive deswelling of hydrogel particles.

4 Results and discussion

4.1 Glucose biosensor

4.1.1 Characterization of UMEs

Referring to chapter 2.2.1.2 the radius of a microelectrode can be determined using equation (1) based on the diffusion limited steady state current measured under well characterized experimental conditions [73]. Typically, cyclic voltammograms are recorded at the microelectrodes in order to obtain the diffusion-limited plateau current (difference of the current between the reduced and oxidized state of the redox couple) [62]. Transformation of equation (3) leads to equation (5):

$$r = \frac{i_{dif}}{4 * n * F * D * c} \tag{5}$$

where r is the electrode (disk) radius, i_{dif} the diffusion limited plateau current, n the number of electrons transferred at the electrode, F the Faraday constant, D the diffusion coefficient and c the concentration of the redox species.

Redox mediators with rapid heterogeneous electron transfer rates are chosen for electrode characterization [62]. Two redox reactions were used for electrochemical measurements presented in this work: the oxidation of ferrocyanide (E^0 = 0.36 V vs. NHE, in aqueous solution)

$$Fe(CN)_6^{4-} \rightarrow Fe(CN)_6^{3-} + e^-$$

and the reduction of ruthenium hexamine chloride ($Ru(NH_3)^{3+}$) (E^0 = 0.05 V vs. NHE, in aqueous solution)

$$Ru(NH_3)_6^{3+} + e^- \rightarrow Ru(NH_3)_6^{2+}$$

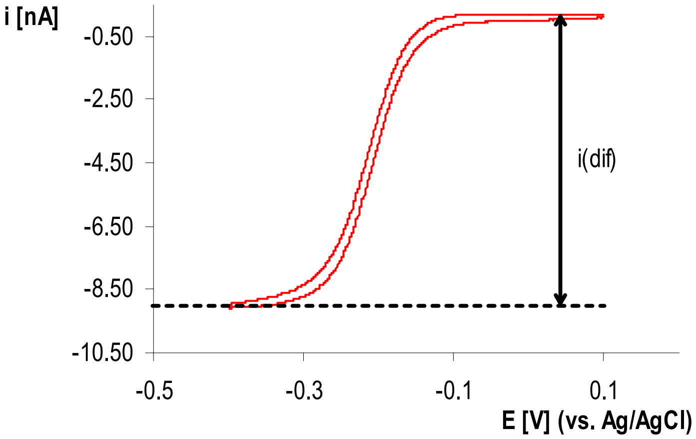

Figure 4.1: Cyclic voltammogram recorded at a 10 µm Au microelectrode in 10 mM RuHex solution (in 0.5 M aqueous KCl as supporting electrolyte); sweep rate: 0.1 V s^{-1}. The diffusion limited plateau current $i_{(dif)}$ is marked with an arrow.

Figure 4.1 shows a typical cyclic voltammogram obtained at a 10 µm Au microelectrode as a representative example. The redox couple used for the experiment was RuHex in a three electrode setup with an Ag/AgCl reference electrode and a Pt counter electrode.

The diffusion limited plateau current obtained from the recorded cyclic voltammogram was 9.1 nA. According to equation (3) the diameter of the electrode can be determined at 7.9 µm (for D = 6*10^{-6} cm^{2} s^{-1}). This value may deviate from the true electrode diameter. For example, recession of the electroactive area within the insulating material leads to decreased diffusion limited plateau currents. Consequently, these results in smaller calculated diameters compared to their true dimensions. SECM can be used to evaluate size and shape of microelectrodes [62]. Increased steady state current values can be attributed to cracks in between insulating material and electrode wire resulting in a determined radius larger than the true radius. Furthermore, the diffusion coefficient may vary from the literature value used for the presented calculations due to a different electrolyte concentration and deviation of the actual temperature. However, the diffusion coefficient was not determined at this stage of the presented thesis even though minor deviations from the literature value to the effective diffusion coefficient may have a significant impact on the calculated dimension.

Instead, in order to verify the electrochemically determined electrode diameters, optical microscopy was used for microelectrode characterization, in respect to e.g. surface roughness, geometry and size of the electroactive area.

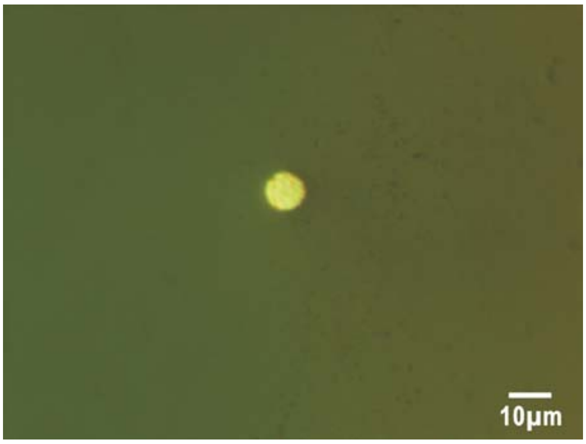

Figure 4.2: Top view of Au microelectrode (50-fold optical magnification). From this image the electrode diameter was determined to be 9.45 µm. The surface of the electroactive area and the insulating material appear very uniform.

Figure 4.2 depicts the top view (50-fold magnification) of a 10 µm Au electrode (same electrode was used for recording cyclic voltammograms shown in Figure 4.1). The electrode surface looks uniform and the electrode diameter was optically determined to be 9.45 µm.

Table 4 summarizes calculated average diameters and standard deviations for all prepared electrodes (n = 25):

Determination	**Average diameter [µm]**	**Standard deviation [µm]**
Electrochemical	8.88	2.26
Optical	8.86	0.56

Table 4: Average electrode diameters and standard deviation for all prepared electrodes.

On average, the electrochemical and optical radius correlates very well. However, the obtained values are smaller than the nominal diameter of the used microwire. The higher standard deviation for the electrochemical determination of the electrode radius may be attributed to imperfections during electrode preparation, which may not be detectable by the optical method, and deviations of the diffusion coefficient and experimental parameters. Additionally and as indicated previously, these preparation and determination artifacts may lead to a decreased electrochemical diameter. Deviating optical diameters are attributed to non-planar alignment of the electrodes during optical microscopy. Minor tilts of the electrodes have an impact on the derived electrode dimensions.

4.1.2 Characterization of microelectrode based glucose biosensors

Glucose oxidase (GOD) is an oxidoreductase containing flavin adenine dinucleotide (FAD) as active site. GOD catalyzes the oxidation of β-D-glucose to δ-gluconolactone using oxygen as electron acceptor, which is reduced to H_2O_2:

$$\beta - D - glu\cos e + O_2 \rightarrow \delta - gluconolactone + H_2O_2$$

H_2O_2 is generated as a by-product of the enzymatic reaction and can be oxidized at the electrode surface. Hence, the presence of the substrate glucose results in a current response, which is proportional to the glucose concentration.

Immobilization of GOD at electrode surfaces was performed using two different approaches: (i) pH shift induced polymerization [20] to entrap the enzyme in a polymer matrix, and (ii) electrode modification with a functionalized SAM for covalent attachment of the biological component/glutaraldehyde mixture [15]. Within the presented work, enzyme entrapment was primarily obtained with the polymerization approach, since the sensitivity of polymer based biosensors is usually enhanced in comparison to covalent attachment via SAMs. Entrapment in polymer matrices, especially polymer suspensions with high water content, ensure high enzyme activity (compared to enzymes in solution) based on a high degree of rotational and translational freedom without conformational changes. However, enzyme immobilization using the covalent approach via SAM layers shows higher stability of the enzymatic biosensing layer.

For fabrication of polymer based glucose biosensors, a procedure was adapted from literature [20]. The optimized GOD stock solution composition (5 mg GOD per mL HPLC grad water and 70 µL polymer solution) published by Kurzawa et al. [20] was used without further modification.

The enzyme activity and, hence, density has a strong impact on the sensitivity of the biosensor and has to be maximized. However, if the enzyme concentration in the pre-polymerization solution exceeds certain limits, agglomeration of the protein may result leading to increased porosity and subsequent collapse or delamination of the polymer network from the electrode surface. A suitable possibility for optimizing the enzyme concentration is based on the sequential deposition of multiple polymer layers. As discussed in chapter 2.2.2.1, theoretically any number of layers can be deposited by applying repeated deposition cycles. However, the layer thickness has a strong influence on the diffusional mass transport of the substrate and reaction products. In case of the glucose biosensor, H_2O_2 has to diffuse through the polymer network to the electrode surface. Therefore, repeated deposition cycles grow thick polymer films increasing the diffusion pathway of enzymatically generated H_2O_2 towards the electrode surface and increasing the probability for loss of H_2O_2 into the bulk electrolyte solution. As a consequence, the response time of the sensor is decreased.

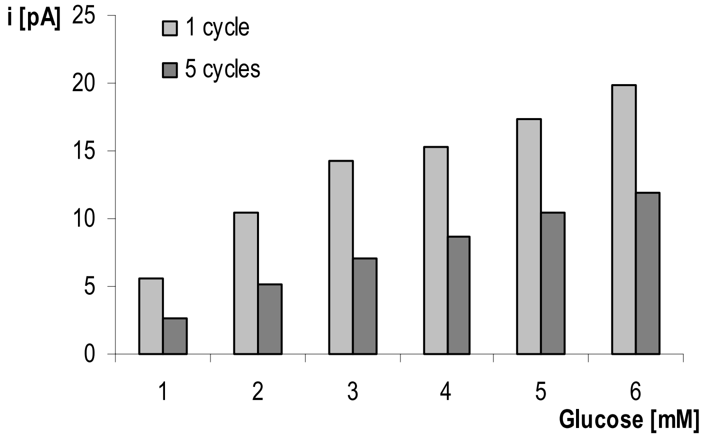

Figure 4.3: Comparison of the current response of glucose biosensors (electrode diameter = 10 µm) prepared via pH shift induced GOD entrapment upon subsequent injections of glucose (increments of 1 mM). The current response for the electrode modified with more cycles is decreased indicating partial delamination of the polymer layer due to lower mechanical stability of thicker polymer films.

In Figure 4.3, the current response of micro enzyme-electrodes (Au, diameter 10 µm) modified via pH shift induced GOD deposition (number of deposition cycles: 1 and 5, respectively) is schematically shown. Remarkable is a decreased current response for the enzyme electrode modified with 5 cycles in comparison to the current response of the biosensor based on only one polymerization cycle. Theoretically, an increase in immobilized enzyme concentration (thicker film) should lead to an enhanced current response. A possible explanation for the observed results is that the probability for (partial) delamination of the polymer is correlated with the electrode size and, hence, increased film thicknesses on micrometer-sized electrodes show an enhanced tendency for delamination, which could be confirmed by optical microscopy. Miniaturizing the developed enzyme electrode for integration into AFM/SECM tips has to deal with even smaller electroactive areas (edge length of integrated frame electrodes is typically in the range of 500 nm to 900 nm), increasing the delamination effect for multiple deposition cycles. Additionally, for simultaneous AFM/SECM imaging thick polymer films are not practicable since the length of the reshaped AFM tip may be in the range of the polymer thickness. Hence, the imaging quality of the AFM measurement would significantly decrease.

Due to these considerations, one deposition cycle was selected to be the optimal approach for miniaturized biosensors in respect to sensor sensitivity and thickness of the polymer film.
During triple pulse deposition comparatively high potentials are applied (2.2 V for 0.2 s and 0.8 V for 1 s, vs. Ag/AgCl) in order to encapsulate the fragile enzymatic component within the polymer film. Hence, the proteins need a certain recovery time before an optimum sensor response is achieved. Prior studies suggest that enzyme electrodes should be stored for at least 12 h in phosphate buffer (0.1 mol l^{-1}, pH 7.4) at 4 °C before use [20]. An enzyme electrode was tested according to its glucose response after different storage periods. Glucose calibrations were performed 2 h, 1 d and 5 d after polymerization. Figure 4.4 shows the resulting calibration plots.

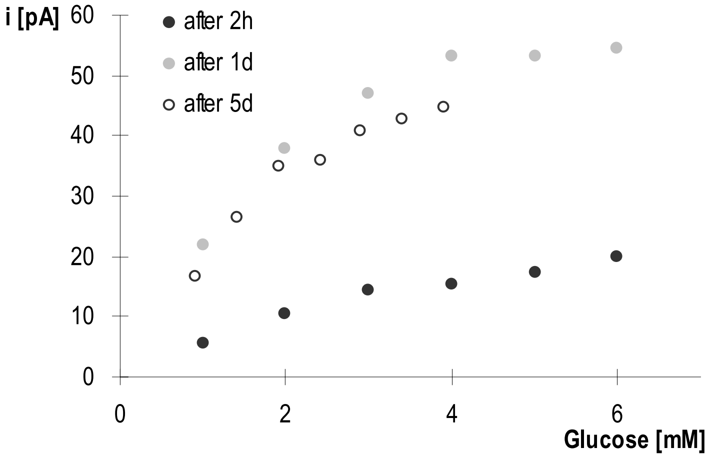

Figure 4.4: Calibration curves of a glucose biosensor after different storage periods (2 h, 1 d and 5 d). The sensor shows the highest current response after a period of 1 day which indicates that sufficient recovery time is provided for the enzymatic component. After 5 days the enzyme activity decreases. This observation is partly attributed to removal of weakly bound enzymes in the outer layers of the polymer film. Hence, hereafter enzyme electrodes were characterized after 12-24 h.

Derived from Figure 4.4 the optimum response of the biosensor was obtained after storing the enzyme electrode for one day in buffer solution at 4 °C. Apparently, after storing for two hours the ability of the enzymes for optimized conversion of glucose was not yet restored resulting in a lower current response. The decrease of the current response after extended storage periods corresponds with prior long term stability studies [20, 102]. This decrease of the current signal is partly attributed to the removal of weakly bound enzyme in the outer layers of the polymer film. In accordance with these studies, the biosensor characterization was usually performed after one day.

Sufficient permeability of the polymer matrix is a prerequisite for diffusion based transport of H_2O_2 to the electrode surface [20]. Hence, the permeability of the immobilization matrix has to be ensured. Using cyclic voltammetry the electron transfer rate of freely diffusing redox species (ferrocyanide) to an unmodified electrode was compared with the diffusion behavior to polymer modified electrodes (Figure 4.5). Differently modified electrodes were prepared by varying the number of deposition cycles leading to different polymer thicknesses (0, 1, 3 and 5 deposition cycles). As shown in Figure 4.5, the peak current derived from the oxidation of ferrocyanide is decreased with increasing number of deposition cycles corresponding to an increasing thickness of the polymer layer due to decelerated diffusion within the polymer film.

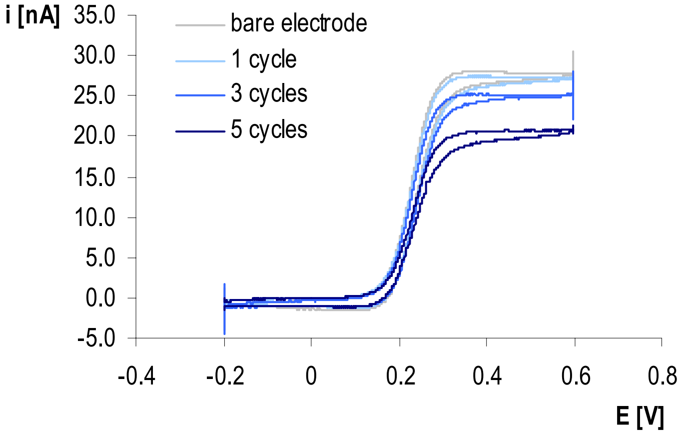

Figure 4.5: Cyclic voltammograms recorded at unmodified and modified microelectrodes in 20 mM ferrocyanide solution (in 0.5 M KCl as supporting electrolyte, vs. Ag/AgCl). A comparison of the electron transfer rate of a free diffusing species (ferrocyanide) was obtained in order to test the permeability of the polymer layer. Thin polymer layers (1 deposition cycle) do not change the diffusion behavior significantly. As expected, the impact on the peak current is enhanced with increasing thickness of the polymer layer due to decelerated diffusion within the film.

Characterization of the glucose biosensors was performed utilizing constant potential amperometry in 0.1 M phosphate buffer solution at pH 7.4. Figure 4.6 (1) depicts a typical hydrodynamic response curve of a glucose biosensor upon several subsequent injections of glucose in increments of 1 mM; (2) shows the corresponding calibration curve.

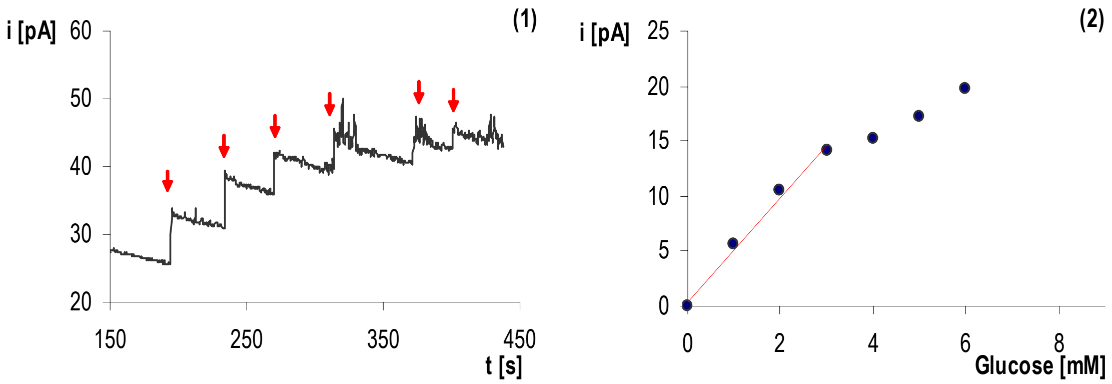

Figure 4.6: (1) Hydrodynamic response of a microbiosensor upon standard addition of glucose (6 x 1 mM) measured in phosphate buffer (0.1 M, pH 7.4) at 0.65 V vs. Ag/AgCl. The biosensor was prepared by entrapping GOD in a polymer film (one deposition cycle). Glucose injections are marked with red arrows. (2) Resulting glucose calibration curve showing linear dependency up to a concentration of ~3 mM.

Multiple enzyme microelectrodes were prepared and the obtained calibration curves were compared. The current response upon standard addition of glucose at different electrodes was found to be fairly varying, although, the same immobilization parameters and electrode dimension were used. However, as indicated in chapter 2.2.2.1 electropolymerization is a complex process strongly depending on multiple parameters such as electrode dimensions, surface roughness, cleanness, the pre-polymerization solution (e.g. exact composition, impurities, temperature, etc.) and the enzyme activity, listing just the most important factors. Considering the complexity of the process and multiple parameters influencing the enzyme entrapment, the achieved results show very good agreement. For quantifiable measurements using the proposed glucose sensor, calibration of each single sensor has to be accomplished prior to use.

Standard addition of decreased volumes of glucose led to a detection limit down to a concentration of 50 µM glucose (typical value 100-150 µM). A linear range of the calibration curve up to 3-4 mM was obtained.

Due to possible errors based on manual injections automated calibration procedures for sensor devices are preferable. Therefore, the calibration of the developed glucose microbiosensor was additionally performed in a flow injection analysis (FIA) set-up. The performance of FIA with electrochemical detection is dependent on the flow cell design and the applied parameters. Hence, prior to the effective measurements the flow cell design had to be optimized. In addition, an optimized sample loop volume (50 µL) and the flow rate (14-20 µL s^{-1}) were determined with constant potential amperometry of ferrocyanide ($Fe(CN)_6^{4+}$) solutions. The optimized parameters were the applied during glucose calibration recorded with the biosensors. Figure 4.7 shows a typical FIA injection curve and the respective calibration curve.

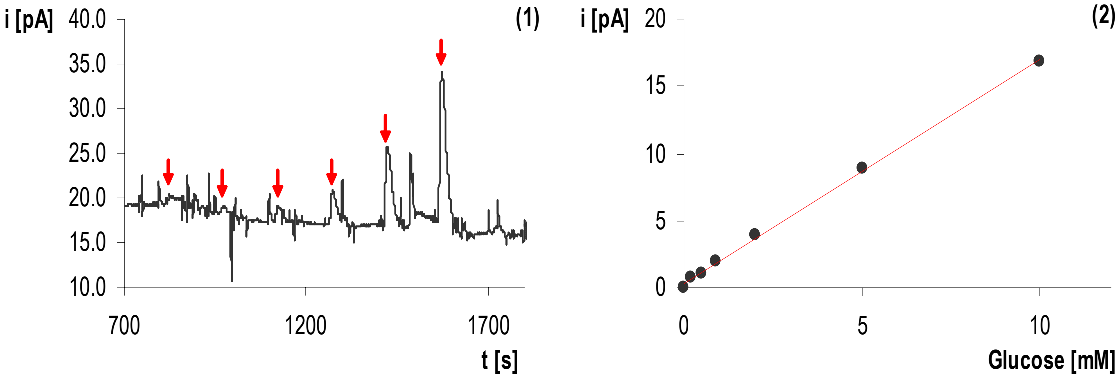

Figure 4.7: (1) FIA injection curve. Current response of polymer based glucose biosensor to several subsequent glucose flow injections (0.2, 0.5, 1, 2, 5 and 10 mM) measured in phosphate buffer (0.1 M, pH 7.4) at 0.65 V vs. Ag/AgCl. (2) Resulting glucose calibration curve showing linear correlation (R^2 = 99.9).

In these studies, a detection limit down to only 200 µM and a measurement range up to 10 mM was achieved. The pumping of the solutions with a peristaltic pump results in a fairly high background noise as shown in Figure 4.7 (1), resulting in a decreased detection limit compared to manually obtained calibration curves.

Improvement of the automated glucose calibration can be achieved by using sequential injection analysis (SIA) instead of FIA in future applications. The syringe pump used in SIA results in a steady flow and, therefore, a decreased noise. Additionally, SIA has the advantage that smaller sample volumes are accommodated, which is in particular advantageous for analysis of toxic or expensive substances.

A second approach for biosensor design based on SAM layers and covalent attachment of GOD/glutaraldehyde mixtures was investigated. Manual glucose calibrations using constant potential amperometry were performed accordingly. The respective hydrodynamic response curve and glucose calibration plot is illustrated in Figure 4.8.

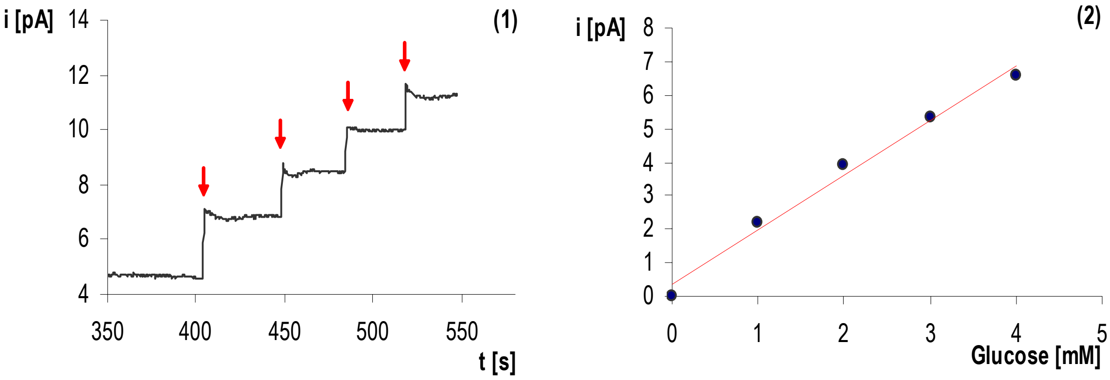

Figure 4.8: (1) Hydrodynamic response of a biosensor to glucose (4 x 1 mM) measured in phosphate buffer (pH 7.4) at 650 mV vs. Ag/AgCl. The biosensor was prepared by covalent linking of GOD/glutaraldehyde to cystaminiumdihydrochloride modified electrode surfaces. Glucose injections are marked with red arrows. (2) Resulting glucose calibration curve showing linear correlation.

As already indicated, immobilization via functionalized self-assembled monolayers generally leads to lower sensitivity of the biosensor, due to a lower enzyme concentration deposited on the electrode surface. In case of direct covalent binding, a monolayer of enzyme is immobilized at the surface. In contrast, cross-linking of the SAM and enzyme with glutaraldehyde, as it was performed throughout this thesis, rather leads to the enzyme being entrapped in a thin cross-linked network instead of an enzyme monolayer. However, the amount of enzyme deposited is decreased in comparison to entrapment in a polymer matrix. To visualize this statement, Figure 4.9 shows a comparison of the current response obtained at the polymer based biosensor and at the SAM modified enzyme electrode upon subsequent glucose addition. As expected, the sensitivity of the latter approach is significantly decreased. However, biosensors based on covalently attached SAM usually provide higher mechanical stability. Depending on the application and concentration of the analyte both approaches are of practical value.

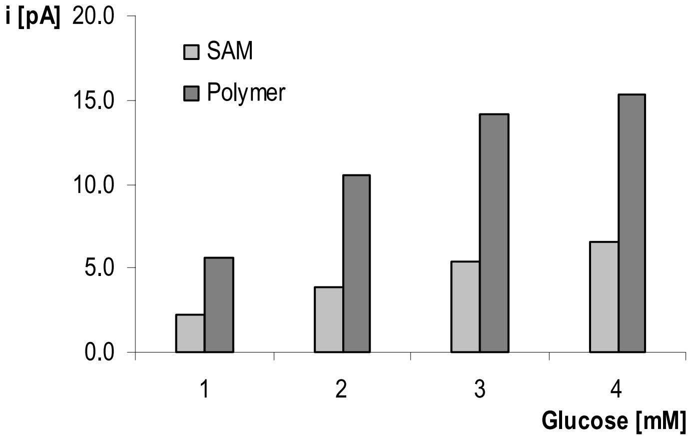

Figure 4.9: Comparison of the current response obtained at enzyme electrodes based on SAM and polymer entrapment immobilization following glucose injection (measurement in 0.1 M phosphate buffer pH 7.4 at 0.65 mV vs. Ag/AgCl). As expected from theoretical considerations, the SAM based biosensor shows a much lower sensitivity.

4.1.3 AFM tip integrated biosensors

Prior to immobilization of enzymes at the surface of the AFM tip integrated electrodes, the functionality of the bifunctional probes was studied in simultaneous SECM feedback and AFM dynamic mode experiments. A microstructured gold grating at a silicon nitride substrate was used as a model substrate.

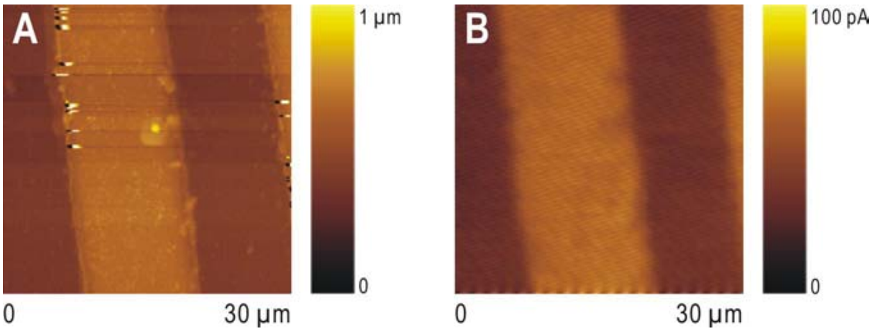

Figure 4.10: Simultaneously recorded AFM dynamic mode and SECM feedback mode measurement of a gold grating on silicon nitride. The topography recorded in dynamic mode operation of AFM (A) and the corresponding current signal (B) show excellent correlation. The images were recorded with a scan rate of 2 Hz (the redox mediator was 20 mM ferrocyanide in 0.5M KCl supporting electrolyte; E_{tip} = 0.65 V vs. Ag/AgCl).

In Figure 4.10: (A), the topography of the substrate shows elevated gold stripes with a width of 10 µm and a height of 200 nm. Figure 4.10: (B) illustrates the simultaneously recorded current information. In both images the elevated gold grating can be clearly seen. Due to positive feedback (based on the recycling of the ferricyanide at the gold feature) an increased current in comparison to the steady state current in bulk solution is obtained. The observed negative feedback over the (insulating) silicon nitride structure is based on partially blocking the hemispherical diffusion of the redox mediator towards the integrated electrode leading to a decreased current (negative feedback). A comparison of the recorded topography and electrochemical information shows excellent agreement of the obtained structures in the images demonstrating the ability of the bifunctional probes to simultaneously recorded topography and electrochemical properties.

As already discussed in previous chapters, bifunctional AFM probe design is not limited to the integration of amperometric electrodes, and can be extended to implement potentiometric electrodes or, as shown in this thesis, for the integration of electrochemical biosensors.

The presented integration of biosensors into AFM probes is an exemplary demonstration serving as basis for more sophisticated integrated sensors based on the immobilization of the biological component in a hydrogel matrix. Therefore, the development of tip-integrated biosensors was not the main objective of this thesis. However, it could be demonstrated that the proposed approach of tip-integrated biosensors is highly promising in respect to the development of imaging microbiosensors.

As a model for the AFM tip integrated biosensors based on the self-assembly approach, horseradish peroxidase (HRP) was immobilized onto the integrated gold microelectrode as previously described (see chapter 3.3.6). A tip generation/substrate collection SECM experiment involving simultaneous detection of tip integrated enzyme activity and AFM topography was performed. The electrochemical signal generation is based on the following reactions:

(1) $H_2O_2 + FMA \rightarrow 2OH^- + FMA^+$ (Enzymatic reaction catalyzed by HRP)

(2) $FMA^+ + e^- \rightarrow FMA$ (Electrode reaction, E = 0.05 V vs. Ag/AgCl)

HRP catalyzes the reduction of hydrogen peroxide, with hydroxymethylferrocene (FMA) acting as a metal organic electron, which is oxidized to ferrocinium methylhydroxide (FMA^+). The electroactive co-product FMA^+ produced in the vicinity of the enzymatic layer diffuses to the microstructured gold spots at the sample surface, which are biased at a potential of 0.05 V vs. Ag/AgCl driving the reduction of FMA^+. Hence, information on the local electrochemical activity with respect to the position of the tip-integrated biosensor is provided. Figure 4.11 shows the respective AFM and SECM images.

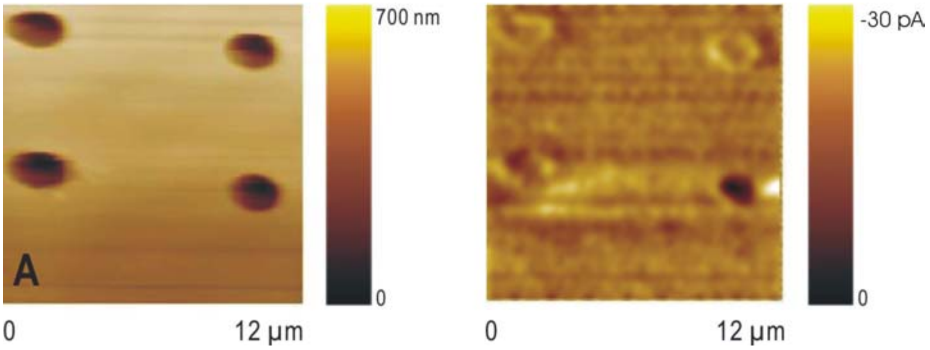

Figure 4.11: Simultaneously recorded topography (A) and tip integrated enzyme activity (B) recorded in generation/collection mode. The substrate (microstructured gold spots) is biased at a potential of 0.05 V vs. Ag/AgCl driving the reduction of FMA⁺. Although the current image is noisy, the location of the gold spots and, hence, the tip integrated enzyme activity can be clearly depicted. The images were recorded with a scan rate of 1.5 Hz.

The studies of laterally resolved glucose membrane transport by AFM tip integrated glucose biosensors involve following reactions:

(1) $\beta - D - glucose + O_2 \rightarrow \delta - gluconolactone + H_2O_2$

(Enzymatic reaction catalyzed by GOD)

(2) $H_2O_2 + FMA \rightarrow 2OH^- + FMA^+$ (Enzymatic reaction catalyzed by HRP)

(3) $FMA^+ + e^- \rightarrow FMA$ (Electrode reaction, E = 0.05 V vs. Ag/AgCl)

Glucose was detected via two different approaches. Figure 4.12 shows a scheme of the experimental setup.

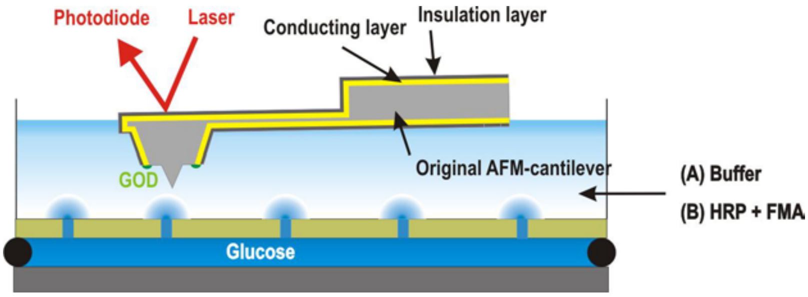

Figure 4.12: Scheme of the experimental setup for glucose membrane transport and glucose sensing. Upper compartment contains buffer (A) or HRP and FMA (B). Ideally, altered current response should be observed only over the pores of the membrane due to the electrochemical conversion of hydrogen peroxide (A) or ferrocinium methylhydroxide (B). Hydrogen peroxide results from the enzymatic conversion of glucose, FMA$^+$ in turn from two consecutive enzymatic reactions with glucose and hydrogen peroxide as the enzymatic substrates.

First, buffer solution was filled into the upper compartment, which was separated from the lower compartment with a track-etched membrane (pore size: 220 nm) containing glucose solution. GOD converts glucose into gluconolactone producing H_2O_2 as the by-product of the enzymatic conversion. The AFM tip was biased at 0.65 V in order to oxidize hydrogen peroxide. Therefore, the localized diffusion of glucose was mapped. Figure 4.13 shows the respective results. The topography of the membrane (A) can be clearly seen. Although, the current response (B) (especially in the upper part of the image) is very noisy, indications of enhanced current response above the pores can be seen in the lower part of the image.

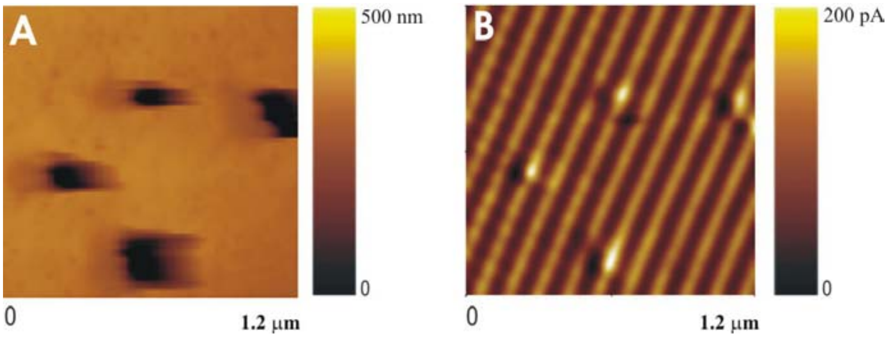

Figure 4.13: Simultaneously recorded topography (A) and current images (B) of the surface of a polycarbonate membrane. The AFM tip integrated electrode was biased at 0.65 v vs. Ag/AgCl in order to oxidize enzymatically produced hydrogen peroxide resulting from the conversion of glucose. The upper part of image (B) is very noisy, however, laterally resolved detection of glucose diffusing from the membrane pores can clearly be imaged. The images were recorded with a scan rate of 1 Hz.

For the second approach involving a bi-enzymatic conversion as shown in the reaction scheme above, the solution in the upper compartment was exchanged with a HRP and FMA solution. In the presence of HRP hydrogen peroxide is reduced catalyzed by the enzyme and ferrocinium methylhydroxide is produced. FMA^+ diffuses to the tip integrated electrode which was biased at a potential of 0.05 V vs. Ag/AgCl. At this potential only FMA^+ and no other species in the solution is converted. Hence the localized diffusion of glucose is mapped in presence of peroxidase. The obtained images are shown in Figure 4.14. Here again, the topography of the membrane can be depicted very well. However, at this stage no significant current change above the pores of the membrane could be observed. It is expected that improvements of the signal processing electronics will improve the S/N ratio in future enabling visualization of the current response.

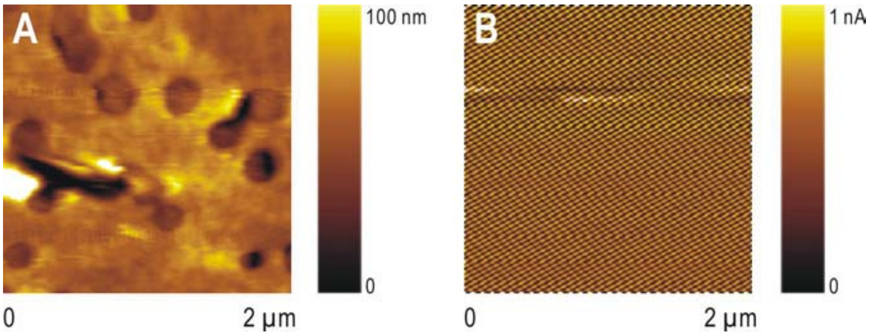

Figure 4.14: Simultaneously recorded topography (A) and current images (B) of the surface of a polycarbonate membrane. The AFM tip integrated electrode was biased at 0.05 V vs. Ag/AgCl, in order to convert enzymatically produced FMA^+. No significant current change above the pores of the membrane could be observed due to very high background noise. The images were recorded with a scan rate of 1 Hz.

4.2 Temperature responsive microgels

4.2.1 AFM studies

Atomic force microscopy is a powerful technique for the investigation of surfaces and interfaces in ambient and liquid environments. AFM investigations of hydrogel films are usually performed to obtain mechanical and structural data on those novel materials [30-32]. However, studies on single hydrogel microparticles (microgels) and in-situ observation of their temperature responsive behavior are a challenge that to date cannot be found in literature. In order to study their functionality and application as novel drug delivery systems and immobilization matrices for biosensors, laterally resolved information on their structure and dynamic behavior is a fundamental prerequisite. In this thesis, first studies were performed to demonstrate the ability of AFM for imaging hydrogel microparticles and to obtain information on the dependence of particle height on the applied tip force prior to in-situ temperature studies.

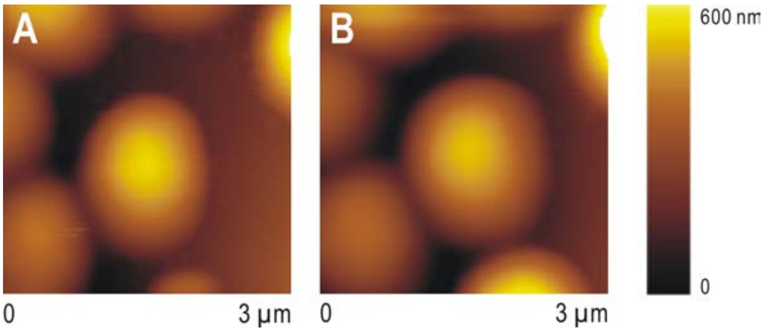

Figure 4.15: In-situ AFM images of hydrogel microparticle swelling in deionized water. (A) 2 min swelling period in water. (B) 5 min swelling period in water. The particles in image (A) are already highly swollen indicating that the swelling process occurs at a very fast rate. The images were recorded with a scan rate of 3 Hz.

By tuning the polymerization conditions, different hydrogel particle sizes can be designed. A microgel particle size of approx. 1 µm (at pH 7, 20 °C) was chosen for all AFM studies, showing a height change due to the temperature induced deswelling effect, which should be well detectable with the AFM. In-situ investigations on the swelling behavior and swelling rate upon addition of deionized water were performed by using a sample stage with a mounted liquid flow cell. Due to re-alignment of the laser from ambient to liquid conditions the first images of the sample surface could not be recorded until 2-3 min after immersion. Image (A) in Figure 4.15 reveals that at this point of time the particles were already swollen to a high extent showing that the uptake of water occurs at a very fast rate. The series were recorded without changing any experimental parameters and without withdrawing the tip from the sample surface. Figure 4.15 shows two images of the swelling process ((A) two minutes, (B) five minutes after immersion of the particles in water). The images were recorded by using AFM contact mode and comparatively high scan rates (~2-3 Hz). A difference in particle diameter can be clearly seen (approx. 1.45 µm at 2 min and approx. 1.75 µm at 5 min). However, it is difficult to derive whether these shape differences results from additional water uptake or if the particles were moved/shifted by the applied force. The dependency of the applied tip force on the particle shape will be discussed more detailed later in this chapter. The swelling process most probably occurs on such a fast time scale that conventional AFM does not offer sufficient temporal resolution to image this process.

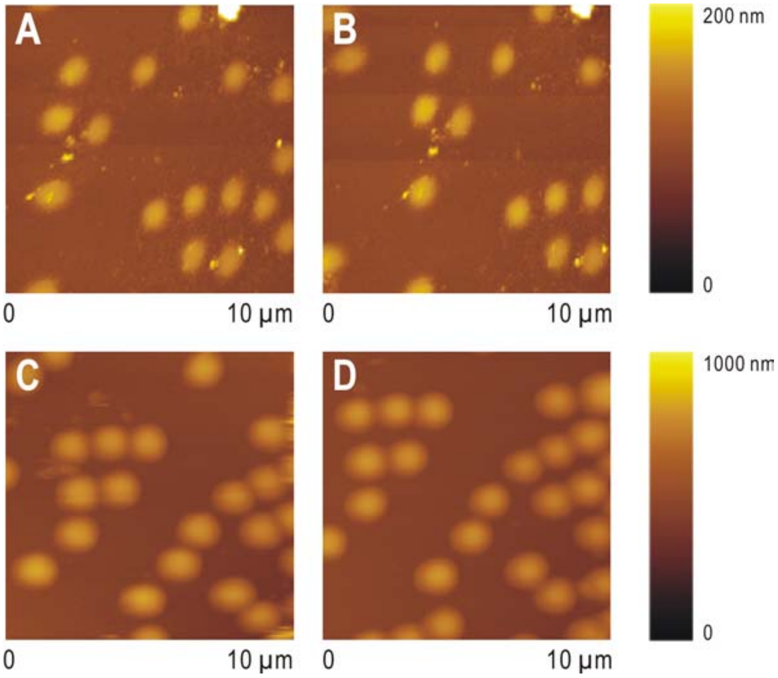

Figure 4.16: AFM images of microgels in air ((A) and (B)) and in deionized water ((C) and (D))-investigating the stability of the samples. The time period between recording image (A) and (B) was 25 min (area was scanned 9 times), and between (C) and (D) 55 min (area was scanned 15 times). As can be derived from the recorded images, immobilization of the electrostatically attached hydrogel particles is strong. It should be noted that although these measurements were performed in AFM contact mode, the soft particles were not detached from the substrate surface. The images were recorded with a scan rate of approx. 1.5 Hz.

To analyze the efficiency of the hydrogel immobilization onto the substrate surface, constant scanning over the same sample area was performed without changing the experimental settings. Typically, 10 to 15 images were recorded during AFM contact mode measurements under both ambient and aqueous (deionized water) conditions. The measurements were repeated at different spots of the 1 x 1 cm sample. The stability of electrostatically attached hydrogel particles was found to be strongly dependent on the respective sample area. Figure 4.16 shows AFM images (air and deionized water) of sample areas with strongly attached particles. Scanning over the same area for 25-55 min (air: 25 min, 9 scans; water: 55 min, 15 scans) does not significantly affect the surface morphology, as can be clearly derived from the images. Apparently, even the use of AFM contact mode applying higher forces to the sample surface in comparison to dynamic mode operation does not significantly influence or destroy the microgels at the scanned spots, which is surprising as the particles have a water content of up to 90 % in their swollen state (in deionized water and below the VPTT). The surface of the swollen particles can be described as spongy and soft resulting in the difficulty of deriving height information on the investigated microparticles.

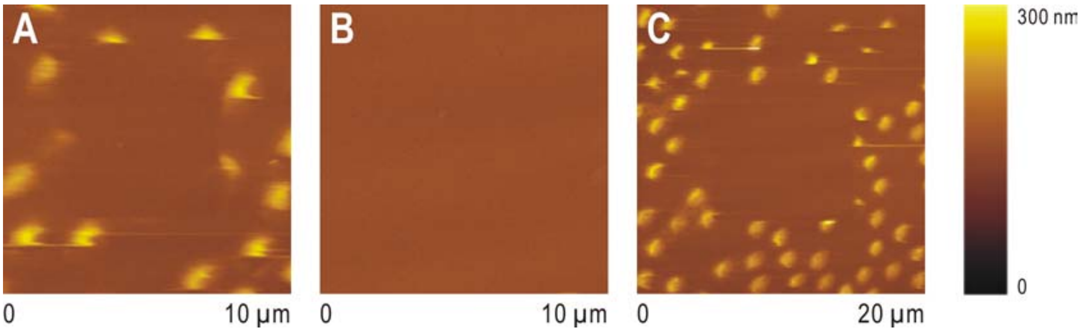

Figure 4.17: AFM studies of hydrogel sample stability (under ambient conditions) at a poorly immobilized sample area. The central, particle free area in image (A) was scanned once before increasing the scan range to obtain image (A). Rescanning of the same area resulted in image (B) showing that the hydrogel particles are detached. After increasing the scan range from 10 µm to 20 µm image (C) was obtained. This series depicts that poor immobilization leads to only weakly bound particles that can be easily detached from the surface with a single scan. The images were recorded with a scan rate of approx. 1.5 Hz.

In contrast to Figure 4.16 it was found that an average sample also contains areas with poorly immobilized microparticles. Hydrogel particles are shifted at or detached from the surface by the impact of the scanning AFM tip. Figure 4.17 shows a series of images were hydrogel particles disappeared after a single scan across the sample section. Upon increase of the scan range on the same spot, the area which was scanned before can be clearly identified due to detached particles. Poor immobilization of microgels can be attributed to inadequate cleaning and/or functionalization of the substrate prior to immobilization leading to incomplete attachment of the particles on those parts of the surface. Sample preparation is an important step in AFM investigation of hydrogel particles, however, samples with uniform stability were rarely observed.

Generally, AFM contact mode has a higher force impact on samples and is therefore recommended for measurements on robust surfaces. However, as mentioned before hydrogels are comparatively soft materials. Hence, in order to reduce the force impact and to lower the probability of removing particle from the surface AFM dynamic mode measurements were considered more suitable for the investigation of hydrogels.

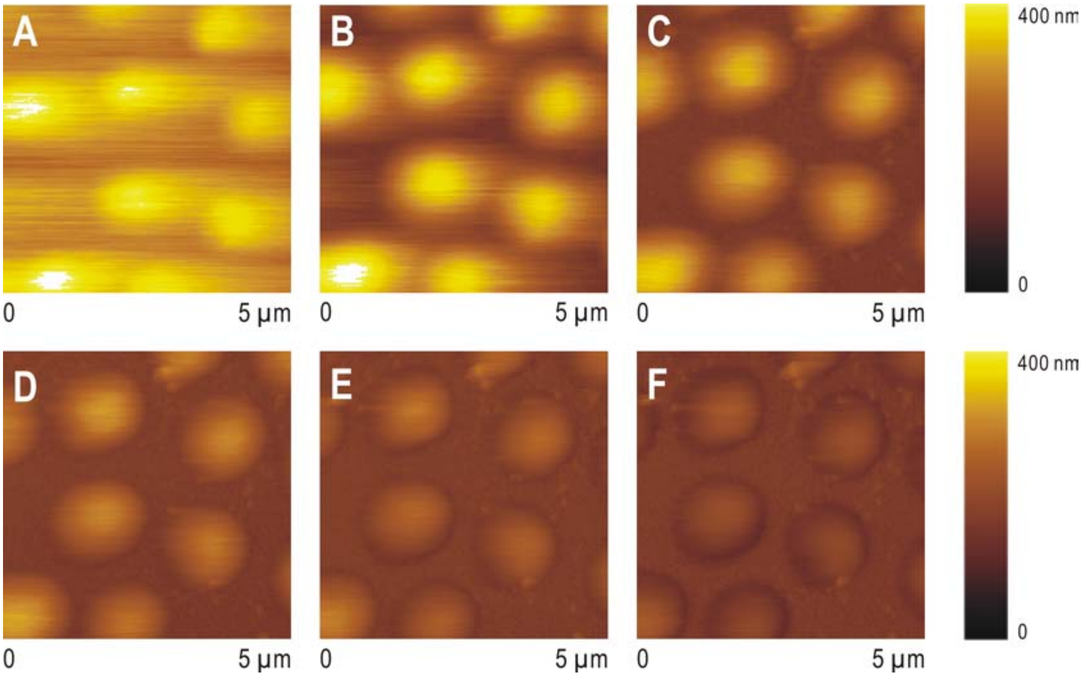

Figure 4.18: AFM studies of the microgel shape in respect to the applied force. Images were recorded in AFM dynamic mode at different values of the amplitude setpoint (in liquid, pH 3). A/A$_0$ (amplitude/free amplitude) settings were as follows: (A) 0.7, (B) 0.675, (C) 0.65, (D) 0.625, (E) 0.6 and (D) 0.575. Images (A) and (B) appear blurred due to inappropriate force settings. In contrast, particles in image (E) and (F) are too intended because the applied force was too high. Force optimization for sufficient imaging quality along with minimization of indentation is a prerequisite for the following in-situ studies. The images were recorded with a scan rate of 2 Hz.

As clearly seen in Figure 4.18, even AFM dynamic mode operation has a certain impact on soft samples, especially when the cantilever is driven acoustically (magnetic drive of the cantilever decreases the force impact [103]). The complex dependence of the imaging results on the imaging parameters is well known [104]. To observe the influence of the applied force on the particle shape, surface areas were continuously scanned while increasing the force impact.

During measurements in ambient conditions the particle height does not significantly change upon stepwise increasing the force. However, the height information of swollen particles (mapped in solution pH 3) showed a strong dependence on the applied force (Figure 4.18). The challenge for imaging soft materials is illustrated in Figure 4.18. In order to still achieve a decent imaging quality, the parameters adjusting the applied force are already influencing the particle shape of the highly hydrophilic soft particles. A compromise between image quality and impact of the force on the height information has to be achieved. If a high force (usually $A/A_0 < 0.6 - 0.65$) is applied the particles are intended leading to misinterpretation of the true particle dimensions.

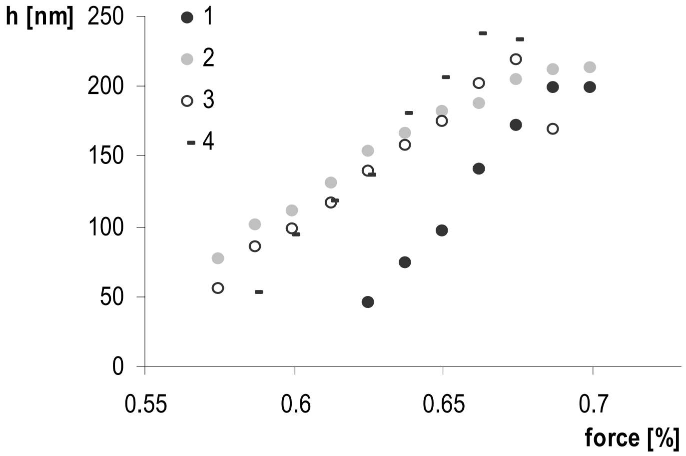

Figure 4.19: Influence of the applied force on the height of hydrogel microparticles. Average values of four sample areas are shown (1-4). Force values are specified in % of the free cantilever amplitude (free cantilever amplitude ~ 8). The particle height values for each area show highly linear dependency, however, sufficient correlation for particle heights in different scan areas could not be obtained.

Figure 4.19 shows a plot of average values of particle height versus applied tip force. Measurements on four different sample spots were performed. Before each series the tip was withdrawn from the surface and the experimental parameters and AFM settings were not changed. The same AFM tip was used for all four sample areas. The curves show a linear dependency. However, the plots of the single scan spots are not correlated, although, the measurement settings were not altered. Hence, the applied force (i.e. the resulting height) is apparently not only dependent on the force setpoint value, but also on factors such as changes in the tip characteristics. Even if the same tip was used, changes due to adsorption of the soft sample material onto the scanning tip may change the tip characteristics and accordingly the force interaction. Therefore, the height information on the hydrogel microparticles derived from AFM measurements within this work is considered to provide only relative values.

4.2.2 AFM-dynamic mode in-situ investigations on temperature responsive deswelling behavior of hydrogel microparticles

Thermoresponsive particles investigated within the presented work show a negative response behavior, which is correlated with a change of shape of the particles resulting in a decreased height during the deswelling process. In general, the deswelling process of poly(N-isopropylacrylamide-acrylic acid) copolymer microparticles (polyNIPAM-co-AAc) is dependent on the ionic strength of the solution, the pH value and the temperature [105]. Due to the complexity of AFM in-situ investigations on hydrogel particles lined out in the previous section, only the temperature effect was mapped at a fixed pH value of 3 without considering ionic strength effects. As discussed in the previous chapter, AFM investigations on the temperature responsive deswelling behavior of microgels requires control of the applied force for evaluation of the involved height changes. Taking into account the dependency of the particle height on the AFM measurement parameters, the following procedure was applied for all temperature experiments. In order to get comparable information on the shape of the particles before and after the VPT within one temperature sweep, the tip was engaged during the temperature cycle without changing the AFM parameters. Hence, the relative height information retrieved from the AFM measurements for one series of data obtained during the temperature induced phase transition is accessible. Aluminum coated silicon cantilevers with a nominal tip height of 15 – 20 µm, and a typical tip curvature of 10 nm were used for all in-situ temperature studies (see Table 5). Gold coated silicon nitride cantilevers could not be applied for in-situ temperature studies due to thermal effects on the resonance frequency caused by different thermal expansion coefficients of the coating and cantilever material [106].

Due to the acrylic acid groups, the investigated polyNIPAM-co-AAc particles reveal an additional pH responsive behavior involving attenuation of the volume phase transition behavior at pH > pK_a (4.25). If the acrylic acid groups are (partially) deprotonated (pH $\geq$ 4.5), the particle size increases and the VPTT shifts to higher values due to chain-chain coulombic repulsion and increased osmotic pressure resulting from influx of counter ions (Donnan potential) [107, 108]. Jones and Lyon [25] reported that dynamic light scattering (DLS) investigations of polyNIPAM-co-AAc particles at pH 6.5 did not show a VPT in the observed temperature window (≤ 40 °C). However, studies reported in literature discuss that on similar particles the volume phase transition at a higher pH was not recorded at temperatures < 60 °C [108]. Additionally, at this pH a very broad transition zone of the highly swollen particles is observed. In order to ensure a sharp volume phase transition, all in-situ temperature AFM studies on the deswelling behavior were performed in solution with pH 3. Due to the lower water content at pH 3, the particles additionally reveal higher particle stiffness. Together with the sharp VPT at low temperatures this allows AFM investigations on in-situ deswelling behavior.

A series of experiments were performed on electrostatically bound microparticles. Usually, the temperature was ramped between 25 °C and 30-33 °C. Typically, a heating, cooling and re-heating cycle was performed without withdrawing the tip or significantly changing the experimental parameters (Figure 4.20). The tip was scanned continuously and the heating was performed in increments of 1 °C with a delay time of approx. 5 min at each temperature ensuring that the sample was tempered in order to obtain images at constant temperature values.

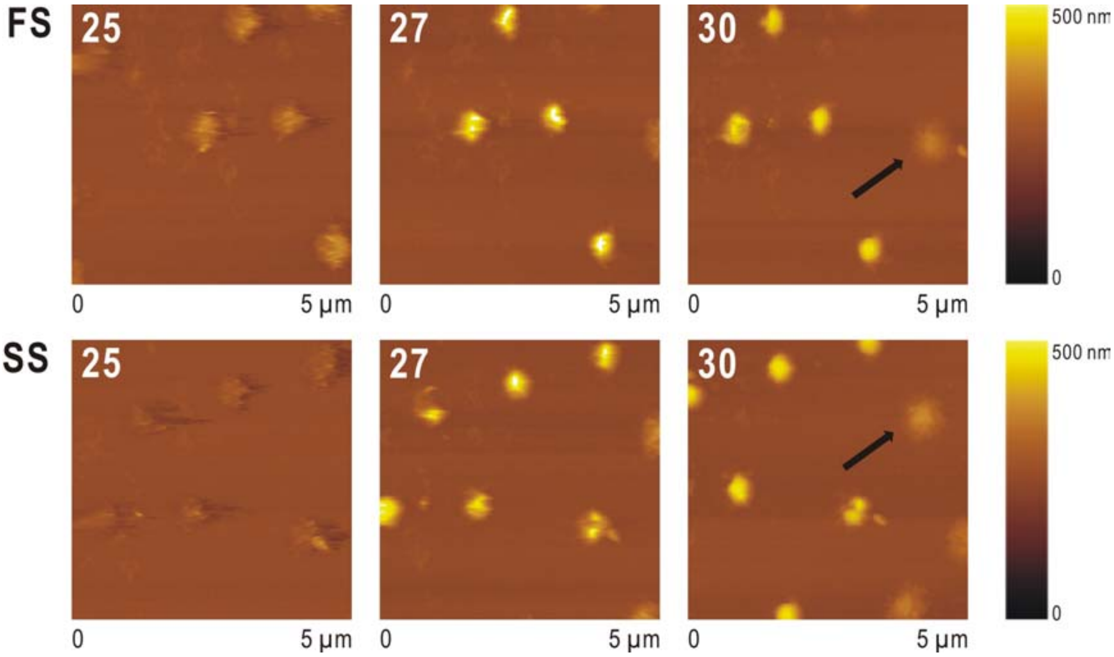

Figure 4.20: AFM images of electrostatically attached hydrogel particles on Au substrate recorded at 25 °C, 27 °C and 30 °C showing the temperature responsive deswelling effect. The experiment was performed while constantly scanning the AFM tip across the surface and recording images in incremental steps of 1 °C. After the first temperature sweep (FS) the sample was cooled and heated a second time (SS) without significantly changing the measurement parameters or withdrawing the tip. The images were recorded with a scan rate of approx. 0.6-0.8 Hz.

Figure 4.20 clearly shows a change of shape of the microgel particles at a temperature of 27 °C. Due the high water content of the particles below their VPT the soft microgel surface is characterized by a loss of imaging quality, whereas at temperatures > VPTT the image quality is improved indicating a change in stiffness of the particles. An additional effect on the imaging quality in comparison to the image presented in Figure 4.16 (B) is related to the changed tip geometry. The increase in aspect ratio of the aluminium coated silicon tips in comparison to the gold coated silicon nitride tips deteriorates the image quality, since the tip apparently penetrates the soft swollen microparticles to a higher extent.

The observed results in change of particle stiffness correlate well with theory describing a water exclusion up to 90 % upon passing the VPTT along with increased stiffness [33].

Additionally it should be noted that the VPTT obtained of the electrostatically bound particles is decreased in comparison to the VPTT obtained in bulk measurements [25]. This effect may be based on the different experimental conditions and also on the fact that the particles are attached to the surface.

According to photon correlation spectroscopy measurements, the deswelling behavior is correlated with a decrease in size of the particles. However, initial AFM experiments as shown in Figure 4.20 surprisingly indicate an increase in height upon passing the VPTT at 27 °C. Only particles at the edge of the scan area show the expected behavior (marked with black arrows). After cooling the sample to the start point of the temperature ramp, the microparticles return to their initial state showing the expected reversibility of the deswelling-swelling process within the AFM measurements. Heating of the sample for a second time reveals the same results. Due to hysteresis of the AFM scanner, which is additionally influenced by the temperature change, the scan range slightly shifts during the experiment. Remarkably, again only particles at the edge of the scan area show the expected behavior (marked with black arrows). These particles follow the expected behavior and their height decreases upon passing the VPT. In order to elucidate this “edge effect” the scan area was increased at the maximal temperature of 30 °C (Figure 4.21) without removing the AFM tip from the sample surface. Hence the increased scan area contains attached microparticles, which were not in contact with the AFM tip during or before the temperature cycle.

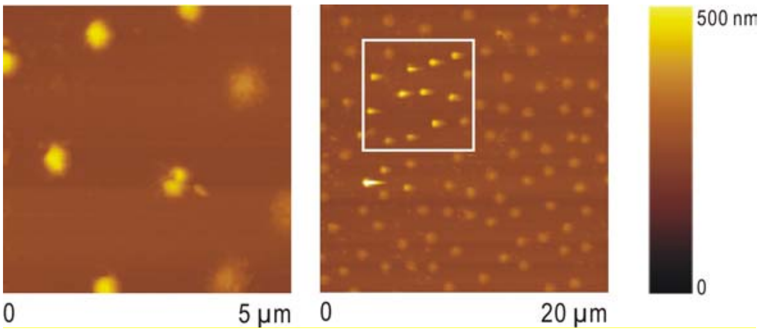

Figure 4.21: AFM images of electrostatically bound microgels recorded at 30 °C. Increase of the scan range indicates that particles that have not been in contact with the AFM tip during or before VPT show a different phase transition behavior compared to particles that were continuously scanned during heating. The white square marks the continuously scanned area. The images were recorded with a scan rate of approx. 0.6-0.8 Hz.

Figure 4.21 indicates a strong influence of the AFM tip on the VPT behavior. Hydrogel particles, which were not scanned before or during the phase transition, appear flat (h = ~100 nm) and show the expected deswelling behavior. Only particles that were in contact with the tip before or during the volume phase transition show the unexpected shape and height change (h > 200 nm). Apparently, the AFM tip interacts to a certain extend with the attached microparticles inducing a change in the volume phase transition behavior. The obtained height values retrieved from the AFM measurements at each temperature are given in Figure 4.22. Height values that were obtained during the first (FS) and the second sweep (SS) correlate well. Since the tip was engaged during the whole temperature experiment, the obtained data provides proof that the force impact on the particles was not significantly changed within the experiment.

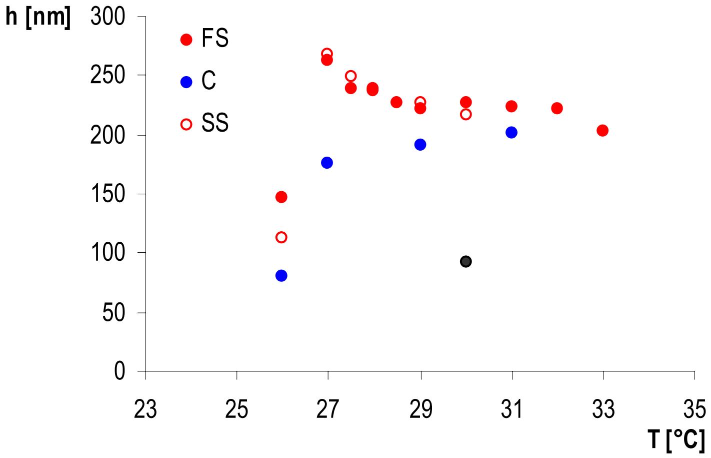

Figure 4.22: Plot of the average hydrogel particle height (electrostatic attachment) vs. temperature: (FS) first temperature sweep, (C) cooling, (SS) second temperature sweep. The observed increase in height for the first and second sweep correlates well. The black dot marks the average particle height (n = 25, average height = 92 ± 12 nm) of particles, which were not scanned before or during the transition phase.

In order to further investigate the influence of the AFM tip on the phase transition behavior, the experimental conditions were changed as follows: in contrast to other AFM instruments the PicoPlus AFM used in all experiments allows keeping the tip engaged at the surface without scanning. Again, the tip was engaged at the surface during the whole temperature sweep to keep the experimental conditions unaltered. However, instead of continuously imaging the sample surface, only one image was recorded after each incremental rise of the temperature (typically in steps of 1 °C).

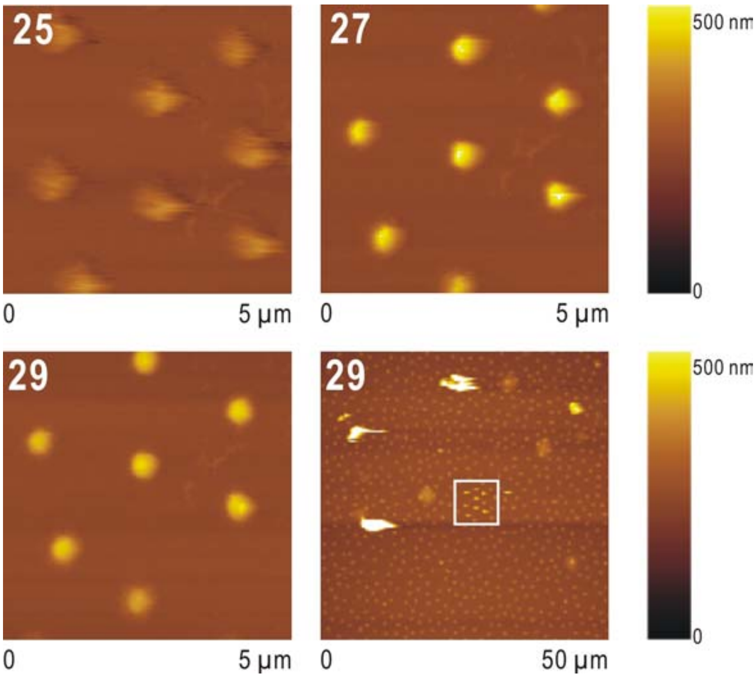

Figure 4.23: AFM images of electrostatically bound hydrogel particles on Au surfaces recorded at 25 °C, 27 °C and 29 °C. During stepwise heating of the sample the tip was engaged at the surface without scanning. The particles abruptly change in shape at 27 °C (VPT). The scan range was increased at 29 °C revealing the same height dependency on prior scans as shown in Figure 4.21 (white square marks the previously scanned area). The images were recorded with a scan rate of approx. 0.4-0.5 Hz.

Figure 4.23 shows the respective AFM images. Although the sample was not scanned continuously, the same height dependency of microgel particles, which were scanned before or during VPT (see Figure 4.21), is observed, which, again, leads to the conclusion that the tip-sample interaction affects the deswelling behavior of hydrogel microparticles.

In order to further minimize the tip-sample interaction, the hydrogel microparticles were exposed to the scanning tip only twice, below (25 °C) and above the VPTT (29 °C). During the temperature ramp the tip was kept engaged, however, was not scanned across the sample surface (Figure 4.24).

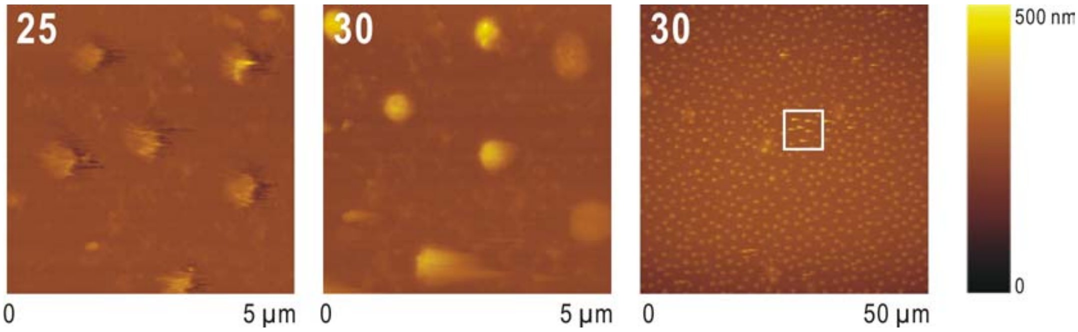

Figure 4.24: AFM images of electrostatically bound hydrogel particles on Au surfaces recorded at 25 °C and 30 °C. After recording the scan at 25 °C, the tip was kept at the surface while increasing the temperature to 30 °C. After mapping the sample surface at 30 °C the scan range was increased showing the same results as obtained in prior experiments (the white square marks the area that was scanned before the VPT). Hence, scanning over the microparticles only once already induces a change of the deswelling behavior. The images were recorded with a scan rate of approx. 0.4-0.5 Hz.

The series of experiments shown in Figure 4.21, Figure 4.23 and Figure 4.24 revealed an increase of the particle height, after the microgel particles were – even only once - in contact with the AFM tip. This behavior appears independent of the number of performed scans. Hence, the observed consistent phenomenon of increased particle height after the VPT indicates an irreversible AFM tip-microgel particle interaction altering the VPT behavior of the previously scanned particles

One possible explanation is that the tip induces a partial desorption of the electrostatically bound particles from the surface causing a change of the particle shape. Due to the high water content of the swollen particles, the imaging quality is poor and this effect is not evident from the AFM data. However, this tip-induced change in footprint and height of the particles induces a different deswelling behavior of the microgels (see also Figure 4.29).

In order to investigate the influence of the proposed partial desorption effect, covalently attached particles were investigated in the following. The covalently attached particles were formed by immobilization to amino-functionalized gold substrates via amide bonds. In order to compare the results of the covalent binding approach with the data obtained for the in-situ temperature experiments of the electrostatically bound particles, the same experimental conditions were applied. The temperature was again incrementally increased in steps of 1 °C and the tip was either continuously scanned or kept engaged at the surface as previously described. Figure 4.25 - Figure 4.27 show the obtained AFM images of these studies.

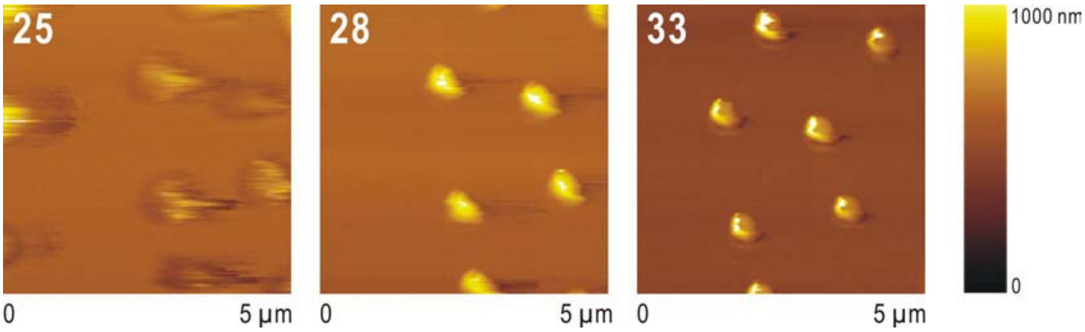

Figure 4.25: AFM images of covalently bound hydrogel microparticles on a functionalized Au surfaces recorded at 25 °C, 28 °C and 33 °C. The tip was continuously scanned across the surface and AFM images were recorded at incremental temperature steps of 1 °C. The images were recorded with a scan rate of approx. 0.55 Hz.

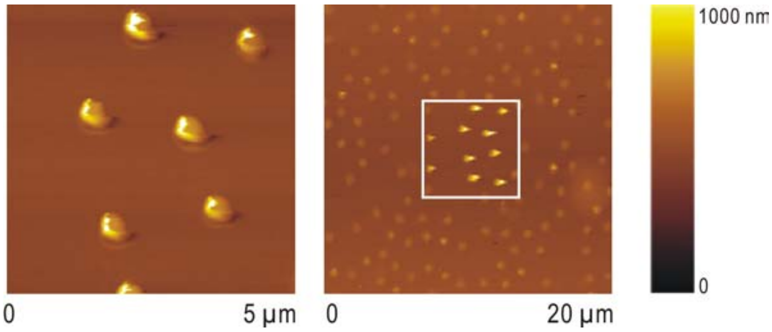

Figure 4.26: AFM images of covalently bound microgel particles recorded at 33 °C. An increase of the scan area shows again the height effect on particles, which were scanned during or prior to the VPT. The white square marks the constantly scanned area. The images were recorded with a scan rate of approx. 0.45-0.55 Hz.

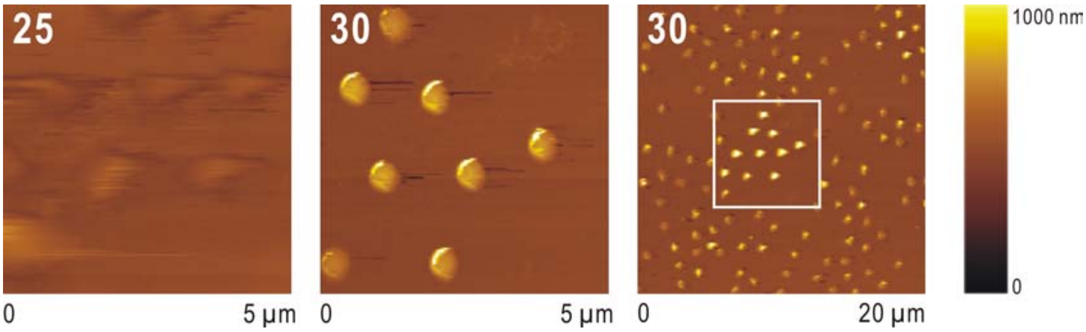

Figure 4.27: AFM images of covalently bound hydrogel particles on Au surfaces recorded at 25 °C and 30 °C. The tip was engaged at the surface without scanning during the temperature ramp. After recording an image at 30 °C the scan range was increased indicating the same effect observed during the temperature experiments on the electrostatically bound particles (white square marks previously scanned particles). The images were recorded with a scan rate of approx. 0.56 Hz.

The volume phase transition of the covalently bound particles proceeds at slightly higher temperatures (28 °C) in comparison to the electrostatically attached particles, which undergo the transition at 27 °C. However, evaluation of the AFM data obtained for the covalently bound particles shows the same results in respect to the height increase during the phase transition similar to the electrostatically bound microgel particles. As the second image in Figure 4.25 demonstrates, the height of the particles is increased after the VPT, whereas particles which were not scanned prior to the temperature sweep (Figure 4.26, right image) again show the expected deswelling behavior along with a reduced particle height. A repetition of the experiment scanning the sample only once, before the VPT, however, keeping the tip engaged as described previously for the electrostatically attached particles, presents the same effect. Figure 4.28 shows a plot of average heights versus temperature during continuously scanning the tip on the sample surface while rising the temperature. Height values obtained in first (FS) and second temperature sweep (SS) correlate well for temperatures higher the VPTT.

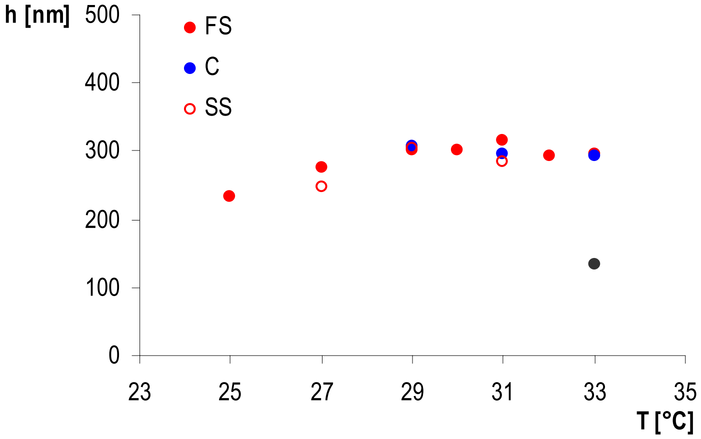

Figure 4.28: Trend of the average height of the hydrogel particle (covalently bound) at the respective temperature ((FS) first temperature sweep, (C) cooling, (SS) second temperature sweep). The black dot at 133 ± 46 nm marks the average particle height in the areas, which were not in contact with the AFM tip during scanning.

It should be noted that optimization of the image quality for covalently attached samples was a tedious procedure. In general, satisfying image quality of the swollen particles could not be achieved leading to uncertainty of the height values, especially below the VPT. In consequence, the plot in Figure 4.28 shows no significant change in the height values at the VPTT. The observed temperature effect on the swelling behavior along with the poor imaging ability is hypothesized as follows: although the microgels are covalently bound, the total adhesion to the surface might be lower compared to the electrostatic attachment due to the lower number of binding sites, as there is a higher density of electric charges on the surface of the particles compared to the sites for possible covalent binding. No further investigations on this issue were performed at this stage of the presented work, but should be a starting point for future experiments elucidating the processes occurring at the sample surface. Additionally, repeated measurements on the covalent attached particles revealed that particles were easily removed from the substrate surface indicating that they were either only weakly bound or still only adsorbed to the surface. Hence, in future the conditions of covalently binding hydrogel particles to the substrate surface have to be improved and optimized in order to obtain more reproducible results and improved imaging quality on the phase transition behavior. Due to limited access to other covalent immobilization processes within this thesis, no further investigations on covalently attached particles were performed.

The results obtained from measurements of the covalently attached microgels are contradictory to the hypothesis of AFM tip-induced desorption. However due to the questionable quality of the samples this theory cannot be conclusively eliminated.

In order to elucidate the contradictory AFM data obtained on the deswelling behavior of the microgels, following model should be discussed.

At the chosen pH value (3) the acidic groups of the acrylic acid present in the hydrogel network are fully protonated. For all in-situ temperature investigations a silicon probe was used. Hence under ambient condition and without further pretreatment the silicon surface is covered with hydroxyl groups (silicon surfaces are known to possess about $5*10^{-14}$ OH-groups/cm^2 under normal laboratory conditions [109]). Hence, hydrogen bonding may be formed between the carboxylic group and the terminated hydroxyl groups leading to attractive adhesion forces. This adhesion effect between tip and particle can result in a change of the initial particle footprint and height of the particles, which were in contact with the AFM tip. Furthermore, this effect can be enhanced due to the high aspect ratio of the silicon tips applied in AFM imaging. The tip is dipped into the soft outer layer of the particles leading to a strong adhesion to the outer shell and changing the shape of the attached particle. Adhesion effects were obtained by Woodward et al. [110] investigating the interaction forces between similar hydrogels (polyNIPAM-co-AAc, with a 5 % lower acrylic acid content than the particles used in the presented studies) microgels and silica surfaces with colloid probe microscopy. These results reveal that only at pH 4 (< pK_a(AAc)), when the carboxylic groups are protonated, adhesive forces were obtained. At higher pH values repulsive forces between the probe and the gels were measured. A suggested mechanism is that the interactions between the outer shell of the microgels and the AFM tip pull the particles up and/or rip them partially off causing a shape change. Hence, this change in shape may induce a different swelling behavior, which leads to a smaller footprint of the particle and increased height instead of the collapsing deswelling effect. However, at the present stage of the investigations it is not clear, why an irreversible change of the particle shape will occur by scanning the tip across the particle. The AFM studies on the electrostatically bound particles do not support a theory of ripping off the particles, since AFM imaging on repeated heating and cooling experiments could be performed at the same sample spot. Furthermore, the hypothesis that the particle remains in the energetic unfavorable "decreased footprint/increased height state" over a period of 30-40 min, appears unlikely for the experimental series where scanning of the tip was only performed once in the beginning of the heating experiment at 25 °C and then after the VPT at 30 °C.

Figure 4.29 summarize a schematic view of the proposed models for tip induced modification of the hydrogel particles.

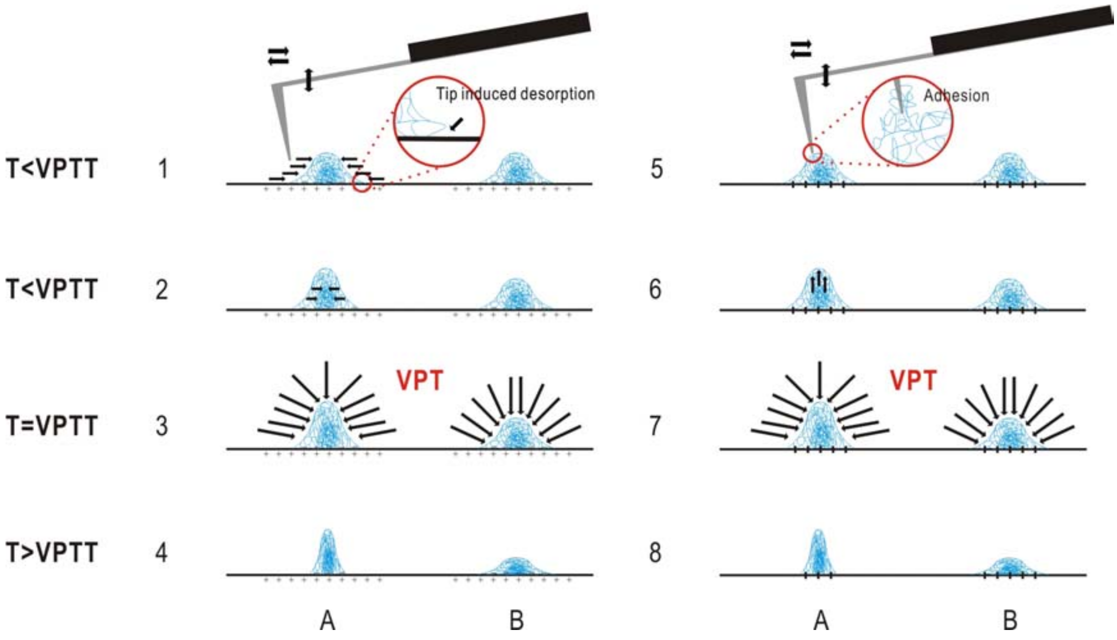

Figure 4.29: represents a scheme of proposed models for AFM tip influence on hydrogel particles. (A) particle that is depicted before the VPT, (B) particle that is not depicted before the VPT. (1) – (4) electrostatic attachment to the surface and tip induced desorption: (1) – (2) scanning of the AFM tip desorbs the side areas of the hydrogel particle and squeezes the particles together (particle A), particle B having no contact to the AFM tip remains unaltered. (5) – (8) covalent attachment to the surface and adhesion of hydrogel to the AFM tip. (5) – (6) adhesion of hydrogel to the tip leads to partial pull-off of the particle in z direction (particle A), again particle B remains unaltered. (3) & (7) During the volume phase

transition particle A deswells not only in z direction of the substrate but additionally in the (x, y) plane (3-dimensional deswelling). Particle B deswells mainly in one dimension only (z direction).

Optimizing the imaging quality of swollen particles obtained with the aluminium coated silicon cantilevers was typically a tedious procedure and measurements were performed using comparatively low scan rates (0.5 - 0.7 Hz). As described before, the high aspect ratio of these tips enables the tip to dip deep into the soft shell of the particle reducing the imaging quality. In contrast, the gold coated silicon nitride tips with a lower aspect ratio resulted in higher imaging quality allowing higher scan rates (up to 3 Hz). This effect is associated with the tip geometry, which is listed in Table 5.

Dimension	**Silicon cantilevers (Al coated)**	**Silicon nitride cantilevers (Au coated)**
tip curvature	<10 nm	15-30 nm
tip height	15-20 µm	2.8 µm

Table 5: AFM tip dimensions of used cantilevers.

The silicon cantilevers can be envisaged as sharp needles, which penetrate the outer shell of polymer network to a certain extent, whereas the silicon nitride tips are hypothesized to predominantly slide across the surface of the hydrogel particles. Figure 4.30 schematically compares imaging of a soft sample with the two cantilever shapes.

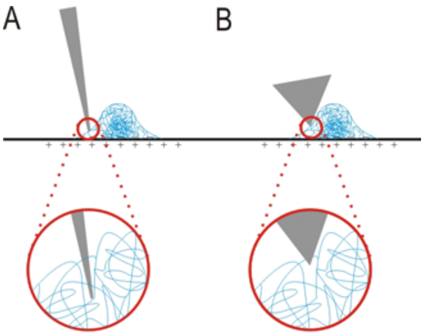

Figure 4.30: Scheme of the applied cantilever shapes. (A) "Needle-like" silicon cantilever (backside aluminium coated). During scanning across the particles the tip penetrates the hydrogel matrix. Adhesion of material leads to easier destruction and blurred images. (B) Silicon nitride cantilever (backside gold coated). Cantilever rather slides across the particles instead of penetrating.

As indicated before, the backside gold coating on the silicon nitride cantilevers leads to a drift in the force setpoint during heating of the sample [106]. Thermal stress within the gold layer upon temperature changes induces a drift of the photodiode signal preventing in-situ studies with an increased imaging time. In order to reduce this thermal drift, the gold layer from the backside of the cantilever mount can be removed in aqua regia (one part conc. HNO_3 and three parts conc. HCl) by dipping the cantilever mount into the acid mixture. Careful removal allows a controlled area of gold remaining at the front of the cantilever to maintain enough reflectivity for subsequent laser alignment. AFM probes modified by this technique do not show unfavorable thermal drifts and, hence, these less invasive tips can in future be used for AFM heating experiments.

An alternative approach can be envisaged including complete removal of the gold coating and subsequent controlled sputtering of a gold layer only on the very end of the cantilever. Additionally, this approach allows to further decrease the curvature of the tip to a desired value of 30 nm - 100 nm. Using a modified AFM tip with a curvature of approx. 130 nm, the temperature responsive deswelling of electrostatic bound particles was investigated. The tip was scanned during the heating process and images were recorded after stabilizing the temperature at 25 °C, 27 °C and 30 °C. At 30 °C the scan range was increased leading to the same results that were achieved in previously performed experiments (Figure 4.31). Previously depicted hydrogel microparticles again show a different behavior upon passing the VPT.

Although a loss in lateral resolution is obtained, future applications will include further modification of the gold coating with a long chain thiol monolayer resulting in a hydrophobic tip, which could be used to finally proof the proposed hypothesis.

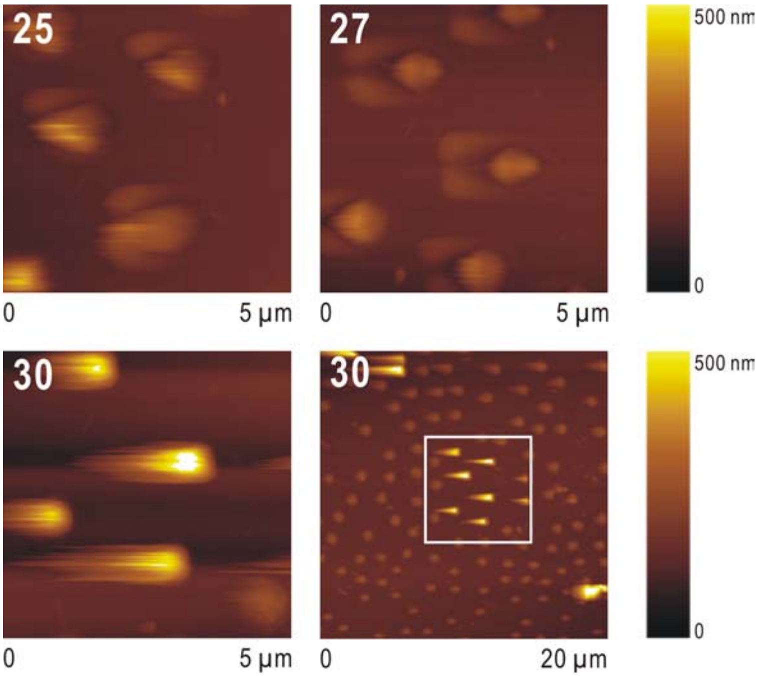

Figure 4.31: AFM images of electrostatically bound hydrogel microparticles on functionalized Au surfaces recorded at 25 °C, 27 °C and 30 °C. A modified silicon nitride cantilever was used (Au sputtered tip, tip curvature ~ 130 nm). The hydrogel particles show the same trend in shape change as during all other experiments in this study. The images were recorded with a scan rate of approx. 0.6 Hz.

For confirmation of the obtained results, additional information using complementary non invasive techniques would be needed. Hence, we propose the combination of optical microscopy measurements of the particle height, with prior scanning of a sample array using the AFM. Therefore, following experiment was performed: AFM was used to pattern a hydrogel surface by scanning the AFM tip once in defined arrays across the sample surface (in solution pH 3). Figure 4.32 shows a scheme of the produced pattern.

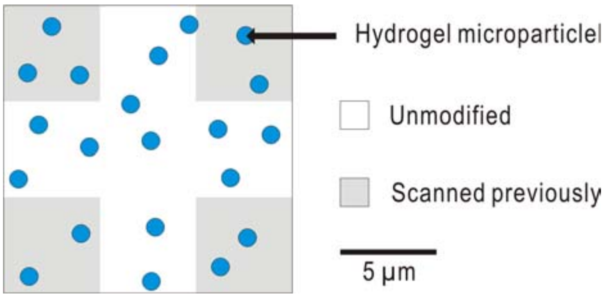

Figure 4.32: Scheme of the microgel particle scan pattern produced by AFM. Grey areas (5x5 µm) were scanned once at 17 °C, white areas remained unmodified (scans were performed in solution at pH 3).

After “patterning” of the sample by AFM, the substrate was transferred into an optical microscope (oil-immersion objective, 100-fold magnification) and the shape change associated with the temperature responsive deswelling was monitored by optical microscopy. The objective of the experiment was to investigate whether the footprints of the particles in the previously scanned area were significantly altered in comparison to the hydrogel particles, which were not in contact to the AFM tip. As proposed in the scheme of Figure 4.29 scanning the particle surface should lead to a tip induced desorption or tip adhesion of the hydrogel particles and, therefore, an altered dimension of the footprint. However, although the scanned area was marked to date it was impossible to locate the scanned spots again in the optical microscope during these preliminary experiments. For future works following experimental changes are suggested: (i) increased AFM scan area; (ii) reduced time between scanning and optical investigation; and (iii) improved marking of the scanned pattern from AFM enabling retrieval of the same area in optical microscopy.

5 Conclusions and outlook

In the presented work strategies for the development of microelectrode based biosensors were investigated with main emphasis on optimization of the experimental conditions for subsequent miniaturization and integration of amperometric biosensors into AFM tips. Beyond established immobilization techniques, novel materials such as hydrogels have been studied with AFM in order to obtain laterally resolved information of their temperature behavior in prospect to their use as novel materials for immobilization of biological components (e.g. enzyme entrapment) and drug delivery systems.

Preparation of the conventional biosensing layers on microelectrodes was achieved using two well established approaches: (i) entrapment of enzymes based on pulsed deposition of electrophoretic polymers and (ii) covalent attachment via self-assembled monolayers. Both approaches have been selected for the integration of biosensing layers into an integrated AFM/SECM probe, since the immobilization can be localized at miniaturized electrodes without involving any manual manipulation of the electrode surface. For the first approach, it was found that pulsed deposition of the enzyme containing film resulted in an optimum of enzyme activity and film stability at the miniaturized electroactive surface if one pulse cycle was applied. In respect to the modification of the AFM tip integrated micro- and nanoelectrodes this parameter is crucial.

The covalent immobilization approach, as expected, showed lower sensitivity of the biosensor due to lower enzyme concentration on the surface via covalent binding. Hence, this approach was demonstrated for the immobilization of horseradish peroxidase at the integrated AFM/SECM probe, however, was not further investigated. The obtained current response for integrated biosensors obtained via polymer entrapment usually was in the pA range [101]. The prepared biosensors based on polymer entrapment had the best current response after storing the fabricated biosensor at 4 °C for 24 h. Micro biosensors with an electroactive diameter of 10 µm were calibrated using manual and automated standard addition. The detection limit determined with manual glucose standard addition was 50 µM, which was lower compared to the detection limit obtained with FIA due to better control of the background noise at this stage of the presented work. During flow injection analysis the use of a peristaltic pump resulted in higher background noise and, therefore, a reduced detection limit. However, the calibration curves obtained in FIA calibration experiments revealed improved linearity and excellent correlation of the obtained data. Due to limited time, more extensive studies on the prepared

AFM tip integrated biosensors could not be performed during this work and will be topic of future studies.

Thermoresponsive hydrogels are novel materials with potential applications as immobilization matrices in biosensor design and drug delivery. Furthermore, they can be used as model systems for soft biological surfaces. A prerequisite for these challenging applications is the fundamental characterization of these materials and understanding of the temperature responsive behavior. To date, studies on the temperature dependent swelling or deswelling are mainly performed in bulk experiments using light scattering techniques. Scanning probe investigations were used to image films before and after passing phase transition. In order to monitor the in-situ changes during the volume phase transition induced by the temperature change, atomic force microscopy was used studying volume changes of single polyNIPAM-co-AAc hydrogel microparticles for the first time. The sample surface was either continuously scanned during cycling of the temperature, or single scans were performed before and after the volume phase transition, however, while keeping the AFM tip engaged at the sample surface. Additionally, the complex phase transition behavior of these particles is dependent on the pH and ionic strength of the solution. To control the experimental conditions, all experiments were performed in a solution of pH 3. The volume phase transition was observed at 27 - 28 °C.

One of the major findings of the conducted experiments is that the interaction of the AFM tip with the immobilized particles significantly influences their volume phase transition behavior. Particles being depicted before the volume phase transition temperature show a difference in shape after passing this temperature, in contrast to particles, which were not in contact with the AFM tip. Even single scans before the VPT induce a change in the phase transition behavior. In order to investigate the immobilization effect on the phase transition behavior, electrostatically bound particles and covalently attached particles were investigated. Several variations of the experiments were performed in order to investigate the effect of the applied AFM tip force and to enable formulating a hypothesis for these surprising results. In summary, it is very likely that the particles are partially desorbed by the AFM tip due to hydrophilic adhesive forces at pH 3. However, further experiments will be conducted with a hydrophobic AFM tip to proof this hypothesis.

The experiments performed within this thesis have also shown new perspectives for future work, in both presented fields, the development of AFM tip integrated biosensors and for in-situ phase transition studies of thermoresponsive hydrogels.

For further maximization of the enzyme concentration (activity) within the recognition layer of tip integrated biosensor providing enhanced sensitivity, further optimization of the pre polymerization solution is suggested. In addition, reproducible fabrication of the enzyme containing layer is a prerequisite for routine application of biosensors. Resulting, lower detection limits open the field for a wide variety of applications. Measurements on living samples, e.g. sensing of the glucose metabolism in vicinity of single cells, requires high sensitivity of the applied biosensors. Future applications may include the combination of scanning AFM tip integrated biosensors with molecular recognition force spectroscopy based on the modification of the tip with biological recognition elements [54, 55, 58]. Immobilization of an enzymatic recognition layer at the integrated electrode surface will result in novel multifunctional scanning probes simultaneously measuring topography, localized bio(electro)activity and binding/rupture events. Additionally, for thorough characterization of the developed biosensors further improvement of the calibration methodology is needed. The application of SIA instead of FIA is a promising alternative for reducing the high background noise. It is expected that further optimization of AFM tip integrated biosensors will lead to innovative applications in a variety of biological/biomedical applications.

In order to enhance the knowledge on the interaction of thermoresponsive hydrogels with AFM probes, several strategies are proposed. First, sample preparation has to be optimized, especially for covalent immobilization of hydrogel particles. Both, more reproducible experimental conditions for AFM measurements along with enhanced knowledge for future applications using hydrogels as immobilization matrices in novel biosensor design can thus be achieved. In order to further elucidate the obtained experimental results on the volume phase transition behavior, following approaches are proposed. AFM measurements with hydrophobic probes are suggested, due to lower adhesive interactions between the sample and the tip. Modification of AFM probes with a long-chained (e.g. C18) thiol monolayer is a promising approach. In addition, magnetically oscillated AFM (MAC mode) can be used for reduced force impact on the sample. To evaluate data obtained with dynamic mode AFM, the results should be correlated with data obtained from other non invasive scanning probe techniques such as NSOM. For elucidation of the change of particle footprints induced by the scanning AFM tip, further experiments combining optical microscopy with in-situ AFM measurement as already described in the discussion section (see chapter 4.2.2) can be envisaged. By simultaneously applying both techniques, independent observations of the volume phase transition will be obtained. The MI AFM used for the experiments in this thesis allows mounting of the AFM on an inverted microscope, which was already applied within our research group for cell investigations. Hence, changes in the phase transition behavior induced by the AFM tip could be simultaneously monitored with independent techniques.

Additionally, recording force distance curves to increase the information on attractive/repulsive forces between the AFM probe and the sample will help understanding the processes occurring during the volume phase transition of the particles.

Combining responsive hydrogels with tip integrated biosensors provides following perspectives for future applications. Hydrogels are highly promising materials for immobilizing biological recognition elements at biosensor surfaces. However, molecule-loaded thermoresponsive microgel particles known to expel solvent - and therefore the loaded component - can be applied for mimicking exocytosis events in a controlled setting. Laterally resolved measurements on the kinetics of this process at individual hydrogel particles would be a valuable asset in the field of drug delivery applications.

6 References

1. Thevenot, D.R., et al., *International Union of Pure and Applied Chemistry Physical Chemistry Division, Steering Committee on Biophysical Chemistry Analytical Chemistry Division, Commission V.5 (Electroanalytical Chemistry) Electrochemical biosensors: proposed definitions and classification. Synopsis of the report.* Sensors and Actuators, B: Chemical, 1996. **B30**(1): p. 81.
2. Scheller, F., et al., *Research and development of biosensors. A review.* Analyst (Cambridge, United Kingdom), 1989. **114**(6): p. 653-62.
3. Schuhmann, W. and E.M. Bonsen, *Biosensors.* Encyclopedia of Electrochemistry, 2003. **3**: p. 350-384.
4. Hulanicki, A., S. Glab, and F. Ingman, Pure Applied Chemistry, 1991. **63**: p. 1247.
5. Goepel, W., *Chemical analysis and sensorics with microstructured devices.* Mikrochimica Acta, 1997. **125**(1-4): p. 179-196.
6. Wang, J., *Amperometric biosensors for clinical and therapeutic drug monitoring: a review.* Journal of pharmaceutical and biomedical analysis, 1999. **19**(1-2): p. 47-53.
7. Clark, L.C., Jr. and C. Lyons, *Electrode systems for continuous monitoring in cardiovascular surgery.* Annals of the New York Academy of Sciences, 1962. **102**: p. 29-45.
8. Cass, A.E.G., et al., *Ferrocene-mediated enzyme electrode for amperometric determination of glucose.* Analytical Chemistry, 1984. **56**(4): p. 667-71.
9. Degani, Y. and A. Heller, *Electrical communication between redox centers of glucose oxidase and electrodes via electrostatically and covalently bound redox polymers.* Journal of the American Chemical Society, 1989. **111**(6): p. 2357-8.
10. Yang, X., G. Johansson, and L. Gorton, *A glucose sensor made by chemically crosslinking glucose oxidase directly on the surface of a carbon electrode modified with palladium/gold for hydrogen peroxide electrocatalysis.* Mikrochimica Acta, 1989. **1**(1-2): p. 9-16.
11. Wang, B., et al., *Amperometric glucose biosensor based on sol-gel organic-inorganic hybrid material.* Analytical chemistry, 1998. **70**(15): p. 3170-4.
12. Kuenzelmann, U. and H. Boettcher, *Biosensor properties of glucose oxidase immobilized within SiO2 gels.* Sensors and Actuators, B: Chemical, 1997. **B39**(1-3): p. 222-228.
13. Nagata, R., et al., *A glucose sensor fabricated by the screen printing technique.* Biosensors & bioelectronics, 1995. **10**(3-4): p. 261-7.
14. Gernet, S., M. Koudelka, and N.F. De Rooij, *Fabrication and characterization of a planar electrochemical cell and its application as a glucose sensor.* Sensors and Actuators, 1989. **18**(1): p. 59-70.
15. Wilhelm, T. and G. Wittstock, *Patterns of functional proteins formed by local electrochemical desorption of self-assembled monolayers.* Electrochimica Acta, 2001. **47**(1-2): p. 275-281.
16. Bartlett, P.N. and J.M. Cooper, *A review of the immobilization of enzymes in electropolymerized films.* Journal of Electroanalytical Chemistry, 1993. **362**(1-2): p. 1-12.
17. Schuhmann, W., *Conducting polymer based amperometric enzyme electrodes.* Mikrochimica Acta, 1995. **121**(1-4): p. 1-29.
18. Cosnier, S., *Biomolecule immobilization on electrode surfaces by entrapment or attachment to electrochemically polymerized films. A review.* Biosensors & Bioelectronics, 1999. **14**(5): p. 443-456.

19. Trojanowicz, M., T. Krawczynski, and T. Krawczynski vel Krawczyk, *Electrochemical biosensors based on enzymes immobilized in electropolymerized films.* Mikrochimica Acta, 1995. **121**(1-4): p. 167-81.
20. Kurzawa, C., A. Hengstenberg, and W. Schuhmann, *Immobilization method for the preparation of biosensors based on ph shift-induced deposition of biomolecule-containing polymer films.* Analytical Chemistry, 2002. **74**(2): p. 355-361.
21. Pelton, R., *Temperature-sensitive aqueous microgels.* Advances in Colloid and Interface Science, 2000. **85**(1): p. 1-33.
22. Soppimath, K.S., et al., *Stimulus-responsive \"smart\" hydrogels as novel drug delivery systems.* Drug Development and Industrial Pharmacy, 2002. **28**(8): p. 957-974.
23. Qiu, Y. and K. Park, *Environment-sensitive hydrogels for drug delivery.* Advanced Drug Delivery Reviews, 2001. **53**(3): p. 321-339.
24. Debord, J.D. and L.A. Lyon, *Synthesis and Characterization of pH-Responsive Copolymer Microgels with Tunable Volume Phase Transition Temperatures.* Langmuir, 2003. **19**(18): p. 7662-7664.
25. Jones, C.D. and L.A. Lyon, *Synthesis and Characterization of Multiresponsive Core-Shell Microgels.* Macromolecules, 2000. **33**(22): p. 8301-8306.
26. Debord, J.D. and L.A. Lyon, *Thermoresponsive Photonic Crystals.* Journal of Physical Chemistry B, 2000. **104**(27): p. 6327-6331.
27. Serpe, M.J., J. Kim, and L.A. Lyon, *Colloidal hydrogel microlenses.* Advanced Materials (Weinheim, Germany), 2004. **16**(2): p. 184-187.
28. Serpe, M.J. and L.A. Lyon, *Nanostructured hydrogel films: Formation and characterization.* Abstracts of Papers, 223rd ACS National Meeting, Orlando, FL, United States, April 7-11, 2002, 2002: p. COLL-281.
29. Plunkett, M.A., et al., *Adsorption of pNIPAM Layers on Hydrophobic Gold Surfaces, Measured in Situ by QCM and SPR.* Langmuir, 2003. **19**(17): p. 6837-6844.
30. Matzelle, T.R., G. Geuskens, and N. Kruse, *Elastic Properties of Poly(N-isopropylacrylamide) and Poly(acrylamide) Hydrogels Studied by Scanning Force Microscopy.* Macromolecules, 2003. **36**(8): p. 2926-2931.
31. Suzuki, A., et al., *Surface domains and roughness of polymer gels observed by atomic force microscopy.* Macromolecules, 1997. **30**(8): p. 2350-2354.
32. Harmon, M.E., D. Kuckling, and C.W. Frank, *Photo-Cross-Linkable PNIPAAm Copolymers. 5. Mechanical Properties of Hydrogel Layers.* Langmuir, 2003. **19**(26): p. 10660-10665.
33. Serpe, M.J. and L.A. Lyon, *Alternate layer deposition of poly(N-isopropylacrylamide) microgels to achieve thermoresponsive, microstructured thin films.* Polymer Preprints (American Chemical Society, Division of Polymer Chemistry), 2003. **44**(2): p. 701-702.
34. Eremeev, N.L., et al., *Shortening the biosensor assay by use of enzyme-containing temperature-sensitive hydrogels.* Biotechnology Techniques, 1999. **13**(5): p. 295-298.
35. Suzuki, H., *Microfabrication of chemical sensors and biosensors for environmental monitoring.* Materials Science & Engineering, C: Biomimetic and Supramolecular Systems, 2000. **C12**(1-2): p. 55-61.
36. Sato, K., et al., *Microchip-based chemical and biochemical analysis systems.* Advanced Drug Delivery Reviews, 2003. **55**(3): p. 379-391.
37. Kueng, A., C. Kranz, and B. Mizaikoff, *Scanning probe microscopy with integrated biosensors.* Sensor Letters, 2003. **1**(1): p. 2-15.
38. Binnig, G., et al., *Surface studies by Scanning Tunneling Microscopy.* Physical Review Letters, 1982. **49**: p. 57.
39. Binnig, G., et al., Applied Physics Letters, 1982. **40**: p. 178.

40. Binnig, G. and C.F. Quate, *Atomic Force Microscope.* Physical Review Letters, 1986. **56**: p. 930.
41. Iwasawa, Y., H. Onishi, and K.-I. Fukui, *In situ STM study of surface catalytic reactions on TiO2(110) relevant to catalyst design.* Topics in Catalysis, 2001. **14**(1-4): p. 163-172.
42. Dieska, P., I. Stich, and R. Perez, *Covalent and Reversible Short-Range Electrostatic Imaging in Noncontact Atomic Force Microscopy.* Physical Review Letters, 2003. **91**(21): p. 216401/1-216401/4.
43. Hartmann, U., *Intermolecular and surface forces in noncontact scanning force microscopy.* Ultramicroscopy, 1992. **42-44**: p. 59-65.
44. Hansma, P.K., et al., *Tapping mode atomic force microscopy in liquids.* Applied Physics Letters, 1994. **64**(13): p. 1738-40.
45. Zhong, Q., et al., *Fractured polymer/silica fiber surface studied by tapping mode atomic force microscopy.* Surface Science, 1993. **290**(1-2): p. L688-L692.
46. Putman, C.A.J., et al., *Tapping mode atomic force microscopy in liquid.* Applied Physics Letters, 1994. **64**(18): p. 2454-6.
47. Le Grimellec, C., et al., *Tapping mode atomic force microscopy allows the in situ imaging of fragile membrane structures and of intact cells surface at high resolution.* Single Molecules, 2000. **1**(2): p. 105-107.
48. Florin, E.L., V.T. Moy, and H.E. Gaub, *Adhesion forces between individual ligand-receptor pairs.* Science (Washington, DC, United States), 1994. **264**(5157): p. 415-17.
49. Lee, G.U., D.A. Kidwell, and R.J. Colton, *Sensing Discrete Streptavidin-Biotin Interactions with Atomic Force Microscopy.* Langmuir, 1994. **10**(2): p. 354-7.
50. Janshoff, A., et al., *Force spectroscopy of molecular systems - single molecule spectroscopy of polymers and biomolecules.* Angewandte Chemie, International Edition, 2000. **39**(18): p. 3212-3237.
51. Willemsen, O.H., et al., *Biomolecular interactions measured by atomic force microscopy.* Biophysical journal, 2000. **79**(6): p. 3267-81.
52. Carrion-Vazquez, M., et al., *Mechanical design of proteins studied by single-molecule force spectroscopy and protein engineering.* Progress in biophysics and molecular biology, 2000. **74**(1-2): p. 63-91.
53. Zlatanova, J., S.M. Lindsay, and S.H. Leuba, *Single molecule force spectroscopy in biology using the atomic force microscope.* Progress in Biophysics & Molecular Biology, 2000. **74**(1-2): p. 37-61.
54. Hinterdorfer, P., et al., *Detection and localization of individual antibody-antigen recognition events by atomic force microscopy.* Proceedings of the National Academy of Sciences of the United States of America, 1996. **93**(8): p. 3477-81.
55. Hinterdorfer, P., et al., *A mechanistic study of the dissociation of individual antibody-antigen pairs by atomic force microscopy.* Nanobiology, 1998. **4**(3): p. 177-188.
56. Ros, R., et al., *Antigen binding forces of individually addressed single-chain Fv antibody molecules.* Proceedings of the National Academy of Sciences of the United States of America, 1998. **95**(13): p. 7402-5.
57. Schwesinger, F., et al., *Unbinding forces of single antibody-antigen complexes correlate with their thermal dissociation rates.* Proceedings of the National Academy of Sciences of the United States of America, 2000. **97**(18): p. 9972-9977.
58. Raab, A., et al., *Antibody recognition imaging by force microscopy.* Nature Biotechnology, 1999. **17**(9): p. 902-905.
59. Schutz, G.J., et al., *Single molecule microscopy of biomembranes (Review).* Molecular Membrane Biology, 2000. **17**(1): p. 17-29.

60. Bard, A.J., *Introduction and Principles*, in *Scanning Electrochemical Microscopy*, A.J. Bard and M.V. Mirkin, Editors. 2001, Marcel Dekker, Inc.: New York. p. 1-15.
61. Wightman, R.M. and D.O. Wipf, *Voltammetry at Ultramicroelectrodes*, in *Electroanalytical Chemistry*, A.J. Bard, Editor. 1985, Marcel Dekker, Inc.: New York. p. 267-353.
62. Zoski, C.G., *Ultramicroelectrodes: design, fabrication, and characterization.* Electroanalysis, 2002. **14**(15-16): p. 1041-1051.
63. Engstrom, R.C., et al., *Measurements within the diffusion layer using a microelectrode probe.* Analytical Chemistry, 1986. **58**(4): p. 844-8.
64. Liu, H.Y., et al., *Scanning electrochemical and tunneling ultramicroelectrode microscope for high-resolution examination of electrode surfaces in solution.* Journal of the American Chemical Society, 1986. **108**(13): p. 3838-9.
65. Bard, A.J., et al., *Scanning electrochemical microscopy. Introduction and principles.* Analytical Chemistry, 1989. **61**(2): p. 132-8.
66. Kwak, J. and A.J. Bard, *Scanning electrochemical microscopy. Theory of the feedback mode.* Analytical Chemistry, 1989. **61**(11): p. 1221-7.
67. Lee, Y., S. Amemiya, and A.J. Bard, *Scanning Electrochemical Microscopy. 41. Theory and Characterization of Ring Electrodes.* Analytical Chemistry, 2001. **73**(10): p. 2261-2267.
68. Liljeroth, P., et al., *Micro ring-disk electrode probes for scanning electrochemical microscopy.* Electrochemistry Communications, 2002. **4**(1): p. 67-71.
69. Liljeroth, P., et al., *Disk-Generation/Ring-Collection Scanning Electrochemical Microscopy: Theory and Application.* Analytical Chemistry, 2002. **74**(9): p. 1972-1978.
70. Zoski, C.G. and M.V. Mirkin, *Steady-State Limiting Currents at Finite Conical Microelectrodes.* Analytical Chemistry, 2002. **74**(9): p. 1986-1992.
71. Lee, C., J. Kwak, and F.C. Anson, *Application of scanning electrochemical microscopy to generation/collection experiments with high collection efficiency.* Analytical Chemistry, 1991. **63**(14): p. 1501-4.
72. Mandler, D., *Micro- and Nanopatterning using the Scanning Electrochemical Microscope*, in *Scanning Electrochemical Microscopy*, A.J. Bard and M.V. Mirkin, Editors. 2001, Marcel Dekker, Inc.: New York. p. 593-602.
73. Newman, J., *Resistance for flow of current to a disk.* Journal of the Electrochemical Society, 1966. **113**(5): p. 501-2.
74. Shao, Y., et al., *Nanometer-Sized Electrochemical Sensors.* Analytical Chemistry, 1997. **69**(8): p. 1627-1634.
75. Hengstenberg, A., C. Kranz, and W. Schuhmann, *Facilitated tip-positioning and applications of non-electrode tips in scanning electrochemical microscopy using a shear force based constant-distance mode.* Chemistry--A European Journal, 2000. **6**(9): p. 1547-1554.
76. Wipf, D.O. and A.J. Bard, *Scanning electrochemical microscopy. 15. Improvements in imaging via tip-position modulation and lock-in detection.* Analytical Chemistry, 1992. **64**(13): p. 1362-7.
77. Wipf, D.O., A.J. Bard, and D.E. Tallman, *Scanning electrochemical microscopy. 21. Constant-current imaging with an autoswitching controller.* Analytical Chemistry, 1993. **65**(10): p. 1373-7.
78. Borgwarth, K., D.G. Ebling, and J. Heinze, *Scanning electrochemical microscopy: a new scanning mode based on convective effects.* Berichte der Bunsen-Gesellschaft, 1994. **98**(10): p. 1317-21.

79. Ludwig, M., et al., *Topography feedback mechanism for the scanning electrochemical microscope based on hydrodynamic forces between tip and sample.* Review of Scientific Instruments, 1995. **66**(4): p. 2857-60.
80. Betzig, E., P.L. Finn, and J.S. Weiner, *Combined shear force and near-field scanning optical microscopy.* Applied Physics Letters, 1992. **60**(20): p. 2484-6.
81. Katemann, B.B., A. Schulte, and W. Schuhmann, *Constant-distance mode scanning electrochemical microscopy (SECM)-part I: Adaptation of a non-optical shear-force-based positioning mode for SECM tips.* Chemistry--A European Journal, 2003. **9**(9): p. 2025-2033.
82. Williams, D.E., T.F. Mohiuddin, and Y.Y. Zhu, *Elucidation of a trigger mechanism for pitting corrosion of stainless steels using submicron resolution scanning electrochemical and photoelectrochemical microscopy.* Journal of the Electrochemical Society, 1998. **145**(8): p. 2664-2672.
83. Treutler, T.H. and G. Wittstock, *Combination of an electrochemical tunneling microscope (ECSTM) and a scanning electrochemical microscope (SECM): application for tip-induced modification of self-assembled monolayers.* Electrochimica Acta, 2003. **48**(20-22): p. 2923-2932.
84. Shi, G., L.F. Garfias-Mesias, and W.H. Smyrl, *Preparation of a gold-sputtered optical fiber as a microelectrode for electrochemical microscopy.* Journal of the Electrochemical Society, 1998. **145**(6): p. 2011-2016.
85. Lee, Y. and A.J. Bard, *Fabrication and Characterization of Probes for Combined Scanning Electrochemical/Optical Microscopy Experiments.* Analytical Chemistry, 2002. **74**(15): p. 3626-3633.
86. Korchev, Y.E., et al., *Hybrid scanning ion conductance and scanning near-field optical microscopy for the study of living cells.* Biophysical Journal, 2000. **78**(5): p. 2675-2679.
87. Macpherson, J.V. and P.R. Unwin, *Combined Scanning Electrochemical-Atomic Force Microscopy.* Analytical Chemistry, 2000. **72**(2): p. 276-285.
88. Macpherson, J.V. and P.R. Unwin, *Noncontact Electrochemical Imaging with Combined Scanning Electrochemical Atomic Force Microscopy.* Analytical Chemistry, 2001. **73**(3): p. 550-557.
89. Jones, C.E., P.R. Unwin, and J.V. Macpherson, *In situ observation of the surface processes involved in dissolution from the cleavage surface of calcite in aqueous solution using combined scanning electrochemical - atomic force microscopy (SECM-AFM).* ChemPhysChem, 2003. **4**(2): p. 139-146.
90. Kranz, C., et al., *Integrating an Ultramicroelectrode in an AFM Cantilever: Combined Technology for Enhanced Information.* Analytical Chemistry, 2001. **73**(11): p. 2491-2500.
91. Melngailis, J., *Focused ion beam technology and applications.* Journal of Vacuum Science & Technology, B: Microelectronics and Nanometer Structures, 1987. **5**(2): p. 469-95.
92. Lugstein, A., et al., *Integrating micro- and nanoelectrodes into atomic force microscopy cantilevers using focused ion beam techniques.* Applied Physics Letters, 2002. **81**(2): p. 349-351.
93. Kueng, A., et al., *Integrated AFM-SECM in tapping mode: Simultaneous topographical and electrochemical imaging of enzyme activity.* Angewandte Chemie, International Edition, 2003. **42**(28): p. 3238-3240.
94. Kueng, A., et al., *Combined scanning electrochemical atomic force microscopy for tapping mode imaging.* Applied Physics Letters, 2003. **82**(10): p. 1592-1594.

95. Kranz, C., et al., *Mapping of enyme activity by detection of enzymatic products during AFM imaging with integrated SECM-AFM probes.* Ultramicroscopy, 2004. **100**(3-4): p. 127-134.
96. Schuhmann, W., et al., *Pulse technique for the electrochemical deposition of polymer films on electrode surfaces.* Biosensors & Bioelectronics, 1997. **12**(12): p. 1157-1167.
97. Monk, P.M.S., *Fundamentals of Electroanalytical Chemistry*. Analytical Techniques in the Sciences, ed. D.J. Ando. 2001, Chichester, England: John Wiley & Sons Ltd. 361.
98. Heinze, J., *Cyclic voltammetry - the \"spectroscopy\" of the electrochemist.* Angewandte Chemie, 1984. **96**(11): p. 823-40.
99. Fan, F.R.F. and C. Demaille, *The preparation of tips for Scanning Electrochemical Microscopy*, in *Scanning Electrochemical Microscopy*, A.J. Bard and M.V. Mirkin, Editors. 2001, Marcel Dekker, Inc.: New York. p. 75-110.
100. Shiku, H., et al., *Dual immunoassay of human chorionic gonadotropin and human placental lactogen at a microfabricated substrate by scanning electrochemical microscopy.* Journal of Electroanalytical Chemistry, 1997. **438**(1-2): p. 187-190.
101. Kueng, A., *manuscript in preparation.*
102. Kueng, A., C. Kranz, and B. Mizaikoff, *Amperometric ATP biosensor based on polymer entrapped enzymes.* Biosensors & Bioelectronics, 2004. **19**(10): p. 1301-1307.
103. Han, W., S.M. Lindsay, and T. Jing, *A magnetically driven oscillating probe microscope for operation in liquids.* Applied Physics Letters, 1996. **69**(26): p. 4111-4113.
104. Magonov, S.N., et al., *Tapping-mode atomic force microscopy study of the near-surface composition of a styrene-butadiene-styrene triblock copolymer film.* Surface Science, 1997. **389**(1-3): p. 201-211.
105. Snowden, M.J., et al., *Colloidal copolymer microgels of N-isopropylacrylamide and acrylic acid: pH, ionic strength and temperature effects.* Journal of the Chemical Society, Faraday Transactions, 1996. **92**(24): p. 5013-5016.
106. Shen, F., et al., *Thermal effects on coated resonant microcantilevers.* Sensors and Actuators, A: Physical, 2001. **A95**(1): p. 17-23.
107. Fernandez-Nieves, A., et al., *Charge controlled swelling of microgel particles.* Macromolecules, 2000. **33**(6): p. 2114-2118.
108. Ito, S., et al., *Preparation of Thermosensitive Submicrometer Gel Particles with Anionic and Cationic Charges.* Langmuir, 1999. **15**(12): p. 4289-4294.
109. Wasserman, S.R., Y.T. Tao, and G.M. Whitesides, *Structure and reactivity of alkylsiloxane monolayers formed by reaction of alkyltrichlorosilanes on silicon substrates.* Langmuir, 1989. **5**(4): p. 1074-87.
110. Woodward, N.C., et al., *Measurement of the Interaction Forces between Poly(N-isopropylacrylamide-acrylic acid) Microgel and Silica Surfaces by Colloid Probe Microscopy.* Langmuir, 2002. **18**(6): p. 2089-2095.